Weft Knit Strain Sensors for Human Motion Capture

Emmanuel Olawuyi Olawole Ayodele

School of Electronic and Electrical Engineering

University of Leeds

A thesis submitted for the degree of

Doctor of Philosophy

December 2020

Declaration

The candidate confirms that the work submitted is his own, except where work which has formed part of jointly authored publications has been included. The contribution of the candidate and the other authors to this work has been explicitly indicated below. The candidate confirms that appropriate credit has been given within the thesis where reference has been made to the work of others.

Part of the work in this thesis has appeared in the following publications:

In Chapter 4:

Emmanuel Ayodele, Syed Ali Raza Zaidi, Jane Scott, Zhiqiang Zhang, Qingxiang Kong, Des Mclernon, "Weft Knit Smart Data Glove", 2019 IEEE International Conference on Wearable and Implantable Body Sensor Networks.

Emmanuel Ayodele, Syed Ali Raza Zaidi, Jane Scott, Zhiqiang Zhang, Ali Hayajneh, Samson Shittu and Des Mclernon, "A Weft Knit Data Glove" submitted to IEEE Transactions on Instrumentation and Measurement, November 2020 (revised).

In Chapter 5:

Emmanuel Ayodele, Bao Tianzhe, Syed Ali Raza Zaidi, Jane Scott, Zhiqiang Zhang, Ali Hayajneh, Des Mclernon, "Grasp Classification with Weft-knit Data Glove using Convolutional Neural Networks", IEEE Sensors Journal, 2021 *(accepted for publication)*.

Emmanuel Ayodele, Syed Ali Raza Zaidi, Jane Scott, Zhiqiang Zhang, DesMclernon, "A Review of Deep Learning Approaches in Glove-Based Gesture Classification" in Machine Learning, Big Data and

IoT for Medical Informatics, P. Kumar, Ed; Elsevier, 2021 *(accepted for publication)*.

In Chapter 6:

Emmanuel Ayodele, Syed Ali Raza Zaidi, Jane Scott, Zhiqiang Zhang, Maryam Hafeez, Des Mclernon,"Effect of Tuck and Miss Stitches on a Weft Knit Sensor", Sensors, 21(2), 358, 2021.

The candidate, Emmanuel Olawuyi Olawole Ayodele, is the sole contributor to the technical part and writing of these publications. The design of all sensor configurations, the design and implementation of all simulations and experiments; and the writing of all drafts of the manuscript were solely performed by the candidate.

All publications were written under the meticulous guidance of supervisors Syed Ali Raza Zaidi, Jane Scott, Zhiqiang Zhang and Des Mclernon. They helped to provide technical feedback on the ideas, results and manuscripts.

Bao Tianzhe, a member of the same working group, recommended CNN and the initial hyperparameters and provided feedback on written drafts. Qingxiang Kong contributed to the programming of the ESP-8266 WiFi module in the wireless prototype of the weft knit data glove. Ali Hayajneh, Maryam Hafeez and Shittu Samson also provided editorial feedback on written drafts.

Acknowledgements

First and foremost, I would like to give God all the glory for it is only by His will that I am where I am today.

I would like to say a big thank you to Dr Syed Ali Raza Zaidi for taking a chance on a masters student who wanted his supervision for his MSc project. In the last five years, I have learnt a lot from you as a supervisor and as a mentor. I will forever appreciate the freedom you provided for me to pursue research that aligns with my career goals.

Special thanks to Dr Jane Scott. Our meeting was a pure coincidence but you took me under your wing and provided meticulous supervision. Thank you for providing all the required materials for me to understand knitting technology and promptly replying to my overwhelming emails and drafts.

I would like to also thank Dr Zhiqiang Zhang for his support and guidance since my application to the PhD program. I really appreciate your guidance into research in wearable technology.

I would like to also offer my gratitude to Dr Des Mclernon. Thank you for your thorough feedback throughout this research. Your method of communicating important information with an infusion of lighthearted jokes is remarkable.

I would also like to thank Ian Rees for his help in fabricating every sensor used in this research. I am also grateful for my fellow colleagues and friends (Dr Samson Shittu, Dr Harith Kharrufa, Tianzhe Bao, Qingxiang Kong, Noman Naftab, Prof Ping Liu, Dr Ali Hayajneh etc.) who made adapting to Leeds a lot easier.

My unending appreciation goes to my family. Particularly, my parents for the financial support throughout my stay in the UK. For the long phone calls on weekends listening to me speak about weft knit strain sensors. I can't pay you back for all of these but I will pay it forward! I would also like to thank my sisters for their continued belief and emotional support. Finally, I would like to thank the love of my life, Sianny, for her love, patience and support during this period. I came to Leeds for a world-class education and I'm also leaving with a world-class partner.

Abstract

Weft knit strain sensors are textile sensors that measure motion at the joints of a human body. These sensors are formed by the weft knitting of conductive yarn and can be implemented as wearable devices that resemble normal clothing. The conductive yarn is a tactile yarn with electrical properties formed from a composite of stainless steel and polyester filaments. Although, it can be mechanically manipulated to create a woven or knitted fabric that measures strain, weft knitting is the optimal method because of its elastic structure. Due to the novelty of this research area, there are a lot of gaps that prevent the wide-scale adoption of this sensing mechanism. This thesis aims to address two of these gaps. Firstly, the lack of a model that accurately simulates the electromechanical behaviour of structural variations of a weft knit strain sensor. Secondly, the lack of a wearable device framework that illustrates the design of the sensor, its implementation in a wearable device and the processing of its acquired data using machine learning algorithms.

Firstly, an electromechanical model that simulates the behaviour of plain knit sensor with only conductive yarn is proposed. The length resistance are obtained from the loop and interlocking angles of the conductive loops in the sensor and the contact resistance is derived using a novel algorithm. The model was validated by a tensile test performed on sensors with the simulated knitting parameters. It was shown that the simulation results agreed with the experimental results. In particular, the proposed model has a lower percentage error in comparison to previous studies. Furthermore, the effect of changes

in the loop and interlocking angles on the piezoresistivity of the sensor is simulated.

Thereafter, this model is applied on a novel sensor configuration comprising of a conductive yarn and a non-conductive elastomeric yarn. The simulation results provide a very accurate representation of the empirical piezoresistivity of the sensor. Subsequently, we create a wholly textile data glove by knitting its support structure and its weft knit strain sensor in a single manufacturing process using WholeGarment technology. The data glove measures motion at the interphalangeal joints in a human hand. The consistency of the glove is verified and classical machine learning algorithms are applied to classify the data acquired using a robotic hand.

In addition, deep learning is evaluated in a grasp classification using the weft knit data glove on human participants. A convolutional neural network (CNN) algorithm is proposed to classify the grasp type from the acquired data. Classical machine algorithms are also used to classify the data to provide a comparative performance. The results illustrate that the CNN algorithm achieved a higher accuracy than the classical machine algorithms in the classification scenarios.

Finally, the effect of miss and tuck stitches on the piezoresistivity of the sensors is investigated. Miss and tuck stitches affect structural properties such as the length, width and extension of a knit fabric and therefore, may affect the piezoresistivity of a weft knit strain sensor. By adapting the electromechanical model to geometrical properties of miss and tuck stitches, several sensor configurations comprising of varying amounts of tuck or miss stitches are simulated. Subsequently, a tensile test is performed on knitted sensors with the simulated properties. The simulation results generally agree with the experimental results. Moreover, it is observed that increases in miss and tuck stitches decrease the initial and mean resistance of the sensor. In addition, the results show that increasing the percentage of

tuck stitches in the sensor increases the linearity of a weft knit strain sensor.

Contents

List of Figures

List of Tables

Abbreviations

ADC	Analog digital converter
ANN	Artificial neural network
AUC	Area under curve
CNN	Convolutional neural networks
CNT	Carbon nanotubes
DIP	Distal interphalangeal
EM	Expected maximisation
FBG	Fibre-braggs grating
FC	Fully-connected
FFT	Fast fourier transform
FPR	False positive rate
HMC	Human motion capture
HMM	Hidden Markov model
k-nn	k-nearest neighbour
LR	Linear regression
NB	naïve Bayes
NP	Nanoparticles
NWs	Nanowires
PDMS	Polydimethylsiloxane
PIP	Proximal interphalangeal
RC	Respiration cycle
RELU	Rectified unit layer
ROC	Receiver operating curve
RR	Respiration rate
sEMG	surface electromyography
SVM	Support vector machines
TPR	True positive rate
ZnONW	Zinc-oxide nanowire

List of Symbols

A_{cr}	Cross-sectional area of tunneling junction
C	Course spacing or height of a loop
C_n	Number of course
d	Diameter of conductive yarn
d_c	Diameter of an elliptical cylinder
d_n	Distance between the conductive nano-materials
e_c	Charge of a single electron
h_{pl}	Plank's constant
L_h	Length of the loop head
L_l	Length of the loop leg
m_e	Mass of an electron
R_{eq}	Equivalent or total resistance of the sensor
R_h	Resistance of the loop head
R_l	Resistance of the loop leg
R_s	Resistance of the loop sinker
R_{tunnel}	Tunneling resistance
S_d	Stitch density
w	Width of knit loop
W_n	Number of wales
α	Loop angle
β	Interlocking angle
ϵ	Strain
λ_{eb}	Height of energy barrier
θ	Inclination
ρ	Resistivity of the conductive yarn
ρ_e	Photo-elastic expansion coefficient

Chapter 1

Introduction

1.1 Introduction

Human motion capture (HMC) involves the measurement of movement at specific joints in the human body. It is a broad research field that stems across several industries including sport science, medical rehabilitation, and human-computer interaction [1, 2]. There are two research approaches in the capture of human motion. The first approach involves the use of computer vision in which cameras are used to record motion which is then analysed using different image processing techniques to generate the required information [3]. However, there are disadvantages with this approach. Firstly, in the current geopolitical climate, users are apathetic in using such devices due to the fear of intrusion of their privacy [4]. In addition, the use of a stationary camera limits the movement of the users to within the camera's viewpoint. This restricts applications that require the continuous monitoring of user while they perform their regular activities. Furthermore, camera-based approaches utilise substantial computational resources as a result of the pre-processing required in segmenting features from the image data.

The second approach involves the use of wearable motion capture devices. These devices when worn by their users are capable of monitoring the users' activities without restricting their movements. A popular example of a commercial wearable device is the Apple watch. Although, this device has a silhouette of a watch, its main features are tracking the health of its users through its

configuration of various sensors; and its telecommunication features that enable users access the internet, make phone calls and send text messages. In 2019 alone, 31 million Apple watch devices were sold [5]. Furthermore, according to an industry-led review [6] published by the government of the United Kingdom, wearable technologies are expected to add $70 billion to the world's economy by 2024.

For wearables used strictly for the capture of human motion, it is imperative that they are located as close to the joint as possible for accurate measurement. This requirement leads to size and weight constraints on the wearable device. Traditionally, these motion-capture wearables were designed by integrating conventional electronic sensors into textile support structures. However, this has resulted in a bulky design that has reduced the commercial adaptation of these devices.

Due to this challenge, a new research area comprising of E-textiles has emerged. E-textiles are textiles with inbuilt electrical properties. They have the advantage of the feel and comfortability of clothing while retaining electrical capabilities. The applications of E-textiles include displays, transistors, antennas, strain sensors among others [7, 8, 9, 10]. Particularly, by using E-textiles as strain sensors, human motion capture systems can be designed to be lightweight, unobtrusive and accurate. Weft knitting provides an optimal approach in creating textile strain sensors because a weft knit fabric has an elastic structure regardless of the elasticity of the yarn used in knitting the fabric [11, 12]. This enables the use of inelastic conductive yarns in creating electrical strain sensors.

1.2 Motivation and Problem Statement

The potential of weft knit strain sensors to replace conventional strain sensors in wearable devices is very promising. They can be easily integrated into the popular knit garments (e.g. gloves, sweaters, socks etc.) without being conspicuous. Particularly, they can be implemented as lightweight wearable clothing that continuously monitor the progress of rehabilitation patients. In addition, weft knit strain sensors can become invaluable in the sports science industry. Functional

clothing embedded with weft knit strain sensors can replace current motion capture devices for athletes. These clothing such as a wearable device in the form of socks can provide valuable data that can be utilised in boosting the performance of the athlete.

However, the commercial adaption of weft knit strain sensors is limited by some factors. Firstly, there is no complete framework that illustrates the design of a weft sensor, its implementation in a wearable device and the processing of its data using machine learning techniques. In addition, theoretical models that can aid the design of weft knit strain sensors are very limited. There have been interesting experimental studies on some weft knit strain sensor configurations that characterise the piezoresistivity of weft knit strain sensors but there have been very few studies that illustrate models that justify the electrical behaviour of the sensor. The few models [13, 14] that exist have significant errors between their simulation and experimental results.

In addition, drift can adversely affect the output of a piezoresistive strain sensor's output. Drift occurs when the output of the weft knit strain sensor changes independently of the sensor's extension. Although, researchers have observed the presence of drift in a weft knit strain sensor's output [15], there has been no investigation on its effect in classification applications.

Furthermore, there have been very few wearable device prototypes that have integrated weft knit sensors into conventional textile garments. The few studies that exist are limited to the design of these devices. Particularly, the use of these devices in classification applications is very rare and are restricted to classical machine learning algorithms. Moreover, no deep learning approach has been applied in classifying the data obtained from a weft knit strain sensor. Lastly, most studies on weft knit strain sensors are limited to the characterisation and application of the sensing mechanism of a specific knit architecture, thereby neglecting the potential of other knit architectures in creating optimal weft knit strain sensors.

Therefore, this research aims to develop a framework for the application of weft knit strain sensors in a human motion capture system. This framework shown in Figure 1.1 begins with the design of an electromechanical model that accurately simulates the sensing mechanism of the proposed sensor. Subsequently, the simulation of the model is validated empirically by a tensile test. The sensor

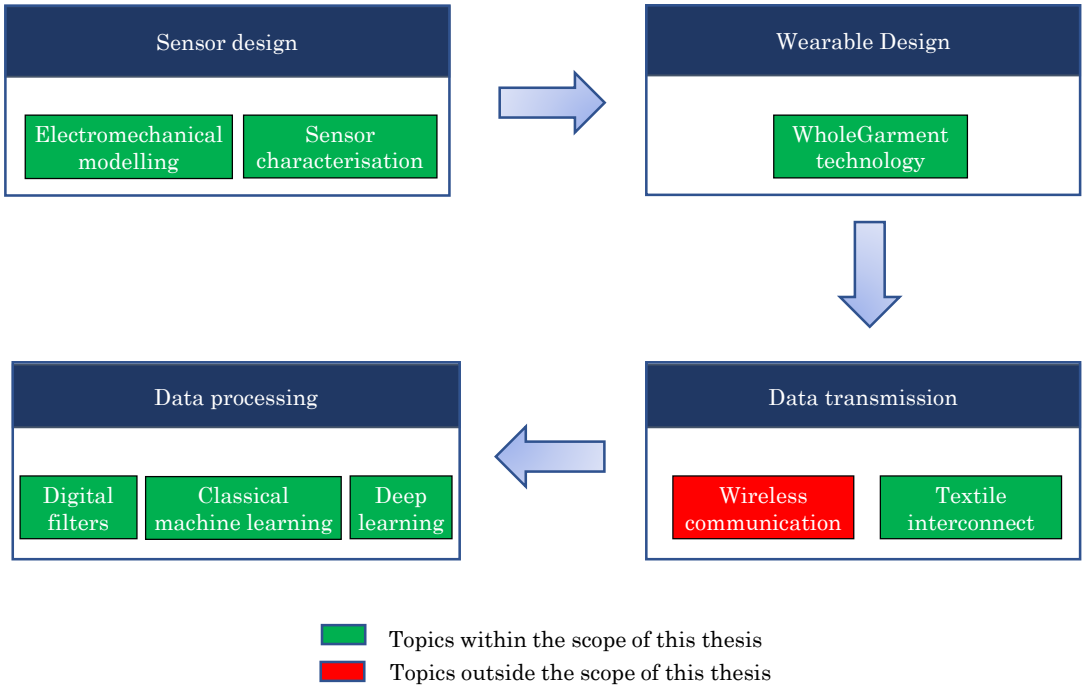

Figure 1.1: Development framework of a weft knit wearable device.

is then implemented in a wearable device and the data captured from the motion at the human joint is processed using machine learning techniques. In this study, the wearable device is a lightweight textile data glove that is optimal in weight-sensitive applications such as the progress measurements in recovering stroke and rheumatoid arthritis patients. However, this framework can be employed in the creation of other wearables that capture the motion of any joint in the human body. In addition, we present the characterisation and electromechanical models of several sensors with varying knit architectures. These architectures can help to improve the linearity of the sensor and consequently, the accuracy of the applied classifiers.

1.3 Contribution and Thesis Organisation

This thesis illustrates the results of a multi-disciplinary research that spans over several research areas. The research areas are illustrated in Figure 1.2.

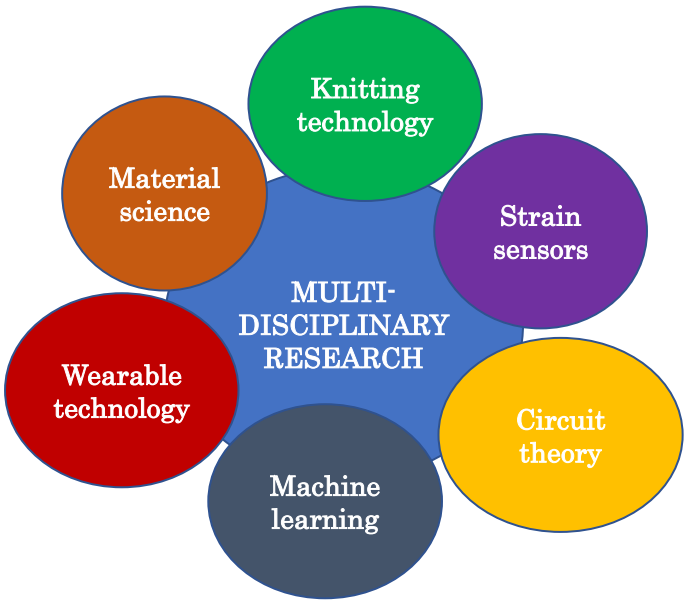

Figure 1.2: Research disciplines covered in this thesis.

In Chapter 2, the fabrication methods, sensing mechanisms and performance metrics of textile strain sensors are discussed. Thereafter, the knitting terminologies that will be encountered in this thesis are outlined. The base knitting structures are also described in this chapter. In addition, the relevant past studies on weft knit strain sensors are reviewed. In particular, the current electromechanical models of weft knit strain sensors are explored. Moreover, the effect of knitting parameters on the electrical behaviour of the sensors are reviewed. Finally, the current applications of weft knit strain sensors in human motion capture systems are explored.

In Chapter 3, a novel electromechanical model of a plain knit sensor is presented. The length resistances are derived from Postle's geometrical model [16]. An algorithm that derives the contact resistance from the equivalent resistance is developed. The simulation results are validated experimentally by fabricating sensors with the same numerical parameters used in the simulation and performing a tensile experiment on the sensors. The results show that my proposed model is more representative of the sensor's electromechanical behaviour than previous studies. Furthermore, the effect of loop and interlocking angles on piezoresistiv-

ity of the sensor are investigated in a parametric study. Under width and length jamming constraints, it is observed that changes in the interlocking angles have a bigger impact on the sensor's piezoresistivity than changes in the loop angle.

In Chapter 4, a more flexible sensor configuration that combines an elastic non-conductive yarn and an inelastic conductive yarn is presented. The model implemented in Chapter 3 is expanded to simulate this sensor's electromechanical behaviour. A tensile test was also performed on the sensors knitted with the new configuration. The simulation results illustrate a more accurate representation of the sensor's piezoresistivity observed empirically. In addition, this sensor configuration is utilised in designing a data glove that measures the flexion at the interphalangeal joints in the hand. The performance of the glove is validated in a repeatability experiment using a robotic hand. It was observed that the sensor's output was consistent, especially after a simple filter was implemented to remove the noise. Subsequently, the effect of drift on the performance of machine learning algorithms is evaluated in a data glove classification scenario. It was observed that drift reduces the accuracy of linear classifiers.

In Chapter 5, a deep learning approach in a real-world classification application with human participants is explored. Data is acquired by participants grasping objects of different shapes with the data glove. Thereafter, a convolutional neural network (CNN) is employed to classify the data and recognise the grasp type of objects grasped by the participants. Moreover, popular machine learning techniques are utilised to perform the same tasks and compare their performance to our CNN algorithm. It was observed that our CNN algorithm is more accurate than the comparative machine learning techniques.

In Chapter 6, the impact of miss and tuck stitches on the piezoresistivity of a weft knit strain sensor is explored. These stitches alter the architecture of the sensor geometrically, therefore it was imperative to understand the effect that they may have on the sensor's electrical behaviour. Several sensors having varying percentages of miss or tuck stitches are designed. The respective electromechanical models of the sensors are developed based on the model implemented in Chapters 3 and 4. The sensor configurations are also knitted using the numerical parameters in the models and undergo a tensile test. The simulation results are compared with the empirical results obtained in a tensile tests and are shown

to mostly agree. It was also observed that increases in the percentage of tuck stitches in the sensor increase the linearity of the sensor.

Chapter 7 describes the conclusions of the study and proposes ideas for further research on the use of weft knit strain sensors in HMC applications.

1.4 Publications and Awards

1.4.1 Awards and Nominations

The research in this thesis has led to the following awards and nominations:

- Digital Innovation Challenge 2019 (£2,500 award).
- University of Leeds postgraduate researcher of the year 2019 nominee.
- EPSRC Connected Nation Pioneers 2018 semi-finalist.
- Future Engineers' Leadership and Innovation Academy (Nanjing, 2018).

1.4.2 Publications

- Emmanuel Ayodele, Syed Ali Raza Zaidi, Jane Scott, Zhiqiang Zhang, Maryam Hafeez, Des McLernon,"Effect of Tuck and Miss Stitches on a Weft Knit Sensor", Sensors, 21(2), 358, 2021.
- Emmanuel Ayodele, Syed Ali Raza Zaidi, Jane Scott, Zhiqiang Zhang, Des McLernon, "A Review of Deep Learning Approaches in Glove-Based Gesture Classification" in *Machine Learning, Big Data and IoT for Medical Informatics*, P. Kumar, Ed; Elsevier, 2021 *(accepted for publication)*.
- Emmanuel Ayodele, Bao Tianzhe, Syed Ali Raza Zaidi, Jane Scott, Zhiqiang Zhang, Ali Hayajneh, Des McLernon, "Grasp Classification with Weft-knit Data Glove using Convolutional Neural Networks", IEEE Sensors Journal, 2021 *(accepted for publication)*.

- Emmanuel Ayodele, Syed Ali Raza Zaidi, Jane Scott, Zhiqiang Zhang, Ali Hayajneh, Samson Shittu and Des McLernon, "A Weft Knit Data Glove" submitted to IEEE Transactions on Instrumentation and Measurement *(revised)*.

1.4.3 Conference Presentation

- Emmanuel Ayodele, Syed Ali Raza Zaidi, Jane Scott, Zhiqiang Zhang, Qingxiang Kong, Des McLernon, "Weft Knit Smart Data Glove", 2019 IEEE International Conference on Wearable and Implantable Body Sensor Networks.

Chapter 2

Literature Review

This chapter provides a thorough review of textile strain sensors, their fabrication methods and the metrics employed in evaluating their strain sensing performances. Furthermore, we describe the various knitting structures and terminologies that are used in this study to enable a clear understanding of the thesis. Subsequently, a comprehensive review of weft knit strain sensors is presented. In particular, we describe the sensor characterisation results illustrated in past studies alongside the undertaken experimental and simulation methodologies. Finally, we conclude the chapter with the few applications of weft knit strain sensors in wearable devices.

2.1 Textile Strain Sensors

Strain sensors are devices that measure mechanical deformation by converting the changes in their electrical properties due to deformation into an output signal [17]. Strain sensors are popular for their applications in damage detection and health monitoring of civil structures [18]. However, they are also employed in monitoring the movement at different joints in the human body. Textile strain sensors are optimal for monitoring the motion at human joints because they are lightweight, stretchable and can be seamlessly integrated into clothing to create unobtrusive textile wearable devices. In this section, we review current textile sensors. In particular, we describe their fabrication techniques, sensing mechanisms and performance metrics.

2.1.1 Fabrication Techniques

Textile sensors are usually fabricated by embedding conductive nanomaterials on textile polymers. These nanomaterials include carbons (e.g carbon nanotubes (CNT) and graphene), nanowires (NWs) and nanoparticles (NPs). Their combination with flexible polymers (e.g. polydimethylsiloxane (PDMS)) creates a sensitive textile strain sensor that is human-friendly and durable. In this section, we provide a review of the various techniques in which textile sensors are manufactured with nanomaterials.

Coating

Textile strain sensors are typically fabricated by coating a textile substrate. The non-conductive textile substrate is either a fibre, yarn or fabric. The various coating techniques include chemical and vapor polymerisation approaches, spray, dip, roller and rod coating techniques [19]. Particularly, chemical polymerisation was employed in fabricating a strain sensor by coating a lycra fabric with polypyrrole (PPy) [20]. This technique involved soaking the fabric in a mixture of a monomer, an oxidant and a dopant. The fabricated sensor could detect strain up to 60%. Furthermore, a textile strain sensor that could sense strain of up to 6.2% was created by spray coating a fabric with ZnONW [21]. This coating mechanism is illustrated in Figure 2.1.

Strain sensors have also being developed by coating yarn and fibres. Notably, textile sensors were formed by coating spandex and silk fibres with graphite flakes with a Meyer rod [22]. The sensing range was 18% for spandex and 15% for silk fibres. It was also observed that the silk fibre strain sensor displayed high stability, low drift and hysteresis. Furthermore, a strain sensor was developed by coating a Polyurethane (PU) yarn in a negatively charged cellulose nanocrystals and then dipping it in a positively charged chitosan solution [23]. Subsequently, the coated yarn was placed in a PDMS matrix. The strain sensor could detect minute strains as low as 0.1% but was inaccurate for strains $> 5\%$.

In summary, coating is a simple method for fabricating textile strain sensors. However, for HMC applications, coated textile strain sensors need to be robust enough to withstand bodily fluids such as sweat that may degrade their accuracy.

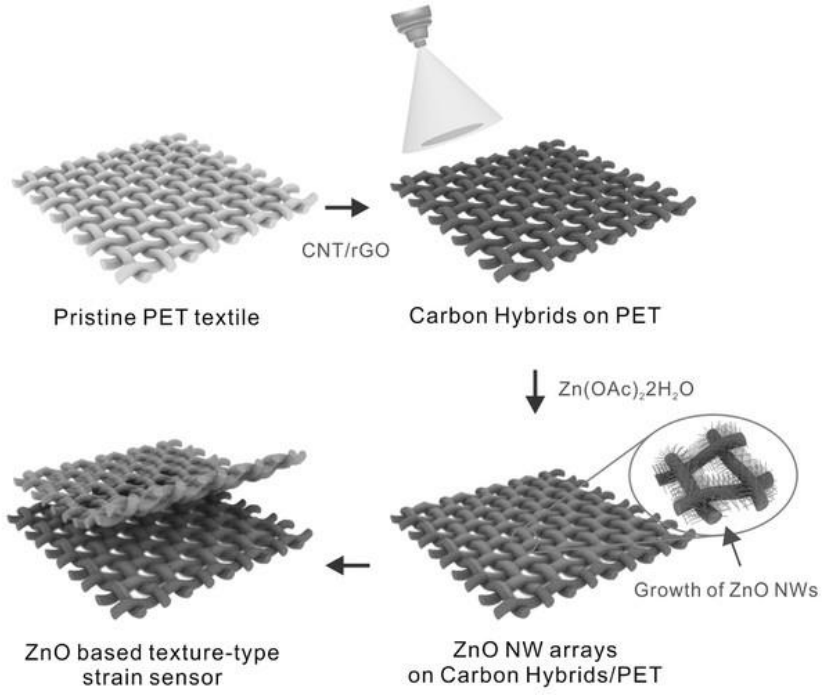

Figure 2.1: Fabrication of ZnONW coated textile strain sensor [21].

Intrinsic Conductive Textile Structures

This section reviews textile strain sensors which are made directly from conductive materials. Although fibres, yarns and fabrics of conductive materials are usually inelastic, they still display piezoresistivity within their limited elasticity. Particularly, carbon fibres were illustrated to detect strains of up to 1.2% [24]. CNT yarns measured strain of up to 3.6% and were relatively stable during the cycle test with a low hysteresis[25]. In addition, when CNT yarns were directly attached to an elastic substrate (Ecoflex substrate), they could measure strains of up to 440%, although at a lower gauge factor that pure CNT yarns. The CNT yarns were encapsulated in the Ecoflex substrate as they were dry spun due to van der Waals interactions [26].

These conductive yarns are usually created by chemical vapor deposition (CVD) [27]. CVD ensures that the conductive material can be grown in a predetermined shape and orientation. Particularly, a graphene woven textile sensor was created by growing graphene on a copper wafer that depicts the architecture

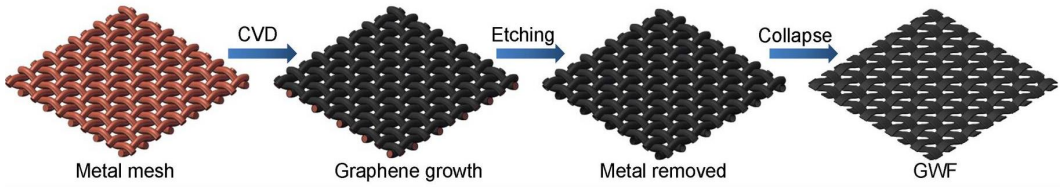

Figure 2.2: Graphen woven fabric sensor [28].

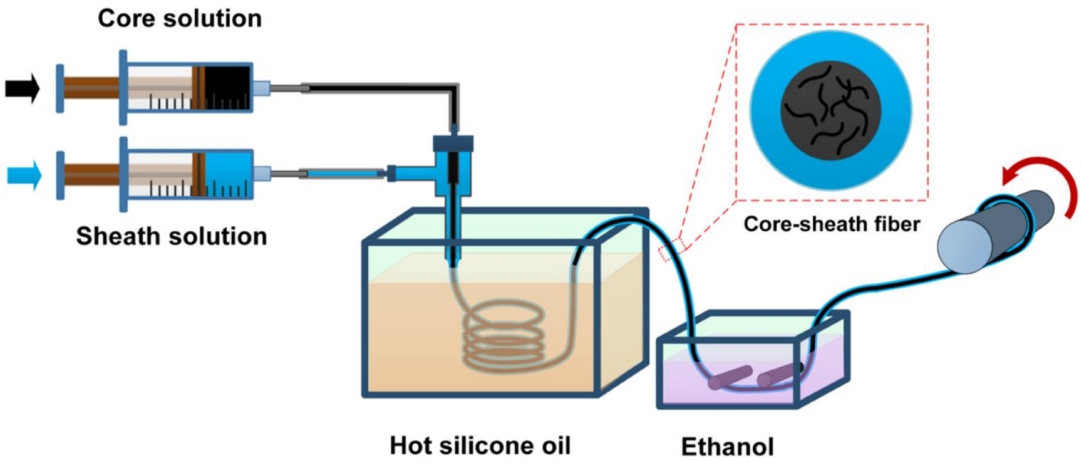

Figure 2.3: Wet-spining fabrication process for coaxial fibre sensor [29].

of a woven fabric [28]. This causes the graphene to grow in the architecture of a woven fabric. Subsequently, the metal wafer is separated from the graphene as illustrated in Figure 2.2. This graphene woven sensor could measure strains of up to 12%. However, significant hysteresis was observed during a cycle test.

Carbonisation of non-conductive textile can convert them to conductive materials. Carbonisation is the heating of a material at high temperatures in the absense of oxygen. A textile strain sensor was created by carbonising silk fabric at 950°c. The carbonised silk sensor when embedded in an Ecoflex substrate was observed to sense strain of up to 500% [30].

Coaxial Fibres

Strain sensors can also be created by employing core-shell structures. These structures comprise a conductive core wrapped by an elastic shell. It is necessary

for the conductive core to be endure high amounts of strain, therefore liquid metals, ionic liquids and elastomeric carbon composites are suitable candidates. A strain sensing coaxial fibre was developed by depositing eutectic indium-gallium-tin (EGaInSn) liquid metal into a PDMS fibre shell [31]. The strain sensor could sense strain from 0.3% to 140%. In addition, a strain sensor was developed by filling a hollow PDMS fibre with an ionic liquid (1-ethyl-3-methylimidazolium tetrafluoroborate, $EMIMBF_4$) [32]. The sensor could measure strain of up to 100% and endure extensions of 230%.

A core-shell strain sensor was also fabricated using wet spinning. Wet spinning involves depositing the sheath polymer and the conductive filler in a suitable solvent and subsequently placing the formulation in a coagulation bath. The fabrication process shown in Figure 2.3 was employed in producing an elastomeric multi-wall CNT (MWCNT) strain sensor [29]. Although, it was able to detect strain of up to 330%, a significant level of non-linearity was observed during strain tests thereby limiting its potential HMC applications.

Knitting

Textile strain sensors are also manufactured by knitting conductive yarn. It is the most preferred method for fabricating textile strain sensors because of its elastic structure. The conductive yarn could be an intrinsic multifilament comprising of conductive fibres and traditional textile fibres or a textile yarn coated with nanomaterials [13, 33]. In particular, initial studies manufactured knit strain sensors with carbon and steel fibres [14, 34]. These sensors exhibited high sensitivity but were limited to an extension of 20%. In addition, sensors knitted with carbon fibres could withstand temperatures of up to 200°C without any significant changes in its piezoresistivity. Recent studies have improved the extensibility of knitted sensors by adding elastic yarns such as Lycra or Spandex [35]. Notably, a textile sensor with extensibility of 160% was created by knitting PEDOT:PSS filaments and Spandex yarns [36]. Furthermore, several studies have shown that different knitting structures or loop configurations result in different sensing behaviours of knitted strain sensors [37, 38]. In addition, embedding knitted strain

sensors in wearable applications is more streamlined that other fabrication methods. WholeGarment^{TM} technology ensures that clothing comprising textile strain sensors can be knitted in a single manufacturing process thus eliminating the use of external attachments. The characterisation, modelling and application of knit strain sensors are further discussed in Section 2.3.

2.1.2 Sensing Mechanisms

In Section 2.1.1, we have illustrated the fabrication techniques of textile strain sensors. Therefore, it is relevant to understand the strain sensing mechanisms of these sensors. Their strain sensing mechanisms can be described as one or more of the following:

Geometrical Effect

According to Poisson's ratio, when a material is stretched in one direction, it tends to contract in the transverse direction. This geometrical effect is important in understanding the sensing mechanisms of most textile strain sensors as it differs across fibres, yarns and fabrics. In conductive yarn/fibre, the change in resistance, R, occurs as a result of the change in the length, L and cross-sectional area, A_r , provided the resistivity, ρ, of the sensor is constant as seen below:

$$R = \frac{\rho L}{A_r}. \tag{2.1}$$

Notably, this sensing mechanism was observed in a coaxial fibre as its electrical resistance was proportional to the square of its length [31]. In contrast, the geometrical effect on resistive fabrics can be more complex and comprise multiple sensing mechanisms. For knit sensors, the piezoresistivity occurs as a result of changes in the contact resistance [13, 14], however it is possible that the piezoresistivity of the fabric may be affected by geometrical changes in the conductive yarn itself.

In addition, the change in capacitance,C_a, of textile capacitive sensors that consist of two electrodes and an insulating dielectric between them is dependent on the geometrical changes of the area of the two electrodes, A_r and the distance between them (thickness of the dielectric), d_0.

$$C_a = \frac{\varepsilon_0 \varepsilon_r A_r}{d_0}, \tag{2.2}$$

where ε_0 and ε_r are the permittivity of vacuum and the relative permittivity of the dielectric constant.

Disconnection Mechanism

Some strain sensors comprise of thin conductive films of nanomaterials within rubber composites thereby creating an overlap between the nanomaterials that allows the flow of electrons in a percolation network. When these sensors are stretched, there are some disconnections in the conductive film that cause an increase in the electrical resistance. This strain sensing mechanism has been employed using nanomaterials such as graphene flakes, and PDMS composites of silver and zinc oxide nanowires (AgNWs-PDMS and ZnONWs-PDMS respectively) [39, 40, 41, 42].

Tunneling Effect

Tunneling occurs when electrons cross a thin non-conductive barrier placed between conductive nanomaterials. Although, the non-conductive barrier prevents a direct electric contact, a tunneling junction occurs because the electrons pass through the barrier. Consequently, a tunneling resistance occurs and can be calculated using Simmons' theory [43, 44]:

$$R_{tunnel} = \frac{V}{A_{cr} J} = \frac{h_{pl}^2 d_n}{A_{cr} e_c^2 \sqrt{2 m_e \lambda_{eb}}} exp\left(\frac{4\pi d_n}{h_{pl}} \sqrt{2 m_e \lambda_{eb}}\right), \tag{2.3}$$

where R_{tunnel} is the tunneling resistance, V is the electrical potential difference, A_{cr} is the tunneling junction's cross-sectional area, J is the current density, h_{pl} is the Plank's constant, d_n is the distance between the conductive nano-materials, e_c and m_e are the charge and mass of a single electron respectively and λ_{eb} is the energy barrier's height.

The tunneling effect was observed to be the main strain sensing mechanism in CNT or graphene polymer nanocomposites [45, 46]. The hexagonal honeycomb structure of CNT and graphene causes them to entangle and fold in their polymer

nanocomposites. Therefore, when strain is applied, the tunneling distance and consequently, tunneling resistance change as the graphene or CNT flakes unfold.

Crack Propagation

Strain sensors have also been developed by coating flexible substrates with nanomaterials such as CNT, gold nanowire (AuNW), silver nanoparticle (AgNP) and graphene [47, 48]. When strain is applied on these sensors, micro-cracks occur on the thin films of nanomaterials. Increased amounts of strain enlarge the cracks and causes a decrease in the electrical conduction and consequently, an increase in the electrical resistance. Furthermore, the removal of the applied strain was observed to diminish the size of the cracks as depicted in Figure 2.4 such that the electrical resistance recovered to its initial steady-state values [49].

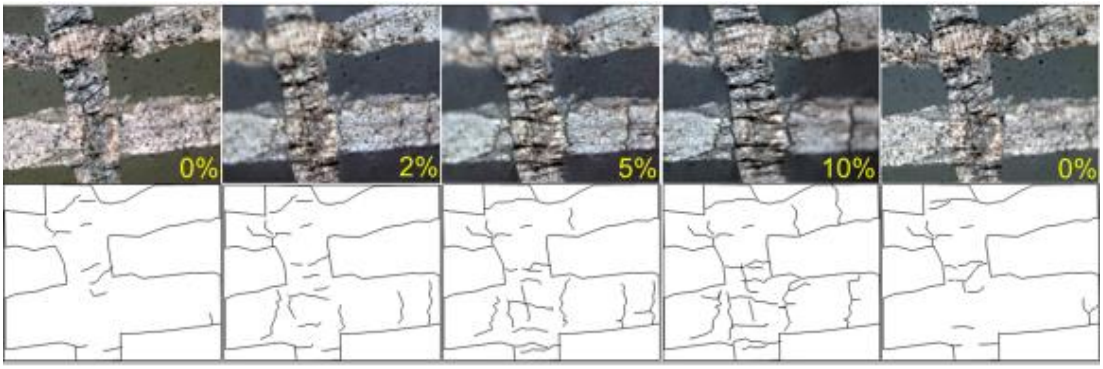

Figure 2.4: Micro-crack propagation and recovery during strain test on graphene PDMS composite [49].

2.1.3 Performance Metrics

The performance of a textile strain sensor can be evaluated by the following metrics. These metrics aid in the characterisation of the sensors and their implementation in HMC applications.

Linearity

The linearity of a strain sensor is very important because non-linearity will complicate the calibration process. The linearity is calculated by the R^2 value of a linear fit of the plot of sensor's electrical output and its mechanical deformation. A sensor with a perfect linearity will have a R^2 value of 1. However, most textile strain sensors exhibit a relatively non-linear response to applied strain. In particular, it was observed that the non-linearity of the textile sensors was a result of changes in the micro-structure or percolation network of nanomaterials [39, 50]. A trade-off relationship can be observed among the linearity, sensitivity and stretchability of a textile sensor. Capacitive textile sensors tend to display a high linearity and a low sensitivity while CNT-hybrid sensors depict low stretchabilty but high linearity and sensitivity [51].

Stretchability

HMC applications require wearable devices to endure up to 50% strain [52]. Therefore, it is imperative that sensors in wearable devices must endure high level of strain without permanent deformation. Unlike metallic strain gauges that have a maximum stretchability of 5%, a key advantage of textile strain sensors is that they can typically achieve high levels of stretchability. Notably, CNT-PDMS composites have been shown to endure strain of up to 280% while graphene-rubber composites can be extended for up to 800% strain [53].

Sensitivity

The sensitivity of strain sensors is measured by its Gauge factor (GF). The GF is calculated as:

$$GF = \frac{\Delta e_p}{e_{p0}\epsilon}, \tag{2.4}$$

where Δe_p represents the change in an electrical property (e.g. resistance or capacitance) and e_{p0} is the initial value of the electrical property. The sensitivity of textile strain sensors varies based on the sensing mechanism. Particularly, sensors whose sensing mechanism is based on crack propagation and disconnection mechanism were seen to have ultrahigh sensitivity (GF $\geq$ 1000) [43, 49]. In contrast,

capacitive sensors such as AgNW-elastomer (silver nanowires) composites exhibit a very low sensitivity because theoretically, their maximum gauge factor is 1 [51].

Hysteresis

Hysteresis occurs when there is a significant difference between the electrical property of the sensor during extension and its contraction to its initial length. For sensors fabricated with nanomaterials fillers, a feasible explanation for hysteresis is that the nanomaterials do not contract as fast as they expanded thereby causing the measured resistance/capacitance values during contraction to lag behind the measured values during extension [54].

Drift

Drift occurs when the resistance or capacitance of the sensor fluctuates at a fixed strain. It is dependent on the response time it take for the sensors to reach their steady-state value. Piezoresistive sensors have a response time of up to 332 ms while capacitive sensors have a shorter response time of <100 ms [55, 56]. The larger response time in piezoresistive sensors such as CNT-Ecoflex composites may have occurred because the flexibility of the Ecoflex does not generate enough force to rapidly restore the CNT's percolation network.

Durability

A textile strain sensor must be durable as it will undergo several strain cycles in its application. It is important that the sensor exhibits consistency in its mechanical and electrical properties after multiple cycles of tension and compression. Therefore, the durability of sensors are tested in a cyclical test, where they are extended and released several times while their electrical output and mechanical durability are measured [37].

2.2 Knitting Technology

Knitting is the manufacture of textile fabric by interlocking succeeding loops of yarn that are bound by the same yarn passing from one loop to another.

There are two major knitting methods and they are weft knitting and warp knitting. These two methods differ in their knitting direction, loop formation and fabric structure [57, 58]. Notably, in warp knitting, loops are interlocked vertically while in weft knitting, loops are interlocked horizontally. This occurs because in weft knitting, loop formation occurs at the needle bed sequentially. In contrast, loop formation in warp knitting occurs when all the needles in the needle bed are knitting simultaneously. Consequently, warp knit fabrics are more structurally stable while weft knit fabrics are more elastic [59]. Therefore, due to its elastic structure, weft knitting is the preferred method in the creation of knit sensors. The rest of this section describes the knitting terminologies, structures and operating principles that will aid in understanding the work undertaken in this thesis.

2.2.1 Knitting Terminologies

- Yarn: A yarn is an aggregation of a fibres or filaments with or without twist [60].
- Fibres: These are the raw materials that are used in the manufacture of yarns. They occur naturally (e.g.wool from animals or cotton from plants) or are manufactured artificially (e.g. polyester).
- Needle loop: A needle loop is the most popular type of knitted stitch. It consists of a head and two legs. The foot of each leg interlocks the head of the previous knitting cycle's loop. As the yarn moves from one foot of a loop into the next foot of another loop, it creates a sinker loop. For most geometrical models of a weft knit structure, the length of yarn in a sinker loop is assumed to be equal to the length of yarn in the head in an adjacent needle loop.
- Courses and Wales: A course is a horizontal row of knitted loops while a vertical column of loops is called a wale. Courses are more prominent to observe on the technical back while wales are easier to detect on the technical face.

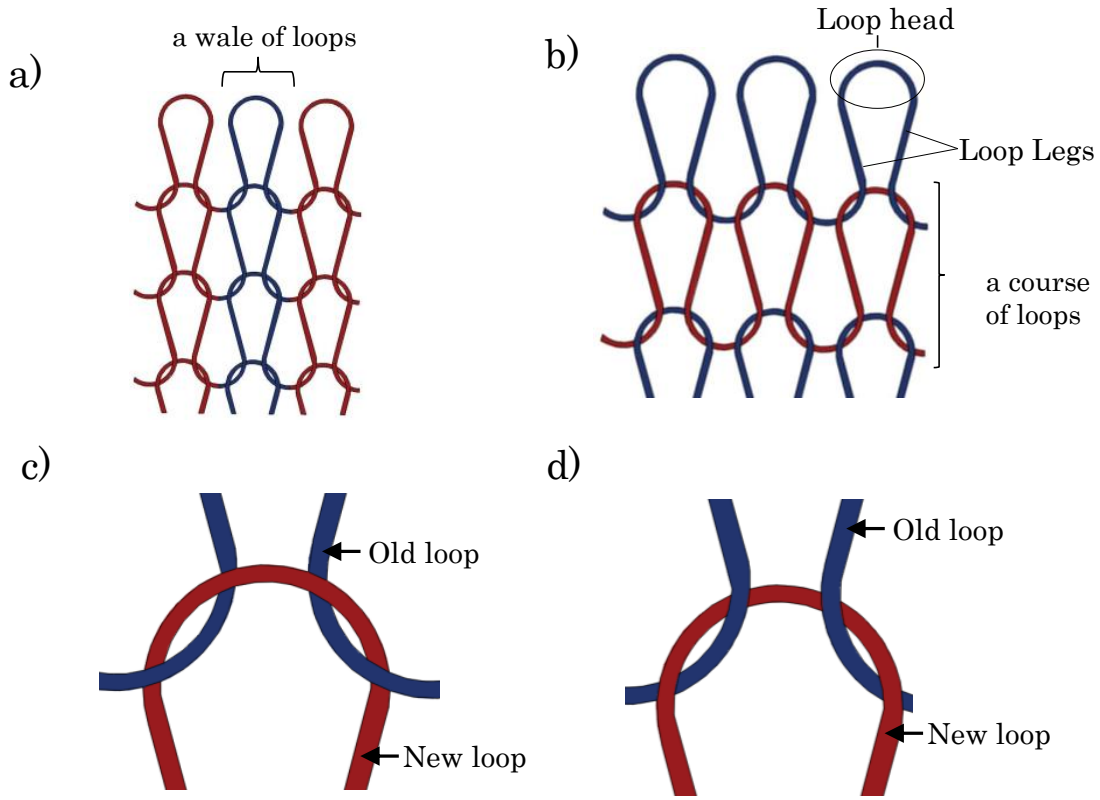

Figure 2.5: a) A wale of loops b) A course of loops c) A reverse loop d) A face loop.

- Stitch density and stitch length: Stitch density is the sum of all loops in a determined fabric area while stitch (/loop) length is the span of a yarn in a loop (including both halves of the sinker loop on each side). The stitch density, S_d, can be calculated as :

$$S_d = C_n W_n, \tag{2.5}$$

  where C_n and W_n are the number of courses and wales respectively.

- Face and and reverse loops: A face loop can be identified as the side of a stitch where loop legs appear to approach the observer as it interlocks the head of an old loop. In contrast, the reverse loop can also be identified as the side of a stitch where the loop legs appear to move away from the

observer as it interlocks an old loop's head. A face loop and a reverse loop are shown in Figure 2.5.

- Technical face and back: The technical face of a fabric illustrates the face loops while the reverse loops are shown on the technical back of the fabric.
- Linear density: The linear density of a yarn or filament is its mass per unit length. The most popular unit of measurement of a yarn's linear density is the tex system where the linear density of a yarn is represented by the weight in grams for 1 kilometre of the yarn [61]. For example, if the weight of 1 kilometre of a yarn is 50 grams, then its linear density is 50 tex or 500 dtex (decitex).
- Input tension: This is the tension on the yarn prior to loop formation. It can be mechanically controlled by the knitting machine and is known to affect the loop length of the fabric [62].

2.2.2 Base Structures

There are four base structures that form the foundation of all weft knitted fabrics [57]. These structures depicted in Figure 2.6 are formed by the changes in the arrangement of the needle bed. These base knitting structures are:

Plain knit

This is the simplest form of weft knitting and it consists of single set of needles that knit loops in the direction of its technical face. The technical face of a plain knit fabric comprise of wale loops resembling the "v" shape and its technical back consists of wales resembling semi-circles formed by the interlocking of the loops head and corresponding sinker loops. Notably, the contact points in a plain knit fabric occur between the loops along the course. Furthermore, plain knitted fabrics are known to endure strain of up to 40% even with non-elastic yarn. This illustrates the advantage of plain knit fabrics in strain sensing applications as its structure enhances elasticity with non-elastic yarns.

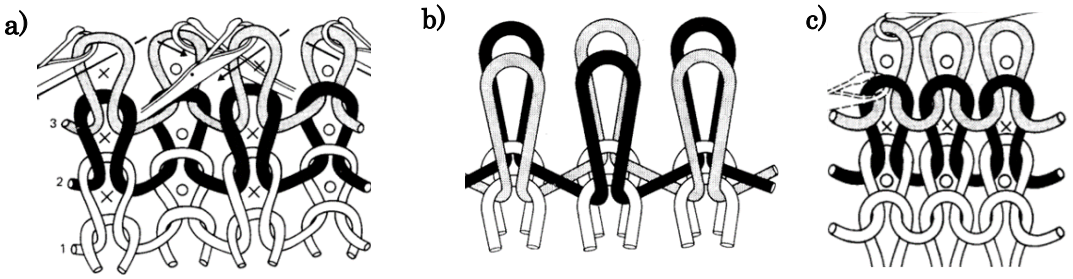

Figure 2.6: a) Technical face (same as technical back) of a 1x1 rib knit fabric b) Technical face of an interlock fabric with its hidden technical back. c) 1x1 Purl knit fabric illustrating both face and back loops on a single side. Adapted from [57].

Rib knit

A rib knit fabric is produced by using two sets of opposite-facing needles. An offset is created between each opposite facing needle to prevent collisions between the two sets of needles. The two sets of needles knit the technical face and back of the fabric. A 1x1 rib knitted fabric is the most elementary form of rib knitting and has both sides of the fabric resembling a plain knitted fabric's technical face. Theoretically, the structure of a 1x1 rib fabric causes its thickness and width to be double and half that of a plain knit fabric respectively.

Interlock knit

Similar to rib knit, interlock knit employs two sets of opposite facing needles. However, unlike in rib knit, there is no offset between the two sets of needles. Collisions are prevented by ensuring that only one set of needles operates at a time. Both sides of an interlock fabric depict the technical face of a plain fabric. Moreover, reverse meshed loops are hidden in the fabric because wales produced by opposite needles are interlocked. Consequently, interlock fabrics are thicker than rib and plain knit fabrics.

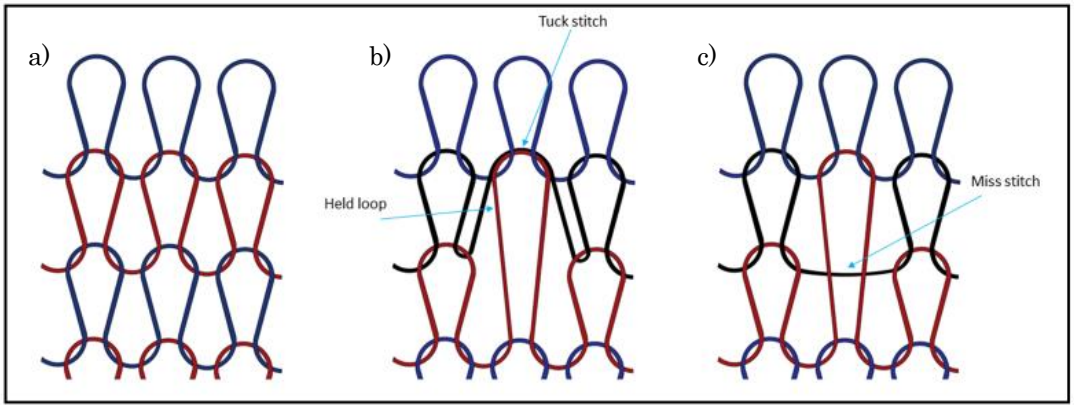

Figure 2.7: a) Knitted loop stitch b) Tuck stitch c) Miss stitch

Purl Knit

A purl fabric is the only weft knit base structure in which both face and reverse loops occur on each side of the fabric. This is achieved because loops are transferred between two sets of opposite needle beds. The simplest purl structure occurs in a 1x1 purl fabric in which a course of face loops is accompanied by a course of reverse loops. A 1x1 purl fabric is estimated to have double the elasticity wale-wise (vertically) of a plain fabric knitted with a similar stitch density and stitch length.

2.2.3 Types of Stitches

A stitch is the fundamental basic unit of a knit structure. There are three main stitches and they are knitted loop stitch, miss (/float) stitch and tuck stitch as shown in Figure 2.7. The knitted loop stitch is the most common form of knitting. It comprises of three or more interlocked needle loops. A knitted loop stitch is produced when a needle hook pulls a new loop by its loop head through a previous loop. Simultaneously, the old loops are dropped by the needles, causing the heads of the old loops to interlock the feet of the new loops [57].

In a tuck stitch, the old loops are not dropped when a new loop is added thereby causing the hook of the needle to accrue two or more loops. A miss stitch, also known as a float stitch occurs when one or more needles are skipped

during the knitting process. This causes the yarn to float over the unused needles. Consequently, miss stitches reduces the number of contact points in a fabric while tuck stitches increases the contact pressure between intermeshed loops in a fabric.

2.2.4 Geometrical Modelling of a Weft Knit Loop

In this section, we analyse the popular geometrical models of a plain knit loop that have been used in describing the electromechanical properties of weft knit strain sensors. The most relevant parameter is the knit loop length which comprises of the lengths of the loop head, loop sinker and 2 loop legs. These lengths are then used to calculate the various length resistances. The resistance of each loop leg is usually calculated as:

$$R_l = \frac{L_l \rho}{A_r}, \tag{2.6}$$

while the resistance of the loop head is calculated as:

$$R_h = \frac{L_h \rho}{A_r}, \tag{2.7}$$

where ρ and A_r are the resistivity and the cross-sectional area of the conductive yarn respectively; and L_l and L_h are the lengths of the loop leg and loop head respectively.

Usually, the length of the loop head and the loop sinkers are assumed to be equal. Therefore, the resistance of the loop sinker is calculated as:

$$R_s = R_h. \tag{2.8}$$

Peirce's loop model

This is the most popular geometrical model used in simulating the length resistances in a weft knit strain sensor. In Peirce's study [63], he proposed that the length of a knit loop could be determined based on the diameter of the yarn, d. Based on geometrical model illustrated in Figure 2.8, the succeeding calculations were made: The height between of the loop, C, also known as the course spacing was calculated as:

$$C = \sqrt{(4d)^2 - (2d)^2} = 3.46d. \tag{2.9}$$

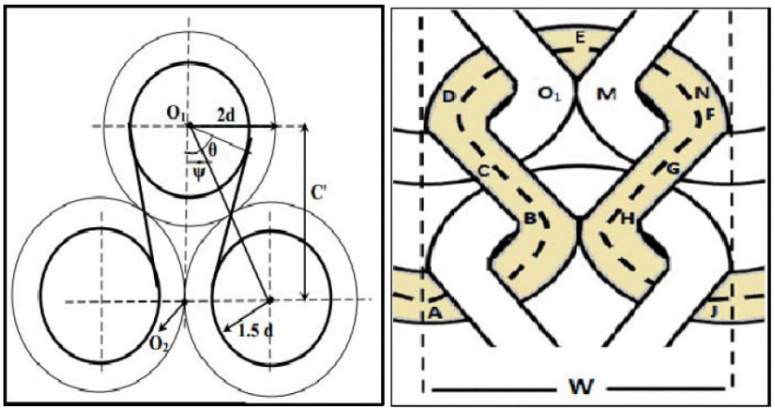

Figure 2.8: Pierce's geometrical model. (a) The yarn's central axis pathway. (b) Model of the knit loop [13].

The length of a loop leg, L_l, was then calculated using Pythagoras theorem as:

$$L_l = \sqrt{d^2 + C^2} = 3.6d. \tag{2.10}$$

Furthermore, the length of the loop head is calculated as the circumference of a semi-circle:

$$L_h = \pi r_h, \tag{2.11}$$

where r_h is the radius of the loop head and is determined as:

$$r_h = 0_1M + MN = d + 0.5d = 1.5d. \tag{2.12}$$

Kurbak's model

Kurbak's geometrical model is illustrated in Figure 2.9. Particularly, the header and the sinker are considered as elliptical curves and the legs of the loops are considered to be helical shapes that encase hypothetical elliptical cylinders parallel to the y axis [64, 65].

The length of the loop head is calculated as:

$$L_h = d(\frac{w}{2d} + d_c)(E(\pi/2, \cos^{-1} e_h), \tag{2.13}$$

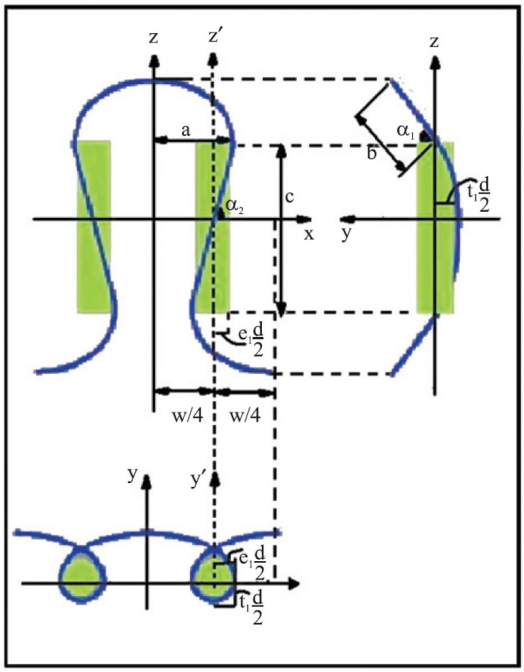

Figure 2.9: Kurbak's geometrical model of a knit loop [65].

where d_c is the diameter of the hypothetical elliptical cylinder, e_h is the eccentricity of the elliptical curve (one-half of the header) and $E(\pi/2, \cos^{-1}(e_h))$ is the complete elliptical integral of the second order.

The length of a loop leg is calculated as:

$$L_l = \left(\frac{d_2\sqrt{1+{d_2}^2} - d_1\sqrt{1+{d_1}^2} + \ln \frac{d_2+\sqrt{1+{d_2}^2}}{d_1+\sqrt{1+{d_1}^2}}}{2a_1} \right), \tag{2.14}$$

where $d_1 = \tan\alpha_1$, $d_2 = \tan\alpha_2$ and $a_1 = \frac{{d_2}^2-{d_1}^2}{2c}$. c is the course spacing, α_2 is the inclination angle of the loop leg to the x-axis and α_1 is the loop angle.

Postle's model

In postle's model [16], the length of a knit loop is determined by its interlocking and loop angles. The loop angle, α, is the angle between the loop's tangent and the y-axis at the centre locus of the loop while the interlocking angle, β, is the

angle at the interlocking locus between the loop's tangent and the y-axis. The loop leg is considered to be a bent beam while the loop head is considered to be two equal segments of a circle.

The length of each loop leg is calculated as:

$$L_l = \frac{p}{\sqrt{2(\sin\alpha + \sin\beta)}} f(k,\gamma), \tag{2.15}$$

where the p is the course spacing and $f(k,\gamma)$ is the difference between the complete and incomplete elliptical integrals. This difference was calculated as:

$$f(k,\gamma) = I(k,\frac{\pi}{2}) - I(k,\gamma), \tag{2.16}$$

where $I(k,\pi/2)$ and $I(k,\gamma)$, the complete and incomplete elliptical integrals respectively are defined as:

$$I(k,\frac{\pi}{2}) = \int_0^{\frac{\pi}{2}} \frac{d\gamma}{\sqrt{1-k^2\sin^2\gamma}}, \tag{2.17}$$

$$I(k,\gamma) = \int_0^{\gamma} \frac{d\gamma}{\sqrt{1-k^2\sin^2\gamma}}, \tag{2.18}$$

and parameters k and γ are calculated as:

$$k = \sin(\frac{\pi}{4} + \frac{\alpha}{2}), \tag{2.19}$$

$$\gamma = \sin^{-1}\left(\frac{1}{k\sqrt{2}}\left(\cos\frac{\beta}{2} - \sin\frac{\beta}{2}\right)\right). \tag{2.20}$$

The length of the loop head was calculated as:

$$L_h = \frac{p(\frac{\pi}{2} - \beta)}{2(\sin\alpha + \sin\beta)}. \tag{2.21}$$

Kawabata's model:

The loop length is calculated based on the inclination angle, and the wale and course spacings [66]. The loop length is calculated as:

$$L_l = w + \frac{2p}{\sin\theta} + \pi d, \tag{2.22}$$

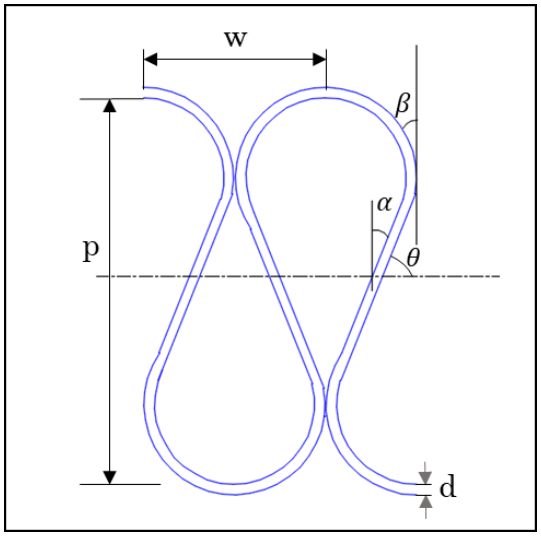

Figure 2.10: Combined knit loop model of Postle and Kawabata models.

where θ is the inclination angle of the loop on the X-axis, the wale spacing,w, is the width of a knit loop and the course spacing, p, is the height of the knit loop.

It is important to note that the length of the loop legs and heads were not specified. Therefore, in order to determine these sectional lengths, this model will have to be combined with other geometrical models [67]. Furthermore, it can be observed in the geometrical model in Figure 2.10, that the relationship between the inclination angle and the loop angle proposed in the Postle and Kawabata models can be determined as

$$\alpha + \theta = 90^{\circ}. \tag{2.23}$$

Others:

Other prominent models include Munden's [68], Leaf [69], Leaf and Gaskin [70]. The application of these models presents a fertile research area as they could provide more accurate simulations of a weft knit strain sensor's electromechanical behaviour.

2.3 Weft Knit Strain Sensors

A weft-knit strain sensor is formed by weft knitting conductive yarn. Conductive yarn can be either a textile yarn (e.g. cotton or polyester) that is coated with nanomaterials [13] or a multifilament yarn consisting of metallic and textile fibres [14, 33]. The sensing mechanism of the sensor is dependent on the contact points between the interlocked loops. Specifically, a contact resistance occurs between interlocked conductive loops. The contact resistance can be calculated using Holm's contact theory as:

$$R_c = \frac{\rho}{2}\sqrt{\frac{\pi H}{nP_r}}, \tag{2.24}$$

where R_c is the contact resistance, ρ is the electrical resistivity, H is the hardness of the material used, n is the number of contact points and P_r is the contact pressure between the conducting materials. Typically, the material hardness and the electrical resistivity are constant based on the properties of conductive yarn used, while the number of contact points is subject to the sensor's design. Therefore, the changes to the contact resistance is dependent on changes to the contact pressure between the loops.

2.3.1 Sensor Characterisation

In [14], a plain knit sensor was knitted with a stainless steel multifilament yarn. The resistance of the sensor was observed to reduce during the extension of the sensor in a strain test. Although the R^2 value was not stated, the resistance-extension relationship of the sensor was seen to be relatively linear. In addition, the resistance of the sensor was also observed to reduce exponentially as the load applied on the sensor increased. A 1x1 rib knit sensor was knitted using stainless steel fibres [71]. Results from the strain test performed on the sensors illustrated an inverse linear relationship between the sensor's extension and its resistance. The piezoresistive behaviour lasted up to extensions of $\approx 85\%$.

Plain and interlock knitted sensors were created with silver-plated yarns and stainless steel multifilament yarns [15]. Subsequently, a strain test was performed on the sensors and the average results were computed. The authors measured the strain sensing mechanism by comparing the change in resistance ($\frac{\Delta R}{R_o}$) to the strain

Configuration	**Piezoresistivity**	**Maximum sensing %**	R^2	**References**
Plain knit	Exponential (inverse)	25	N/A	[14]
Rib knit	Linear (inverse)	85	N/A	[71]
Plain knit	Linear (inverse)	20	0.731	[15]
Elastic plain knit host fabric	Linear	100	0.6652	[15]
Interlock knit	Linear (inverse)	60	0.731	[15]
Elastic interlock knit host fabric	Linear	100	0.831	[15]

Table 2.1: Characterisation of weft knit strain sensors.

of the sensor. It was observed that plain knit sensors showed an inversely linear relationship between the change in resistance and the sensor's strain between 0% and 20% strain. The average R^2 value was calculated to be 0.7847. For strain $>$ 20%, the relationship between the change in resistance and the strain was non-linear. However, no reasons were given for this non-linear piezoresistive behaviour. Furthermore, elastic plain knit sensors were fabricated by knitting single courses of conductive yarn into a host elastomeric plain knit fabric and underwent a strain test. It was observed that a linear relationship between the strain and the change in resistance was observed up to 100%. This occurred because the elastic host fabric increased contact between the heads and sinkers of the individual loops without the intermeshing of these loops. The average R^2 value was calculated to be 0.6652.

A strain test was also performed on the interlock knit sensors. It was observed that the sensors displayed an inversely linear relationship between the strain and its change in resistance up to 60%. A non-linear relationship was observed in further increases in strain. The R^2 value in the linear phase (0% - 60%) was calculated to be 0.731. In addition, five elastic interlock knit sensors were created by knitting single courses of conductive yarn into an elastomeric host interlock fabric. A strain test was performed on these sensors and their average results were calculated. It was observed that a linear relationship was observed between

the strain and the change in resistance of the sensors for up to 100% strain. Particularly, the R^2 value was calculated as 0.816. The increase in the percentage of strain in the linear phase of the interlock knit sensors as compared to the plain knit sensors was deduced to occur as a result of the increase in binding regions in the interlock structure. Based on the R^2 value and the range of the linear phase, the elastic interlock knit sensor was selected as the optimal sensor configuration.

2.3.2 Electrical Modelling

Zhang's Model

The pioneering electrical modelling of a weft knit strain sensor was proposed by Zhang et al. [14]. The authors postulated that a plain knit sensor can be modelled as a resistive circuit because of the contact resistances between intermeshed loops and the length resistance of the yarn itself. The length resistances were categorised into resistances of the loop legs, R_l, and resistances of the loop heads, R_h. The stitch length of a loop head was assumed to be equal to the stitch length of a sinker loop. Therefore, R_h was also used in modelling the resistance of the sinker loop. In a simplified model, the length resistances were assumed to be negligible to the contact resistances and were eliminated.

The simplified model of a single conductive loop is illustrated in Figure 2.11b. V and i_1 - i_3 represent the voltage and hypothetical currents in the circuit respectively. By employing Kirchoff and ohm's laws, the matrix expression was derived as:

$$\mathbf{v} = \mathbf{iR}, \tag{2.25}$$

where

$$\mathbf{i} = [i_1, i_2, i_3]^T, \tag{2.26}$$

$$\mathbf{v} = [0, 0, V]^T, \tag{2.27}$$

and

$$\mathbf{R} = \begin{bmatrix} R_{1,2} + R_{2,1} + R_{1,1} & -R_{2,1} & -R_{1,1} \\ -R_{2,1} & -(R_{2,1} + R_{3,2} + R_{3,1}) & -R_{3,1} \\ -R_{1,1} & -R_{3,1} & R_{1,1} + R_{3,1} \end{bmatrix}. \tag{2.28}$$

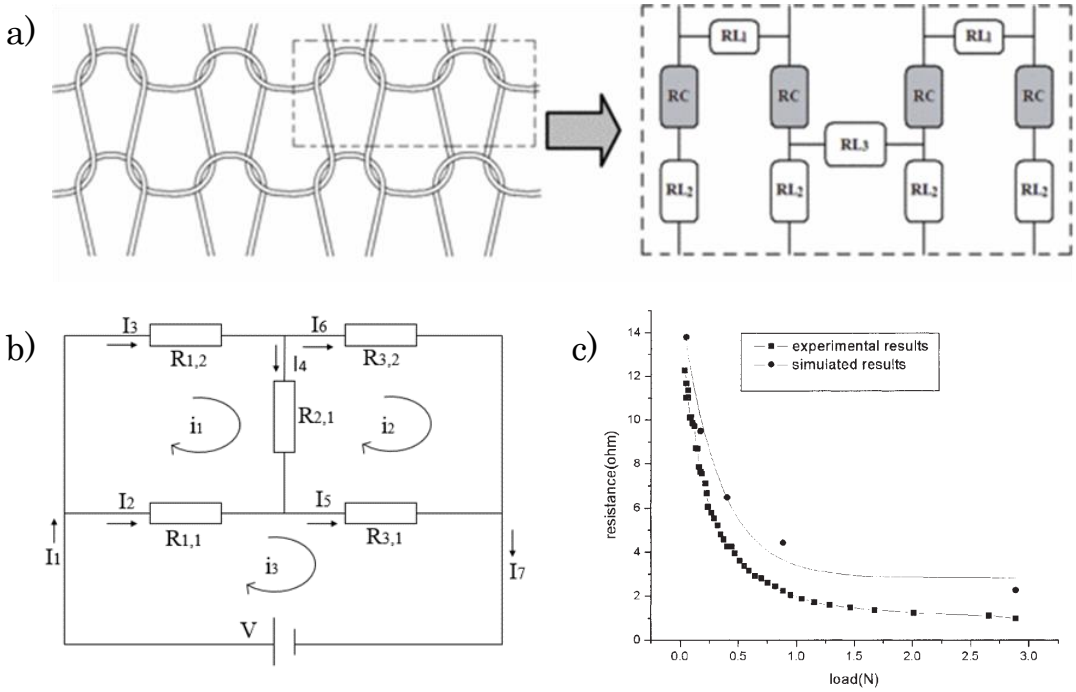

Figure 2.11: a) Electromechanical model of a weft knit strain sensor. b) Resistive model of a single knit loop. c) Simulation and experimental model of strain test. Adapted from [14].

However, the conductive sensor is modelled as a uniform conductive body. Therefore, all contact resistances are equal across the sensor. Consequently, the circuit was modelled as:

$$\begin{bmatrix} 0 \\ 0 \\ V \end{bmatrix} = \begin{bmatrix} 3R_c & -R_c & -R_c \\ -R_c & -3R_c & -R_c \\ -R_c & -R_c & 2R_c \end{bmatrix} \begin{bmatrix} i_1 \\ i_2 \\ i_3 \end{bmatrix}, \tag{2.29}$$

and the equivalent resistance, R_{eq}, was calculated as

$$R_{eq} = \frac{V}{i_3}. \tag{2.30}$$

The contact resistance, R_c, was derived empirically from the contact force, F_n, as:

$$R_c = 4.14 + 7.59 \exp^{-\frac{F_n}{0.0679}}. \tag{2.31}$$

As shown in Figure 2.11c, the simulated result depicted a similar slope to the experimental result but there was a significant distance between the two curves.

Moreover, the percentage error rate was not specified. However, using a graph-to-data software and Matlab, the percentage error between the simulated and experimental results was calculated to be $\approx 26.47\%$. Furthermore, this study postulated that the relationship between the contact resistance, R_c, and the total resistance, R_{eq} of the sensor can be derived as:

$$R_{eq} = R_c \cdot C_v, \tag{2.32}$$

where C_v is a coefficient that varies based on the design of the sensor.

Wang's Model

Another electrical model of a plain knit sensor was proffered by Wang et al. [67]. This model was based on only the length resistance of the conductive loops. Particularly, the contact resistances were neglected to reduce the computation time of the model. This study was purely theoretical and there was no experimental validation.

In Figure 2.12, a sensor comprising of 2 courses and 1 wale was modelled utilising only the length resistances. Kirchoff laws and Ohm's laws were employed in analysing the circuit. The equations below represent the outcome of the circuit analysis:

$$\mathbf{v} = \mathbf{iR}, \tag{2.33}$$

where,

$$\mathbf{i} = [I_1, I_2, I_3, I_4]^T, \tag{2.34}$$

$$\mathbf{v} = [V, 0, 0, 0]^T, \tag{2.35}$$

and

$$\mathbf{R} = \begin{bmatrix} 2(R_h + R_l) & -(0.5R_h + R_l) & -(0.5R_h + R_l) & -R_h \\ -(0.5R_h + R_l) & R_h + R_l & 0 & 0 \\ -(0.5R_h + R_l) & 0 & R_h + R_l & 0 \\ -R_h & 0 & 0 & 2(R_h + R_l) \end{bmatrix}. \tag{2.36}$$

The equivalent resistance was calculated as:

$$R_{eq} = \frac{V}{I_1}. \tag{2.37}$$

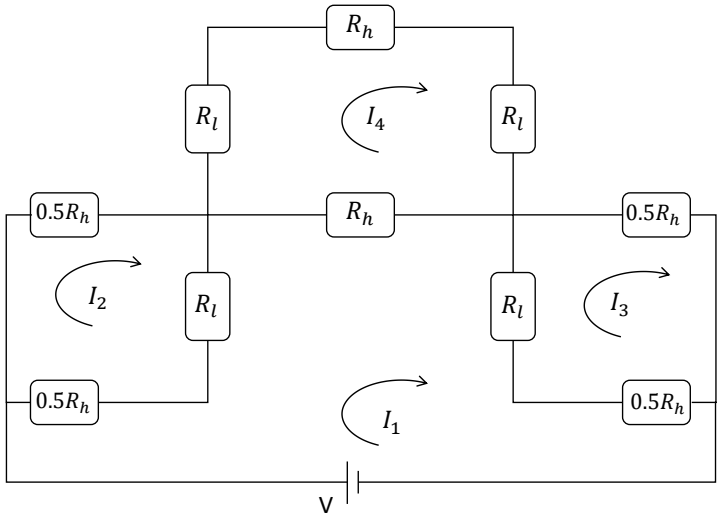

Figure 2.12: Resistive model of a weft knit strain sensor comprising of 2 courses and 1 wale. [67]

Using Matlab, the equivalent resistance was derived as:

$$R_{eq} = \frac{R_h(R_h + 2R_l)}{R_h + R_l}. \tag{2.38}$$

The resistance of the loop head, R_h, and resistance of the loop leg, were derived using Peirce's and Kawabata's models as:

$$R_h = \frac{\rho\pi w(1+\epsilon)}{4}, \tag{2.39}$$

and

$$R_l = \frac{\rho[2l - \pi w(1+\epsilon)]}{4}, \tag{2.40}$$

where w is the width of a knit loop and ρ is the resistivity of the conductive yarn.

Furthermore, this model was implemented in a parametric study [72]. A computer program was developed to simulate the theoretical model. The equivalent resistance was determined directly from the sensor's knitting parameters using the program. The simulation results generally agreed with the experimental results and validated the accuracy of the model.

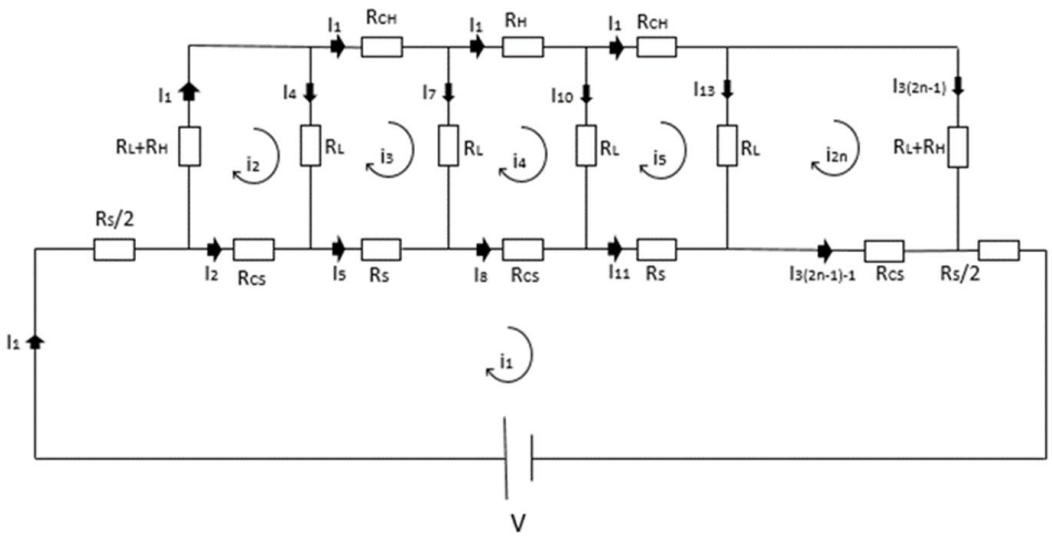

Figure 2.13: Resistive model for an interlock knit sensor [13].

Atalay's model

Atalay et al. [13] proposed an electrical model for an interlock knit fabric implemented in a heart rate monitoring system. Notably, the contact resistances and length resistances were depicted in this model as shown in Figure 2.13. However, the author postulates that the contact pressure at the head of the loops differs from the contact pressure at the sinker loop. This was as a result of experimental observation on microscopic images on the knit sensor during a tensile test as illustrated in Figure 2.14a. Particularly, the conductive loops at the header were observed to separate completely at 20% strain while the conductive loops at the sinker loop were observed to separate completely at 55% strain. This observation has only been recorded in the study while every other study assumes that the conductive pressure is uniform across the sensor. Perhaps, this was as a result of the structure used, as Atalay et al.'s study is the only study that has used the interlock structure.

Similar to Zhang's and Wang's models, Kirchoff's and Ohm's laws were employed in analysing the circuit. For a sensor of 8 courses and 21 wales, the matrix expression was derived from the circuit analysis:

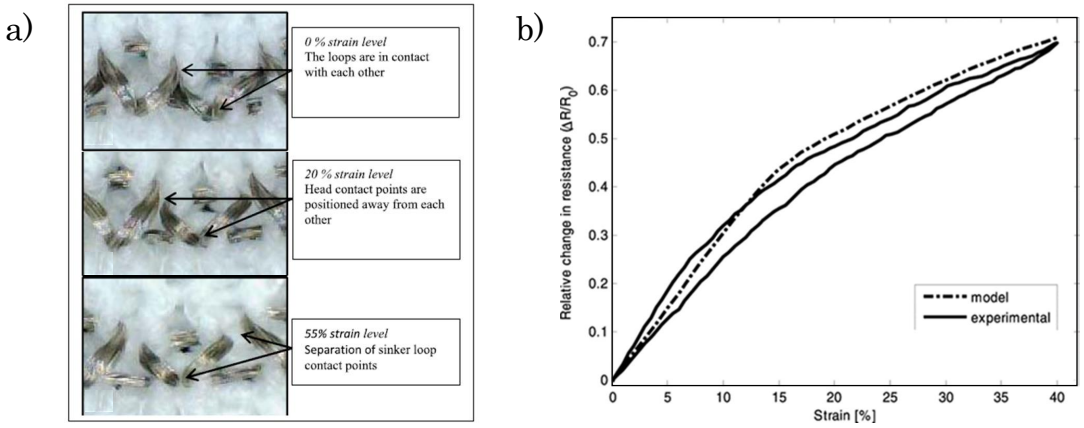

Figure 2.14: a) Contact between interlocked loops during tensile test. b) Simulation and experimental results of tensile test. Adapted from [13].

$$\begin{bmatrix} V \\ 0 \\ 0 \\ 0 \\ \dots \\ 0 \end{bmatrix} = \begin{bmatrix} R_s & R_{cs} & 0 & 0 & R_s & 0 & \dots & 0 \\ 0 & -R_{cs} & R_h + R_l & R_l & 0 & 0 & \dots & 0 \\ 0 & 0 & 0 & -R_l & -R_s & R_{ch} & \dots & 0 \\ 0 & 0 & 0 & 0 & 0 & 0 & \dots & 0 \\ \dots & \dots & \dots & \dots & \dots & \dots & \dots & \dots \\ 0 & 0 & 0 & 0 & 0 & 0 & \dots & R_h + R_l \end{bmatrix} \begin{bmatrix} i_1 \\ i_2 \\ i_3 \\ i_4 \\ \dots \\ i_{21} \end{bmatrix}, \tag{2.41}$$

where R_{ch} and R_{cs} are the contact resistances of the loop head and sinker respectively. R_s,R_h and R_l are the length resistances of the sinker, head and legs of the knit loop.

The equivalent resistance of the sensor was derived as:

$$R_{eq} = \frac{V}{i_1}. \tag{2.42}$$

The length resistances were calculated using Postle's model. Therefore:

$$R_h = R_s = \rho L_o(1+\epsilon), \tag{2.43}$$

$$R_l = \rho \frac{l_f - 2L_o(1+\epsilon)}{2}, \tag{2.44}$$

where l_f and L_o are the length of the knit loop and the steady-state length of the loop head.

Although, the paper explains that the contact resistance occurs as a result of Holm's contact theory, the parameters used in simulating the contact resistance are vaguely explained. Furthermore, the percentage error was not reported but it can be observed in Figure 2.14b that the simulation and experimental results generally agree.

2.3.3 Effect of Knitting Parameters

Effect of Mechanical preconditioning:

Christina et al. [33] studied the impact of preconditioning on the piezoresistivity of the sensor. In this study, 4 samples of sensors with knitted with 3 samples having less than 50% combination of miss and tuck stitches and the last sample having only knit loop stitches. The last sample served as the control sample. These samples were preconditioned by performing 250 stretch-recovery cycles to 16% extension along its course direction. This experiment was repeated at different elongation rates of $9.6mm/s$ and $12mm/s$, and at different currents. It was observed that the peak-to-peak span of the sensor's resistance increased rapidly in the first few cycles till it got to its maximum value and then reduced till it got to a settling time after which its peak-to-peak span was relatively constant. This experiment was repeated after a rest interval. It was observed that mechanical preconditioning, reduced the maximum peak-to-peak span and also the settling time of each sensor. Figure 2.15 illustrates the experimental results for one of the samples. It can be observed that after the preconditioning that occurred in the first session, the settling time for the second session, T_{s2}, is far lower than the settling time for the first first session, T_{s1}.

Effect of elastomeric yarn input tension

In [37], the effect of elastomeric yarn input tension was studied. The weft knit strain sensors were knitted by embedding a course of conductive yarn in a host fabric knitted in an interlock structure with an elastomeric yarn. Sensors were knitted with the same yarns and number of course and wales. However, the input tension of the elastomeric yarn was varied to observe its effect on the

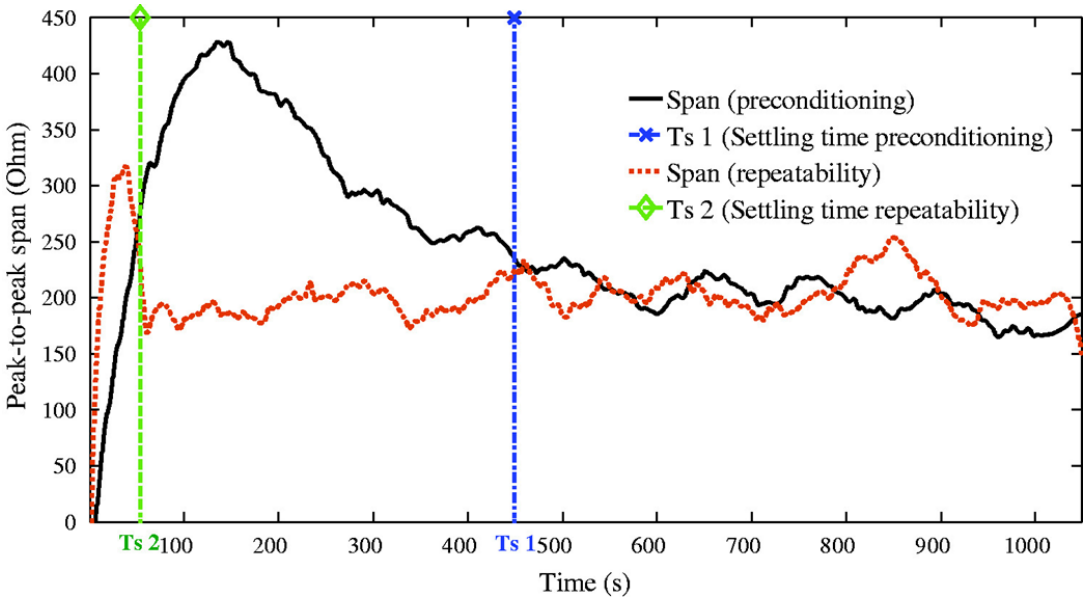

Figure 2.15: Impact of mechanical preconditioning on a weft knit strain sensor [33]

sensor's electrical behaviour. It was observed that the steady-state resistance of the sample group with the higher input tension of the elastomeric yarn was lower than the sample group with a lower input tension. This occurred because the higher input tension of the elastomeric yarn increased pressure at the contact points in the sensor. Consequently, in accordance with Holm's contact theory [73], the contact resistance reduces due to the increased contact pressure which then reduces the equivalent resistance of the sensor. In addition, it was observed that the gauge factor and the R^2 values, which are indicators of the accuracy of the sensor for linear strain measurements were higher in the sample of sensors with the higher elastomeric yarn input tension.

Effect of elastomeric yarn type

In order to observe the effect of elastomeric type, different sensors were fabricated with elastomeric yarns of varying densities. The sensors were also created by embedding a course of conductive yarn in a host fabric knitted in an interlock structure with an elastomeric yarn. All other parameters such as the input

tension of the elastomeric yarn and the number of courses and wales were kept constant so that only the impact of the different elastomeric yarns would be observed [38]. Subsequently, the sensors were stretched to 40% strain during the strain test. It was observed that sensors whose elastomeric yarn had the highest densities produced the highest R^2 values. Furthermore, the results showed that the increases in the linear density of the elastomeric yarn caused an increase in the gauge factor of the sensor. These phenomenon occurred because of the increased thickness of the elastomeric yarn. From these results, we can summarise that an increase in the contact pressure at the contact points, regardless of whether it is caused by an increase in the density or the input tension of the elastomeric yarn leads to a more linear sensor. It is likely that this phenomenon occurs because a larger starting contact area leads to a longer period for contact between conductive loops to exist during extension. During the period where contact occurs the resistance of the sensor is relatively linear to its extension. Therefore, a lower starting contact area or pressure will lead to a lower linear phase of extension and thus a lower linearity of the sensor.

Effect of conductive yarn input tension

Weft knit strain sensors were fabricated using the same methodology in previous sections by embedding a course of conductive yarn in a host fabric. The host fabric was knitted in an interlock structure with an elastomeric yarn. The input tension of the conductive yarn was varied among the sensors while other knitting parameters were kept constant [38]. Contrary to the effect of elastomeric yarn input tension, increases in the conductive yarn input tension resulted in an increase in the initial electrical resistance of the sensor. This occurred as a result of the interlock structure used in the sensor. Particularly, the increase in the input tension of the conductive yarn led to a lower stitch length used in the interlock structure. Consequently, this led to a lower contact pressure at the contact points and therefore a higher contact resistance and equivalent resistance of the sensor. However, the higher input tension led to a reduced gauge factor and R^2. This confirms our observation that a lower contact pressure/area leads to lower gauge factor and R^2 value which are representatives of the sensor's accuracy.

Effect of number of courses and wales

The effect of changes in the number of courses and wales on a weft knit strain sensor was investigated by Li et al. [74]. Weft knit strain sensors were fabricated with varying amount of wales and courses. The results of the study showed that for a sensor comprising of a small number of wales and a large number of courses, increases in the number of of wales led to a decrease in the sensor's resistances and increases in the number of courses led to an increase in the sensor's resistance. In contrast, for sensors consisting of a small number of courses and a large number of wales, increases in the number of courses caused a decrease in the resistance of the sensor while increases in the number of wales cause an increase in the sensor's resistance. The reason for this phenomena was not explained in this study as the authors were more concerned about producing an accurate electromechanical model. However, this phenomena demonstrates the impact of asymmetry on the resistance of the sensor as an increase in its asymmetry caused an increase in its resistance while a decrease in its asymmetry caused a decrease in its resistance.

The effect of changes in number of wales and course was also illustrated in [72]. It was observed that at each percentage of strain, increases in the number of courses caused a decrease in the electrical resistance while increases in the number of wales caused an increase in the electrical resistance.

2.3.4 Applications

Although, the use of weft knit strain sensors in HMC applications is nascent, this section provides a comprehensive review of the few HMC applications utilising weft knit strain sensors. In particular, Atalay et al. employed an interlock knit sensor in creating a respiration monitoring system [13]. This system was a belt that was to be worn on the abdomen (belly). Breathing was measured by the strain on the knit sensor caused by the expansion and contraction of the abdomen. Fast fourier transform (FFT) analysis was used to classify data obtained during various activities such as walking, running, sitting and standing.

A wireless knee sleeve was fabricated by knitting PU/PEDOT:PSS fibres which were created in a wet spinning process [36]. The knee sleeve was used

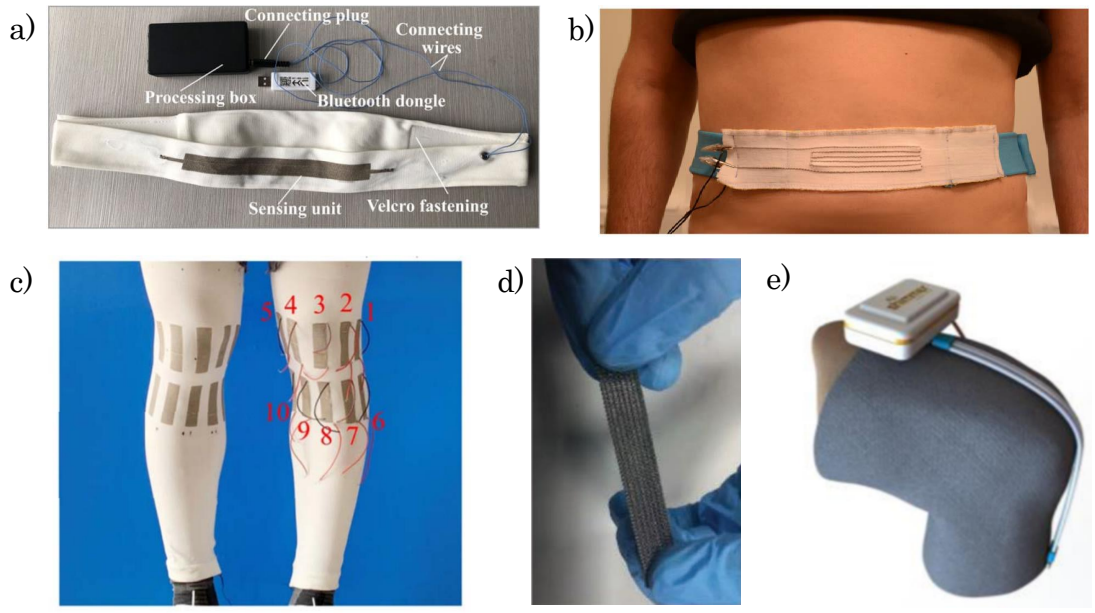

Figure 2.16: Human motion sensing applications using weft knit strain sensors. a) Respiration monitoring band with rib knit sensor [75]. b) Respiration monitoring belt with interlock knit sensor [13]. c) Running tights with embedded weft knit strain sensor [76]. d) Multi-use sensing band [77]. e) Wireless knee sleeve [36].

to monitor movements at the knee joint during rehabilitation activites. The collected data was transfered to a PC for further processing using a Shimmer wireless sensor. Furthermore, a graphene-coated knitted band was created for multiple sensing applications [77]. It consisted of a knitted polyester fabric coated with graphene. The sensing band was employed in detecting motion in different parts of the body including at the throat, finger, wrist and cheeks.

A knee sensing sleeve was manufactured by integrating weft knit strain sensors into running tights [76]. The weft knit strain sensors were knitted using silver-plated conductive yarn and a elastic spandex yarn. The sensing system was employed to detect the activities performed by the user and classify them into running, walking, descending steps and climbing. In addition, another classification scenario was implemented to recognise whether the user was walking, sitting or squatting. The gait motion recognition method was based on the decision tree algorithm and it utilised the maximum, variance, median and average

resistances as selected features.

Furthermore, a 1x1 rib knit sensor was implemented in a respiration sensing belt [75]. The respiration data obtained from the belt was used in detecting the standing, sitting and reading posture of the 20 participants. Subsequently, the authors examined the effect of participant's weight, height, gender and ethnicity on the respiration rate (RR) and cycle (RC). Although, the implementation of a rib knit sensor in this wearable was interesting, the results of the experiments are speculative. Particularly, Asian male participants were observed to have higher respiration indices than the African male participants while African female participants were observed to have higher respiration values than their Asian female counterparts.

2.4 Chapter Summary

2.4.1 Research Gaps in Textile Strain Sensors

Although research in textile strain sensors is very promising, most studies have focused on the nanomaterials used to fabricate these sensors. In particular, the various textiles structures such as knitting and weaving have been largely neglected. Most studies have only focused on the elasticity of the structures and have neglected the impact of these structures on the piezoresistivity of the sensors. Therefore, investigating the impact of the textile structures on the sensors creates a novel research gap as there are several textile structures already employed in traditional textile applications that can be used in creating a strain sensor. Moreover, the electromechanical behaviour of textile strain sensors is poorly understood. Current studies are limited to the behaviour of the metallic materials in the sensor. Therefore, investigating the electromechanical model of the sensor in terms of the textile structure presents a novel research gap. Geometrical models of these structures can be adapted to accurately simulate the piezoresistivity of the sensors.

In addition, textile sensors are known to have high elasticity, but they also tend to have a low linearity, a high hysteresis and a high drift. Therefore, designing a sensor configuration that has a high linearity, a low hysteresis and low drift

while still maintaining the high elasticity will increase its performance in HMC applications. Furthermore, the use of machine learning to classify the output of textile sensors is underutilised. Machine learning algorithms may still accurately classify the output of the sensors in spite of the drift and hysteresis. In particular, the use of machine learning in the classification of the output of textile sensors can aid the adoption of textile strain sensors in HMC applications.

Finally, there are very few HMC applications that comprise of textile strain sensors. Although, textile sensors have the potential to disrupt wearable technology because of their inherent advantages, there are very few studies to illustrate this potential in HMC applications. Therefore, a research framework is needed to illustrate the incorporation of textile sensors in a wearable device.

2.4.2 Conclusion

In this chapter, a comprehensive review of textile strain sensors has been provided. Thereafter, knitting terminologies were described to aid the understanding of this thesis. Furthermore, an exhaustive overview of research on weft knit strain sensors was presented. All relevant studies on the characterisation, modelling, simulation and application of weft knit strain sensors were discussed in this chapter.

Chapter 3

Electromechanical Model of a Weft Knit Strain Sensor: Influence of Loop and Interlocking Angles.

In this chapter, a novel electromechanical model of a weft knit strain sensor is proposed. This model comprises of length resistances derived by Postle's geometrical model and contact resistances derived from the equivalent resistance. The accuracy of this model is validated experimentally. In addition, a parametric study is simulated to investigate the effect of changes in the interlocking and loop angles on the piezoresistivity of the sensor.

3.1 Introduction

Research into the use of weft knitting to create textile sensors has rapidly advanced due to their potential to create wearable devices (wearables) which are wholly textile [78]. Additionally, these wearables are less obtrusive than conventional alternatives and have a higher chance of commercial adoption especially in motion capture applications. Particularly, they can serve as a more comfortable and less intrusive progress monitor and an input device for AR/VR rehabilitation exercises.

Although the potential applications of weft knit strain sensors in wearables are remarkable, most studies are purely experimental and do not provide enough theoretical background that may guide design choices in applications. However, there are a few studies that have presented a theoretical analysis of the electromechanical properties of weft knit strain sensors. In particular, Zhang et al. [14] proposed a model based on the hexagon model derived by Wu et al. [79] to simulate the electromechanical properties of a weft knit fabric made from conductive yarn. Furthermore, the model was based on a plain knit, a base structure of weft knit and the conductive yarn was modelled as a perfect intrinsic conductor. However, the model attempted to simulate the relationship between the resistance of the fabric and the load applied but neglected to justify the relationship between the fabrics resistance and its extension. Moreover, the model overlooks the effect of length resistances (i.e. resistances of the heads and legs of the loops) on the total resistance of the fabric.

Additionally, Wang et al. [67] proffered a hexagon electromechanical model of a weft knit strain sensor created from conductive yarn. The total loop length was calculated using the Kawabata model [66], while the Peirce loop model [80] was used to determine the length of the head and legs of the loop. In a subsequent study [72], an optimised model was developed by simulating the tensions in the legs and heads of the loops using Popper model [81] to determine the force applied on the sensor. However, both studies only modelled the resistance of the sensor on the length resistances and failed to consider the contact resistance between the conductive loops.

Conversely, Atalay et al. [13] postulated the electromechanical model of a weft knit strain sensor which was based on the interlock knit, another base structure of weft knitting. Furthermore, this model simulated both the contact resistances and the length resistances. The length resistances were also calculated with Peirce's model.

Although, the various electromechanical models used in these studies provide a reasonable accurate simulation of the sensor's piezoresistivity, they do not illustrate how knitting parameters might affect the sensor's resistive behaviour.

In contrast, there are experimental studies that have investigated how knitting parameters affect the sensor's piezoresistivity. Particularly, Atalay et al. [37]

[38] investigated the effect of the input tension and the linear density of the elastomeric yarn, and the input tension of the conductive yarn. It was observed that increasing the input tension of the elastomeric yarn decreased the electrical resistance of the sensor while increasing the input tension of the conductive yarn increased the electrical resistance of the sensor. Furthermore, increasing the linear density of the conductive yarn decreased the electrical resistance of the sensor. These phenomena occurred because the input tension and linear density affected the contact pressure between the interlocking loops. Additionally, the effect of mechanical preconditioning was investigated in [33]. It was observed that preconditioning reduced the peak-to-peak span of the sensor's resistance till it reached a stabilised value. These studies although yielding interesting results do not provide a theoretical model to analyse the cause of these effects.

It is clear that in order to design a weft knit strain sensor, a concise analysis of how knitting geometrical parameters affect the sensor's resistive behaviour must be understood. In this chapter, an electromechanical model of the sensor's behaviour is proposed using two major knitting parameters, the loop and interlocking angles. The accuracy of this model is verified experimentally. Furthermore, a parametric study of the impact of loop and interlocking angles on the sensor's piezoresistivity is performed.

3.2 Methodology

3.2.1 Electromechanical Model of a Weft Knit Strain Sensor

The electromechanical model of a weft knit strain sensor can be best described by a resistive hexagonal model illustrated in Figure 3.1. This model comprises of the length resistances and the contact resistances. The loop resistances are the resistances across the loop head and loop leg which are represented by R_h and R_l respectively while the contact resistance, R_c, is the resistance between the interlocking loops. Additionally, the basic assumptions in this model are:

1. Perfect contact occurs between interlocking loops.

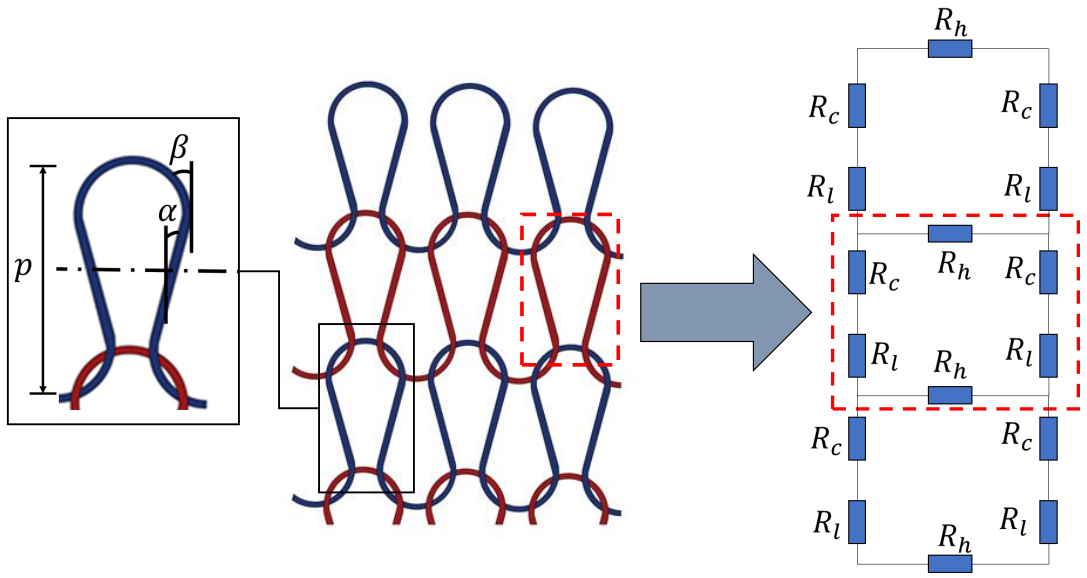

Figure 3.1: Geometrical model and Equivalent Resistive Model of a Weft Knit Strain Sensor. α is the loop angle, β is the interlocking angle and p is the course spacing.

2. All respective lengths of the loop heads and loop legs are equal throughout the sensor.

The resistive model of a weft knit strain sensor with three wales and three courses is illustrated in in Figure 3.2. A circuit analysis is shown below to depict how the equivalent resistance is calculated.

I_n represents the hypothetical currents in n mesh of the circuit. Using Kirchoff's voltage law and Ohm's law, the hypothetical currents are calculated as:

$$\mathbf{i} = \mathbf{R}^{-1}\mathbf{v}, \tag{3.1}$$

where

$$\mathbf{i} = \begin{bmatrix} I_1 \\ I_2 \\ \dots \\ I_{14} \end{bmatrix}, \tag{3.2}$$

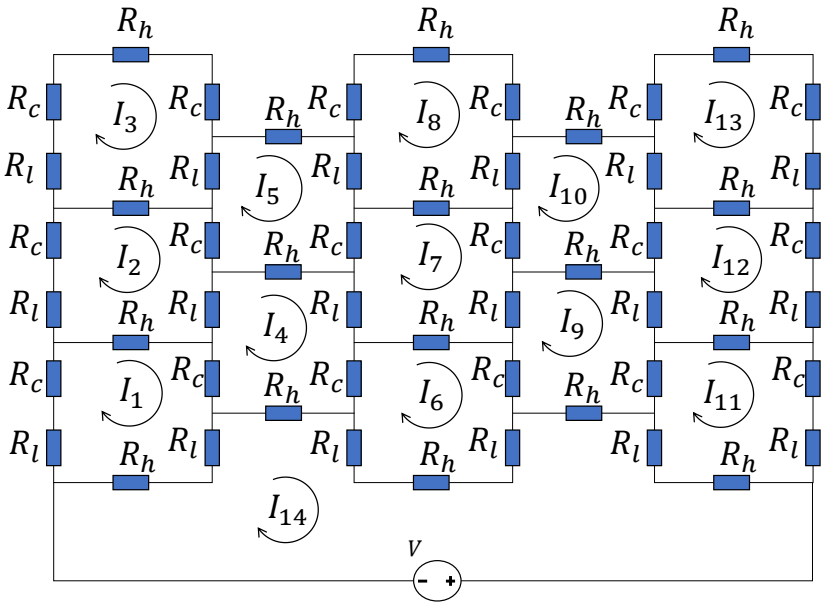

Figure 3.2: Resistive circuit model of a weft knit strain sensor with 3 courses and 3 wales.

$$\mathbf{R} = \begin{bmatrix}
R_{RLC} & -R_h & 0 & -R_c & 0 & 0 & 0 & 0 & 0 & 0 & 0 & 0 & 0 & -(R_l+R_h) \\
-R_h & R_{RLC} & -R_h & -R_l & -R_c & 0 & 0 & 0 & 0 & 0 & 0 & 0 & 0 & 0 \\
0 & -R_h & R_{RLC} & 0 & -R_l & 0 & 0 & 0 & 0 & 0 & 0 & 0 & 0 & 0 \\
-R_c & -R_l & 0 & R_{RLC} & -R_h & -R_c & -R_l & 0 & 0 & 0 & 0 & 0 & 0 & -R_h \\
0 & -R_c & -R_l & -R_h & R_{RLC} & 0 & -R_c & -R_l & 0 & 0 & 0 & 0 & 0 & 0 \\
0 & 0 & 0 & -R_c & 0 & R_{RLC} & -R_h & 0 & -R_c & 0 & 0 & 0 & 0 & -(R_h+2R_l) \\
0 & 0 & 0 & -R_l & -R_c & -R_h & R_{RLC} & -R_h & -R_l & -R_c & 0 & 0 & 0 & 0 \\
0 & 0 & 0 & 0 & -R_l & 0 & -R_h & R_{RLC} & & -R_l & 0 & 0 & 0 & 0 \\
0 & 0 & 0 & 0 & 0 & -R_c & -R_l & 0 & R_{RLC} & -R_h & -R_c & -R_l & 0 & -R_h \\
0 & 0 & 0 & 0 & 0 & 0 & -R_c & -R_l & -R_h & R_{RLC} & 0 & -R_c & -R_l & 0 \\
0 & 0 & 0 & 0 & 0 & 0 & 0 & 0 & -R_c & 0 & R_{RLC} & -R_h & 0 & -(R_l+R_h) \\
0 & 0 & 0 & 0 & 0 & 0 & 0 & 0 & -R_l & -R_c & -R_h & R_{RLC} & -R_h & 0 \\
0 & 0 & 0 & 0 & 0 & 0 & 0 & 0 & 0 & -R_l & 0 & -R_h & R_{RLC} & 0 \\
-(R_l+R_h) & 0 & 0 & -R_h & 0 & -(R_h+2R_l) & 0 & 0 & -R_h & 0 & -(R_l+R_h) & 0 & 0 & 5R_h+4R_l
\end{bmatrix}, \tag{3.3}$$

$$R_{RLC} = 2(R_c + R_l + R_h), \tag{3.4}$$

$$\mathbf{v} = \begin{bmatrix} 0 \\ 0 \\ \dots \\ V \end{bmatrix}. \tag{3.5}$$

The equivalent resistance is then calculated as:

$$R_{eq} = \frac{V}{I_{14}}. \tag{3.6}$$

3.2.2 Determination of Length Resistances

The length of the loop head and legs are derived using the Postle model [16]. In this study, the loop length of the head and legs can be derived from the loop angle and the interlocking angles. The loop angle, α, is the angle between the loop's tangent and the vertical at the centre locus of the loop while the interlocking angle, β, is the angle at the interlocking locus between the loop's tangent and the vertical.

To derive the length of the loop leg, it is considered as a bent beam. The difference between the complete and incomplete elliptical integral is first obtained as:

$$f(k,\gamma) = I(k,\frac{\pi}{2}) - I(k,\gamma), \tag{3.7}$$

where $I(k,\pi/2)$ and $I(k,\gamma)$, the complete and incomplete elliptical integrals respectively are defined as:

$$I(k,\frac{\pi}{2}) = \int_0^{\frac{\pi}{2}} \frac{d\gamma}{\sqrt{1-k^2\sin^2\gamma}}, \tag{3.8}$$

$$I(k,\gamma) = \int_0^{\gamma} \frac{d\gamma}{\sqrt{1-k^2\sin^2\gamma}}, \tag{3.9}$$

and parameters k and γ are calculated as:

$$k = \sin\left(\frac{\pi}{4} + \frac{\alpha}{2}\right), \tag{3.10}$$

$$\gamma = \sin^{-1}\left(\frac{1}{k\sqrt{2}}\left(\cos\frac{\beta}{2} - \sin\frac{\beta}{2}\right)\right), \tag{3.11}$$

The length of the loop leg is then calculated as:

$$L_l = \frac{p}{\sqrt{2(\sin\alpha + \sin\beta)}} f(k,\gamma), \tag{3.12}$$

where p is the course spacing.

To determine the length of the loop head, L_h, the loop head is considered to be two equal segments of a circle with a diameter, d. The length of each segment, l_{seg} is defined as:

$$l_{seg} = \frac{(\frac{\pi}{2} - \beta)d}{2}, \tag{3.13}$$

where the diameter, d, is defined as:

$$d = \frac{p}{2(\sin\alpha + \sin\beta)}. \tag{3.14}$$

Hence, the length of the loop head,L_h is calculated as:

$$L_h = \frac{p(\frac{\pi}{2} - \beta)}{2(\sin\alpha + \sin\beta)}. \tag{3.15}$$

R_l and R_h are length resistances based on the resistivity of the conductive yarn and the loop length of the fabric and are described as:

$$R_l = \frac{\rho \cdot L_l}{A_r}, \tag{3.16}$$

$$R_h = \frac{\rho \cdot L_h}{A_r}, \tag{3.17}$$

where ρ is the resistivity of the conductive yarn and A_r is the cross-sectional area of the conductive yarn.

3.2.3 Determination of Contact Resistance

The contact resistance is usually determined using Holm's contact theory which postulates that a contact resistance exists when there is sufficient contact between two conductors. This theory was applied to the weft knit strain sensor because of the conductive properties of its conductive yarn. Therefore, the contact resistance can be calculated as:

$$R_c = \frac{\rho}{2}\sqrt{\frac{\pi H}{nP_r}}, \tag{3.18}$$

where, R_c is the contact resistance, ρ is the electrical resistivity, H is the hardness of the material used, n is the number of contact points and P_r is the contact pressure between the conducting materials.

Typically, the material hardness and the electrical resistivity are constant based on the properties of conductive yarn used, while the number of contact points is subject to the sensor's design. Therefore, the changes to the contact resistance is dependent on changes to the contact pressure between the loops.

Consequently, the weft knit strain sensor is a piezoresistive sensor because its contact pressure varies based on the strain applied to the sensor. However, the geometrical complexity of a weft knit strain sensor has prevented the researchers from predicting or measuring the contact pressure between interlocking loops. Therefore, alternative methods such as measuring the contact force experimentally during tensile strain have been proposed to determine the contact resistance [14] [13].

Furthermore, Zhang et al. [14] proposed from empirical observations that the contact resistance of the sensor can be determined from the equivalent resistance of the sensor. This relationship was presented as:

$$R_{eq} = R_c \cdot C, \tag{3.19}$$

where C is a variable coefficient based on the number of courses and wales. By observing the calculation of the equivalent resistance from the circuit analysis in equations (3.1)-(3.6). We derive that:

$$\mathbf{R}_{end}^{-1} = R_{eq}, \tag{3.20}$$

where $\mathbf{R}_{end}^{-1}$ is the last element in the inverse matrix of the resistance matrix, $\mathbf{R}$. Therefore,

$$\mathbf{R}_{end}^{-1} = K \cdot R_c, \tag{3.21}$$

where K is the coefficient of the contact resistance in $\mathbf{R}_{end}^{-1}$ and can also be represented as a function of the length resistances.

$$K = f(R_h, R_l). \tag{3.22}$$

This method is satisfactory for simulating fabrics with a small amount of courses and wales but it is very computationally intensive to simulate relatively large fabrics (>15 wales and >15 courses). Therefore, we propose a method that determines the contact resistance from the experimental equivalent resistance in a less computationally demanding control algorithm. This method is illustrated in Algorithm 1. By initialising K with any positive value, the contact resistance can be determined from the experimental equivalent resistance. Subsequently,

the algorithm optimises the contact resistance by comparing the current simulated resistance to its previous value. The algorithm stops updating the contact resistance when the difference between the current contact resistance and the previous value is less than 3% of the current contact resistance. This threshold was selected because the difference in the accuracy of the model becomes insignificant below the threshold.

Algorithm 1 Contact Resistance solution

Initialise:
$R_{sim} \leftarrow 0$
$K \leftarrow 0 < K < \inf$
Loop:
$R_c = R_{exp}/K$
Input R_c into modelled circuit to determine R_{sim}
if $|R_{sim(n)} - R_{sim(n-1)}| > (0.03 \cdot R_{sim(n)})$ **then**
    $K = R_{sim(n)}/R_c$
    goto *Loop*
else
    Return R_c
end if
▷ R_{sim} and R_{exp} are the simulated and experimental equivalent resistances respectively

3.2.4 Model Simulation and Validation

The model proposed above is simulated using Matlab and LTspice with parameters shown in Table 3.1. Additionally, the proposed model was validated experimentally by fabricating a sensor plain knitted with a conductive multifilament yarn. The conductive yarn was a Schoeller multifilament yarn comprising 80% polyester and 20% stainless steel and was purchased from Uppingham Yarns Ltd. The yarn is fairly inelastic although it is stated to have a maximum extension of 5.5% according to its specification sheet. Its yarn count and linear density were also stated as $2/50Nm$ and 400 dtex respectively.

(a) (b)

Figure 3.3: (a) Experimental setup with Instron 3369 and multimeter, (b) Weft knit strain sensor.

The sensor illustrated in Figure 3.3 was fabricated with Shima Seiki Mach2s and dry relaxed for 48 hours to ensure it reached its stable-equilibrium state. It was then subjected to a tensile test in the wale-wise direction using an Instron 3369 tensile machine at a speed of 10mm per minute till the sensor reached its breaking point while its resistance was measured simultaneously with a multimeter. The experimental setup is also depicted in Figure 3.3. Subsequently, the percentage error between the results of the proposed model and the experimental results was determined.

In addition, we investigate the impact of changes in the loop and interlocking angles on the piezoresistivity of the weft knit strain sensor. In particular, we perform a parametric study by creating varying simulation cases with different loop and interlocking angles to observe their effect. Furthermore, the range of angles selected in the simulation cases are based on geometrical limitations imposed by width and length jamming [16].

Table 3.1: Numerical Parameters for Simulation and Experimental Validation.

Parameters	Values
Number of courses	72
Number of wales	72
$\alpha(^\circ)$	24.75
$\beta(^\circ)$	10.85
$\rho(ohm \cdot mm)$	300
Loop spacing (mm)	3
Yarn Diameter (mm)	0.4

3.3 Results

3.3.1 Model Simulation and Validation

Figure 3.4 shows the simulation and the experimental results while Figure 3.5 shows the percentage error between the two results. It can be observed that the resistance curves between extension span of 2% and 14.6% are very similar. During this span, the mean percentage error was 10.4%. However, Between the 0%-2% span, there was a significant disparity between the simulated and experimental results. This is likely as a result of the 2-dimensional limitations of the proposed model because in reality the sensor is 3-dimensional.

Another factor for this disparity might be the lack of mechanical preconditioning which was intentionally avoided as it was outside the scope of this study. Particularly, mechanical preconditioning would have led to a reduced initial resistance as a result of stabilisation. Furthermore between the ranges 14.6%-16%, the disparity is also significant. This occurred because the sensor was close to its breaking point. Although the sensor is modelled in ideal conditions where contact across all loops are equal, it was observed that loops at the middle break contact before other loops. Nevertheless, the mean percentage error between the simulated and experimental results along the entire tensile range was 16.63%. Another empirical observation was the minor instability in the sensor's resistive behaviour under tensile strain. This was caused by sensory noise common to analog sensors and can be smoothened using conventional filtering techniques.

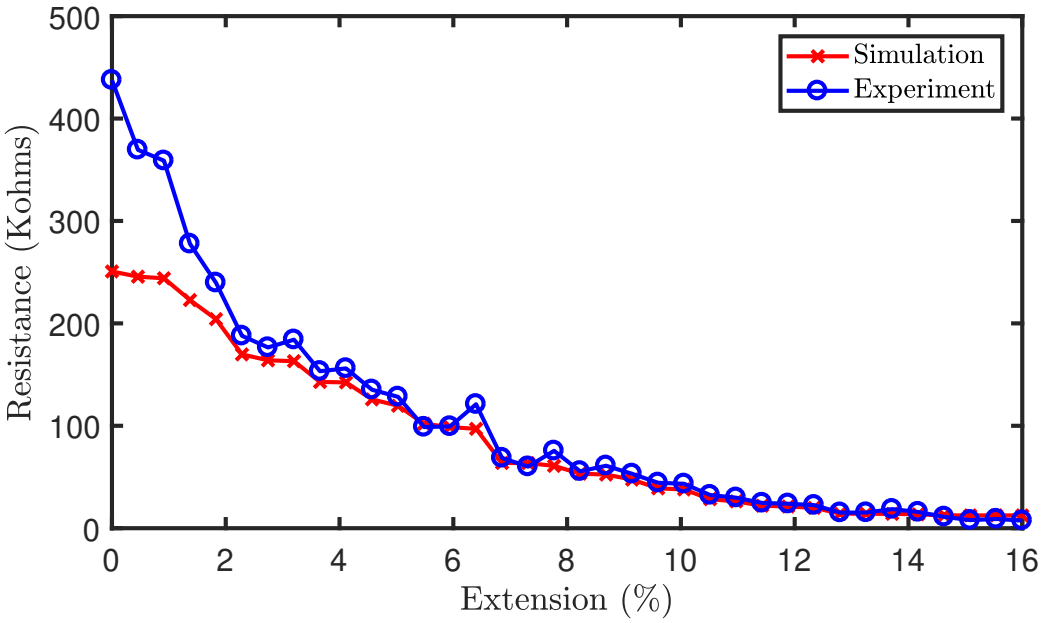

Figure 3.4: Simulated and experimental results of a weft knit strain sensor during tensile test.

3.3.2 Effect of Loop and Interlocking Angles on the Piezoresistivity of a Weft Knit Strain Sensor

The impact of changes in the loop angle is illustrated in Figure 3.6. The interlocking angle and other parameters were kept constant so that only the effect of changes in the loop angle will be observed. As a result of geometrical limitations caused by width and length jamming, only values between 23.7° - 25.8° were simulated as the loop angle. It was observed that although increases in the loop angle were directly proportional to the increases in the initial resistance, the change in the initial resistance between the maximum and minimum loop angles was only 2.27%. This was as a result of the small range of 2.1° between the maximum and minimum loop angles.

The effect of changes in the interlocking angle was also investigated. The loop angle and other parameters were kept constant while the interlocking angle was varied between 3.7° - 18°. This range was also selected due to the geometrical limitations caused by width and length jamming. It was observed in Figure 3.7

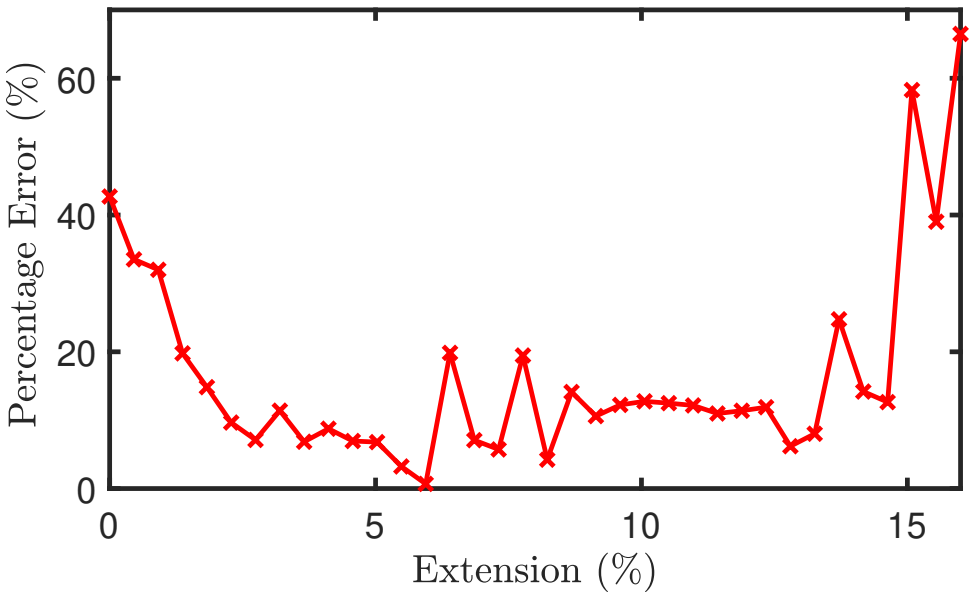

Figure 3.5: Percentage error between the simulated and experimental results.

that increases in the interlocking angle caused the initial resistance to decrease. Particularly, the change in initial resistance between the minimum and maximum interlocking angles was 25.5%. Additionally, the mean resistance across the tensile test reduced as the interlocking angle increased. The decrease in mean resistance was calculated to be 22.2% between the lowest and highest interlocking angles. This occurred because increases in the interlocking angle decreased the lengths of the loop head and the loop legs, which then reduces their respective resistances and thus the equivalent resistance of the sensor.

Furthermore, it was observed that the loop and interlocking angles did not affect the overall exponential relationship between the sensor's resistance and its extension. This is because the loop and interlocking angles only affect the length resistances and not the contact resistance which represents the shape of the sensor's resistance-extension curve.

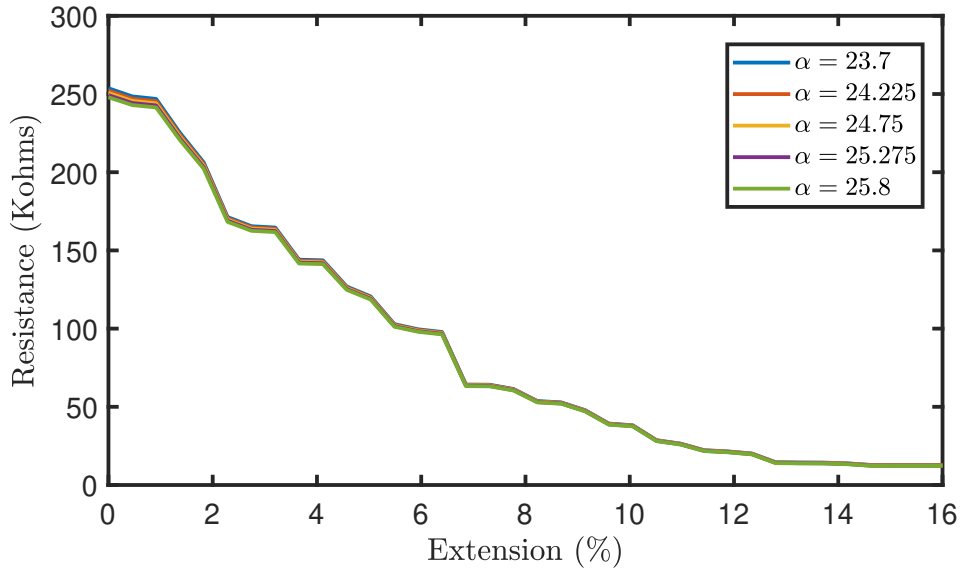

Figure 3.6: Effect of Loop angle on weft knit strain sensor ($\beta = 10.85, Cn = 72, Wn = 72$)

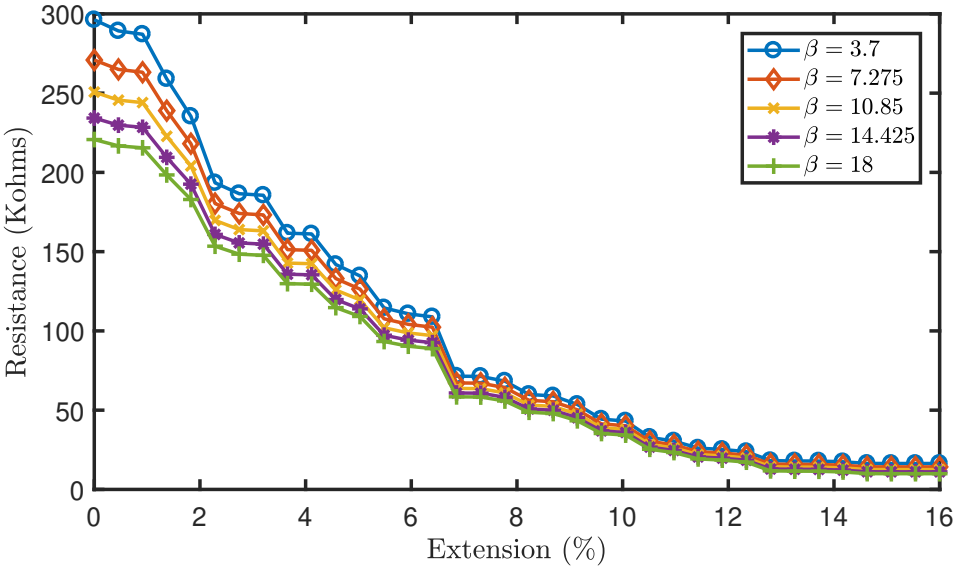

Figure 3.7: Effect of Interlocking angle on weft knit strain sensor ($\alpha = 24.75, Cn = 72, Wn = 72$)

3.4 Conclusion

In this study, we have presented a resistive model of a weft knit strain sensor based on its loop and interlocking angles. Particularly, we have ensured that the length resistances and the contact resistances were considered. Moreover, we simulated this model using Matlab and LTspice software and verified the results experimentally. The mean percentage error between the simulated and experimental results was calculated as 16.63%. Furthermore, a parametric study was performed to investigate the impact of the loop and interlocking angles on the sensor's piezoresistivity. It was observed that increases in the loop angle caused proportional increases in the initial resistance of the sensor up to a maximum increase of 2.27% while increases in the interlocking angle caused a decrease in the initial and mean resistance of the sensor up to a maximum decrease of 25.5% and 22.2% respectively.

Chapter 4

Weft Knit Data Glove

In this chapter, we design a weft knit strain sensor with a novel configuration of conductive yarn and elastomeric yarn to improve the extensibility of the sensor. Thereafter, we simulate the piezoresistivity of the sensor and validate it experimentally using the methodology established in Chapter 3. A lightweight textile glove embedded with these weft knit strain sensors was manufactured using WholeGarment technology. This eliminated the use of an external attachment between the sensors and the rest of the glove as seen in traditional data gloves. Furthermore, the reliability of the glove is verified experimentally and classical machine learning algorithms are implemented in classifying the glove's data.

4.1 Introduction

Stroke is one of the major causes of disabilities in adults. A major challenge most stroke survivors face is the loss of their motor skills, especially the individual finger movements in the hand [82, 83]. Although only 15% fully recover, a large majority will relearn some of their motor skills by performing repetitive tasks in therapy [84]. A key factor in improving rehabilitation is progress measurement. Progress measurement involves collecting the data on the relearning rate of the affected joint and the patient's recovery in general. Furthermore, 45% of post-stroke patients return home and still need ongoing therapy to recover their motor skills [85]. Therefore, only patients who can afford private therapists who visit to take measurements have chances of a full recovery. Even with a private therapist,

there is a chance that their visits might not coincide with rare occurrences that are important to the patient's progress measurement [86].

Therefore, an approach is needed that enables the collection of data from the patient's hand without the need to schedule a therapist's appointment. There are two major methods in measuring the flexion of finger joints and they are camera-based and data glove approaches. Camera-based approach involves the use of a camera and markers in which images acquired are processed to calculate the flexion at the joints [87, 88]. Although the accuracy of this approach has been improved by the use of more novel and complex image processing techniques, they are not commercially feasible in remote monitoring due to privacy concerns as these cameras can be vulnerable to attacks and could be used to record the private lives of the patients. Furthermore, the use of stationary cameras deprives the patient of free movement as they have to be stationary for the camera to accurately capture the fingers motion. Multiple cameras such as in [89] could alleviate this problem but this increases cost and may be higher than the cost of multiple therapist home visits.

In contrast, data gloves provide a cheaper and more efficient alternative as the patient can wear it while performing their daily activities. However, the conventional design of data gloves prevent their large scale adoption in the rehabilitation industry. Particularly, the conventional design comprises of an external attachment that adheres the sensors to the support structure. The support structure is usually a textile glove that places the sensors at the phalangeal joints. This design causes the data glove to be bulky and produce inconsistent results progressively with the degradation of the attachment. Table 4.1 illustrates a summarised review of different data gloves, highlighting their sensors and the method of attachment. Fabric padding is the most common method of attachment in data gloves. It involves placing strain sensors such as fibre-optic and flex sensors in between multiple layers of fabric in a textile glove. Popular commercial data gloves such as Cyberglove and 5DT 5 Ultra have utilised this method [90, 91, 92, 93]. However, this leads to at least three layers of sensor and support structure which causes a bulky data glove and might impede the progress of patients in sensitive applications.

Table 4.1: A Comparison of Data Gloves.

Type of Sensor	Attachment Method	Reference
Conductive elastomer composites	Ink printing	[94]
Fibre optical sensors (5DT 5 Ultra)	Fabric padding	[90, 91, 93]
Hall effect sensors	Fabric padding	[95]
Piezo-resistive sensors (Cyberglove)	Fabric padding	[92]
Magnetic sensing coils	Electrical wires	[96]
Flex sensors	Fabric padding	[97, 98, 99, 100, 101]
Accelerometers (KHU-1)	Hook-and-loop fasteners	[102]
Flex sensors	Cyanoacrilic glue	[103]
Bend sensors and IMUs	Fabric padding	[104]
Conductive polymer (PEDOT:PSS) ink	Ink jet printing	[105]
IMUs and force sensors	Cable ties	[106]
IMUs	Hook-and-loop fasteners	[107, 108]
Soft sensor	Silicon rubber curing	[109]
IMUs	Textile cables	[110]
Metalized fabric conductors	Sewing and fabric padding	[111]
Bend sensors (Shadow glove)	Plastic sheath padding	[112]
Semi-Conducting scotch tape	Fabric padding	[113]

Ink printing is a great lightweight alternative to the fabric padding method as it involves printing conductive ink on a textile glove at phalanx joint locations. This ensures that the glove is not as bulky as the number of layers are limited to one in most places and two in the phalanx joints [94][105]. However, conductive inks are vulnerable to environmental degradation which will lead to inconsistent results when the data gloves are not used in the optimal environmental conditions. Other chemical methods of attachment such as silicon rubber curing and cyanoacrilic glue are also degradable and will eventually lead to distorted results.

In contrast, weft knit strain sensors present a unique potential in the design of wearable devices as the sensors and the support structure can be created in a

single knitting process. Particularly, knee sleeves and respiration belts have been developed using weft knit strain sensors [13, 36, 76]. However, there has been no data glove created with weft knit strain sensors.

Therefore, this chapter presents a weft knit smart data glove capable of measuring the finger flexion at the interphalangeal joints is proposed. Furthermore, this glove utilises WholeGarment technology to fabricate the sensors and the support structure in a single manufacturing process thus eliminating the need for an external attachment. This ensures that the glove is unobtrusive, lightweight and accurate. Additionally, the glove is commercially feasible because custom-sized data gloves can be manufactured easily as we depart from a one-size-fits-all philosophy.

In addition, a novel loop configuration comprising of an elastomeric yarn and a conductive yarn is knitted in a plain structure to create the sensor. Moreover, the electromechanical behaviour of this sensor is modelled using Postle's geometrical model [16] and validated experimentally. The advantage of using Postle's model is that it enables the modelling of the length of the loop legs and head based on the loop's interlocking and loop angles. Finally, the weft knit data glove is validated in terms of its consistency and the performance of some classical machine learning algorithms on the application of the glove in a classification scenario is evaluated.

4.1.1 Related Work

Weft knitting is one of the most popular knitting techniques and it involves interlocking loops of yarn in a horizontal direction such that the feet of the loop legs lock with the head of the previous knitting cycle's loops [57]. Therefore, when conductive yarn is weft knitted, contact resistances occur because of the interlocking of conductive loops. The contact resistance is dependent on the contact pressure between the interlocked loops which varies based on the load applied on the sensor [74, 114, 115].

Consequently, the weft knit strain sensor is classified as a piezoresistive sensor due to the changes in the resistance of the sensor caused by the applied load. The conductive yarn could be a yarn coated with conductive ink or a multifilament yarn comprising of stainless steel fibres. Multifilament conductive yarns are

preferable to silver-coated yarns in the creation of wearable sensors because they are more environmentally stable [78]. Furthermore, the behaviour of the sensor is dependent on the sensor's knit structure and its knitting parameters.

The strain sensing properties of weft knit fabric knitted with conductive yarn was investigated in [14]. The sensor was knitted in a plain knit structure with a stainless steel multifilament conductive yarn and tested experimentally to observe the sensor's piezo-resistivity. It was observed that the resistance of the sensor reduced exponentially as the load applied increased. This occurred because the contact resistance formed by the contact between the interlocked loops of conductive yarns varied due to the change in contact pressure caused by the load applied.

Furthermore, the effect of mechanical preconditioning was investigated in [33]. Different sensors were knitted in a plain knit structure but with different loop configurations and were experimentally tested. Subsequently, it was observed that mechanical preconditioning caused the resistance of the sensors to reduce till it reached a stabilised value.

In addition, Atalay et al. [37, 38] investigated the effect of the conductive yarn's input tension and linear density on the sensor's piezo-resistivity. In contrast, the sensor was knitted in an interlock structure. It was observed that the electrical resistance of the sensor increased when the input tension or the linear density was decreased. This effect materialised because the input tension and the linear density affected the contact pressure between the intermeshed loops.

Despite the breakthroughs in these investigations, there have been few studies illustrating the application of weft knit strain sensors in motion capture. Particularly, a heart monitoring belt was developed using an interlock knit strain sensor [13]. The belt measured heart rate from the expansion and contraction of the abdominal area. Moreover, the sensor's electromechanical model was derived from the Peirce's [63] geometrical model. This model derived the lengths of the loop head and legs from the diameter of the yarn used. Additionally, the sensor was knitted with conductive yarn made by coating non-conductive yarn with silver.

Conventionally, the creation of knitted garments followed the design methodology of current data gloves. It involved knitting the different parts of the garment separately and then attaching them by sewing. However, the introduction

of WholeGarment technology has facilitated the fabrication of entire knitted garments in a single process. This is relevant in the creation of textile sensors because it enables the creation of both the sensors and the non-conductive support structure in the same fabrication process. Additionally, in applications which might require a complex design of the sensor such as for progress measurement in the knee or ankle, it enables the creation of the sensor in a single process. This is advantageous because sewing different parts of the sensor together will impact the extensibility and the piezoresistive behaviour of the sensor.

4.1.2 Contributions

The main contributions of this chapter are as follows:

1. We propose a novel sensor configuration comprising conductive yarn and elastomeric yarn to increase the flexibility of a weft knit strain sensor. In addition, we modify the electromechanical model in Chapter 3 to simulate the piezoresistivity of the sensor configuration. The accuracy of the simulated model is verified experimentally in a tensile test.

2. We design a novel textile data glove comprising of weft knit strain sensors with no external attachment between the sensors and the support structure. The configuration of the sensors are novel and we observe their repeatability in a flexion-extension experiment.

3. We investigate the effect of drift in the sensor's output on the performance of machine learning algorithms in a classification scenario. Notably, it is the first time machine learning algorithms have been utilised in classifying data from a weft knit strain sensor.

4.2 Weft Knit Strain Sensor

The weft knit strain sensor was designed with a novel combination of conductive and elastomeric yarn knitted in a plain knit structure. The design is illustrated

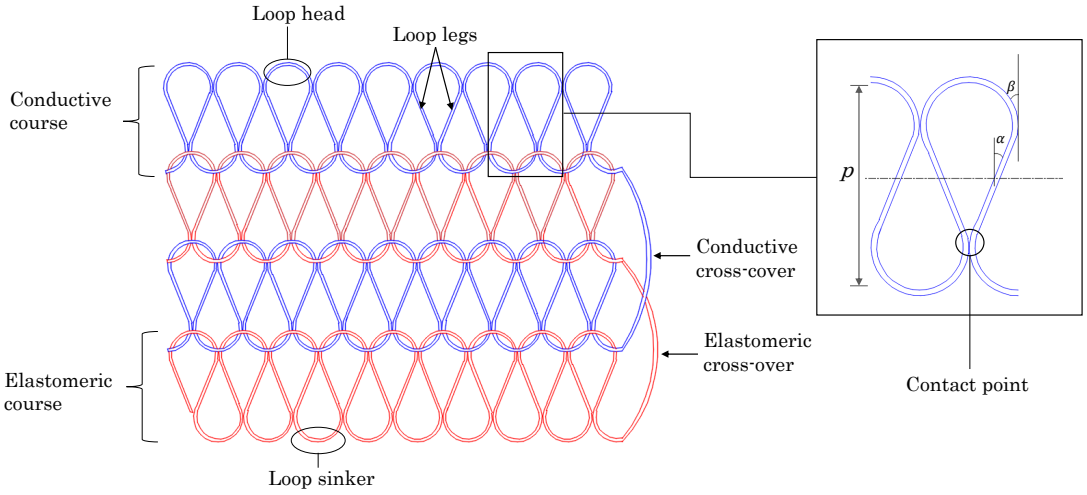

Figure 4.1: Design of the weft knit strain sensor. α is the loop angle, β is the interlocking angle and a course represents a horizontal row of knitted loops.

in Figure 4.1. Unlike in Chapter 3 where the sensor was knitted with only conductive yarn, we integrated an elastomeric yarn to create a more elastic sensor. Particularly, we achieve this by knitting 50% of the courses with elastomeric yarn in a pattern where a course of conductive yarn courses is succeeded by a course of elastomeric yarn loops and is repeated till the last course of the sensor. The elastomeric yarn is a double covered yarn comprising of 82.76% Nylon and 17.24% Lycra. It has a maximum extension of 320% and was purchased from Stretchline UK. In addition, a plain knit structure was selected ahead of an interlock structure because interlock knitted fabrics are less extensible than plain knitted fabrics.

4.2.1 Electromechanical Model

The circuit in this sensor differs from the sensor shown in the Chapter 3 because of the addition of a non-conductive elastomer. However, the methodology used to derive the length and contact resistances in Chapter 3 is utilised in the electromechanical model of this sensor. Moreover, the same conductive yarn is used in the fabrication of this sensor. It is a multifilament yarn comprising of 80% polyester and 20% stainless steel. Due to its metallic properties, its length resistances of

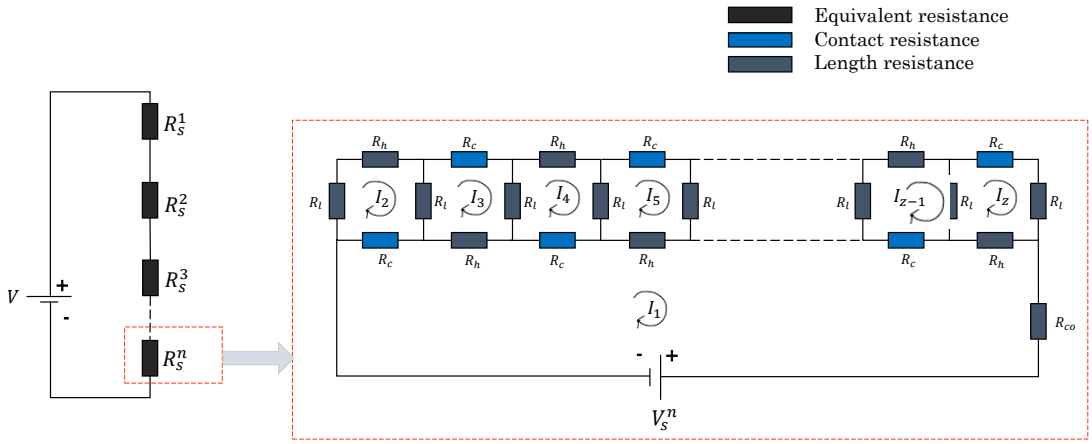

Figure 4.2: Circuit model of the weft knit strain sensor. $(Z-1)$ is the number of wales in the sensor.

the loop head and legs were modelled as R_h and R_l while the contact resistances between interlocking conductive yarn loops were modelled as R_c. The model also follows the basic assumption that the geometry of each loop is constant across the sensor.

As a result of the knitting action of the cam box in a knitting machine, when two yarns are used interchangeably across different courses, there is a crossover at the edge of the fabric between the previous and the current course knitted by the same yarn. In this sensor, the crossover between the conductive courses is modelled as R_{co}. The combination of the resistances in a conductive course and its respective crossover is termed as a conductive section. The equivalent resistance of each n conductive section is modelled as R_s^n. Therefore, the circuit of the sensor represented in Figure 4.2 represents a series network of conductive sections and the number of conductive sections is equal to the number of conductive courses in the sensor.

V_s^n represents the voltage across each conductive section. Due to the aforementioned modelling assumption stating that the geometry of each conductive loop is constant across the sensor, the equivalent resistances of the conductive sections are equal. Thus, the voltage across each conductive section, V_s^n is calculated as:

$$V_s^n = \frac{V}{n}, \tag{4.1}$$

where V is the voltage across the sensor. Let I_1 - I_Z represent the hypothetical currents flowing in the meshes of the circuit (as shown in Figure 4.2) and are solved using Kirchoff voltage law and Ohm's law as:

$$\mathbf{i} = \mathbf{R}^{-1}\mathbf{v}, \tag{4.2}$$

where in a sensor with 72 courses (36 conductive courses) and 36 wales (i.e. Z=37),

$$\mathbf{i} = [I_1, I_2, \ldots, I_{36}, I_{37}]^T, \tag{4.3}$$

$$\mathbf{v} = [V_s^n, \underbrace{0, \ldots, 0, 0}_{36 zeros}]^T, \tag{4.4}$$

$$\mathbf{R} = \begin{bmatrix} 18(R_c + R_h) + R_{co} & -R_c & -R_h & \ldots & -R_h \\ -R_c & R_c + R_h + 2R_l & -R_l & \ldots & 0 \\ -R_h & -R_l & R_c + R_h + 2R_l & \ldots & 0 \\ -R_c & 0 & -R_l & \ldots & 0 \\ \ldots & \ldots & \ldots & \ldots & \ldots \\ -R_c & 0 & 0 & \ldots & R_c + R_h + 2R_l \end{bmatrix}. \tag{4.5}$$

The equivalent resistance of each conductive section is calculated as:

$$R_s^n = \frac{V_s^n}{I_1}. \tag{4.6}$$

4.2.2 Determination of Length Resistances

The length resistances are derived from the Postle's geometrical model of a weft knit loop [16]. This model determines the length of the loop legs and head from the loop and interlocking angles of the loop. The loop angle, α, is the angle between the loop's tangent and the vertical at the centre locus of the loop while the interlocking angle, β, is the angle at the interlocking locus between the loop's tangent and the vertical.

By considering the loop leg as a bent beam, its length was derived as:

$$L_l = \frac{p}{\sqrt{2(\sin(\alpha) + \sin(\beta))}} f(k, \gamma), \tag{4.7}$$

where p is the course spacing. $f(k,\gamma)$ is the difference between the complete and incomplete integrals and can be calculated as:

$$f(k,\gamma) = \int_0^{\frac{\pi}{2}} \frac{d\gamma}{\sqrt{1-k^2\sin^2(\gamma)}} - \int_0^{\gamma} \frac{d\gamma}{\sqrt{1-k^2\sin^2(\gamma)}}, \tag{4.8}$$

and parameters k and γ are calculated as:

$$k = \sin\left(\frac{\pi}{4} + \frac{\alpha}{2}\right), \tag{4.9}$$

$$\gamma = \sin^{-1}\left(\frac{1}{k\sqrt{2}}\left(\cos\left(\frac{\beta}{2}\right) - \sin\left(\frac{\beta}{2}\right)\right)\right). \tag{4.10}$$

The length of the loop head was considered to be the sum of two equal segments of a circle and is derived as:

$$L_h = \frac{p(\frac{\pi}{2} - \beta)}{2(\sin(\alpha) + \sin(\beta))}. \tag{4.11}$$

The resistances of the held loop's legs and head are then calculated as:

$$R_l = \frac{\rho L_l}{A_r}, \tag{4.12}$$

$$R_h = \frac{\rho L_h}{A_r}, \tag{4.13}$$

where A_r is the cross-sectional area of the conductive yarn. The length of the crossover was empirically observed to be twice the course spacing, p. Therefore, the resistance of the conductive crossover is calculated as:

$$R_{co} = \frac{2p \cdot \rho}{A_r}. \tag{4.14}$$

4.2.3 Determination of Contact Resistance

Contact resistance only occurs when there is contact between two conductors. Particularly, it occurs at the contact between the conductive loop legs as illustrated in the enlarged frame in Figure 4.1. According to Holm's contact theory, the contact resistance can be calculated as:

$$R_c = \frac{\rho}{2}\sqrt{\frac{\pi H}{nP_r}}, \tag{4.15}$$

where, R_c is the contact resistance, ρ is the electrical resistivity, H is the hardness of the material used, n is the number of contact points and P_r is the contact pressure between the conducting materials.

Typically, the material hardness and the electrical resistivity are constant based on the properties of conductive yarn used, while the number of contact points is subject to the sensor's design. Therefore, the changes to the contact resistance is dependent on changes to the contact pressure between the loops.

However, simulating or predicting the contact pressure between the interlocking loops has proven cumbersome due to the geometrical complexity of a weft knit strain sensor. Therefore, alternative methods such as obtaining the contact resistance empirically from the contact force have been proposed [13]. However, Zhang et al. [14] suggested from experimental observations that the relationship between the contact and equivalent resistances can be depicted as:

$$R_{eq} = R_c D, \tag{4.16}$$

where D is a variable coefficient based on the sensor design.

By using a control algorithm illustrated in Algorithm 2, we determine the contact resistance from the equivalent resistance. The algorithm is initialised with any positive value as D. Subsequently, the algorithm employs a control feedback by inputting the calculated contact resistance into the modelled circuit. The output equivalent resistance termed as R_{sim} is then used to determine the new coefficient, D. The optimised contact resistance is produced when the difference between the previous simulated equivalent resistance and its current value is less than 3% of the current value. This threshold was chosen empirically as no significant change in accuracy of the model was detected below the threshold.

4.2.4 Model Validation

This model was verified by fabricating sensors with the aforementioned sensor design and the knitting parameters enumerated in Table 4.2. Subsequently, the sensors were dry relaxed for 48 hours to remove any excess strain between the

Algorithm 2 Contact Resistance Solution

Initialise:
$R_{sim} \leftarrow 0$
$D \leftarrow 0 < D < \text{inf}$
Loop:
$R_c = R_{exp}/D$
Input R_c into modelled circuit to determine R_{sim}
if $|R_{sim(n)} - R_{sim(n-1)}| > (0.03 \cdot R_{sim(n)})$ **then**
    $D = R_{sim(n)}/R_c$
    goto *Loop*
else
    Return R_c
end if

▷ R_{sim} and R_{exp} are the simulated and experimental equivalent resistances respectively.

loops as a result of the knitting process. The sensors were then put through a tensile test in an Instron3369 tensile machine where it was extended till 35% extension while its resistance was measured with a digital multimeter. The loop configuration of the sensor and the experimental setup are shown in Figure 4.3. Furthermore, a simulation of the model was also performed using Matlab and LTspice with the same numerical parameters.

4.3 Data Glove

The weft knit data glove was designed using Shima Seiki's sds one apex3 apparel CAD software such that the weft knit strain sensors were located at the distal and proximal interphalangeal joints while the rest of the glove was knitted with the same elastomeric yarn used in the sensors. Particularly, the sensors were knitted to wrap around the joints to maximise its sensitivity. The elastomeric yarn was selected for the rest of the glove because it provides a tight and flexible fit that is optimal for sensing applications while also providing a comfortable experience for the user. WholeGarment technology enabled the knitting of all sensors and

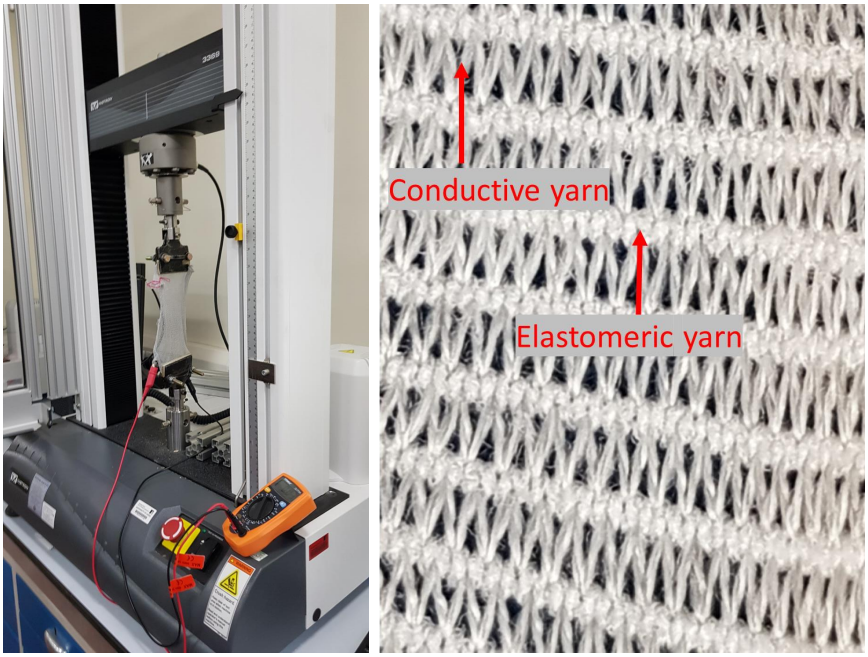

(a) (b)

Figure 4.3: (a) Experimental setup with Instron 3369 and Multimeter. (b) Image of sensor's loop configuration.

the support structure of the glove in a single manufacturing process without any external attachment. The glove design and the fabricated glove are illustrated in Figure 4.4. The glove was knitted with Shima Seiki Mach2s which is equipped with WholeGarment technology. Furthermore, the dimensions used in knitting the glove were selected based on the main author's hand size. This illustrates its commercial feasibility as several data gloves can be fabricated based on sizes similar to the creation of conventional fabrics.

4.3.1 Data Acquisition

A data acquisition system is embedded in the glove to transmit data to a computer. Particularly, it consists of a microprocessor and a set of resistors that form a voltage divider circuit with the ADCs (analog-digital converter) of the microprocessor. The microprocessor used was an Arduino lilypad and it was selected because of its 6 analog inputs which can be connected to the sensors via

Table 4.2: Numerical parameters for Simulation and Experimental Validation

Parameters	Values
Number of conductive courses	36
Number of elastomeric courses	36
Number of wales	36
α	24.75°
β	10.85°
Course spacing	3mm
Yarn diameter	0.4mm
Resistivity	300(ohm·mm)

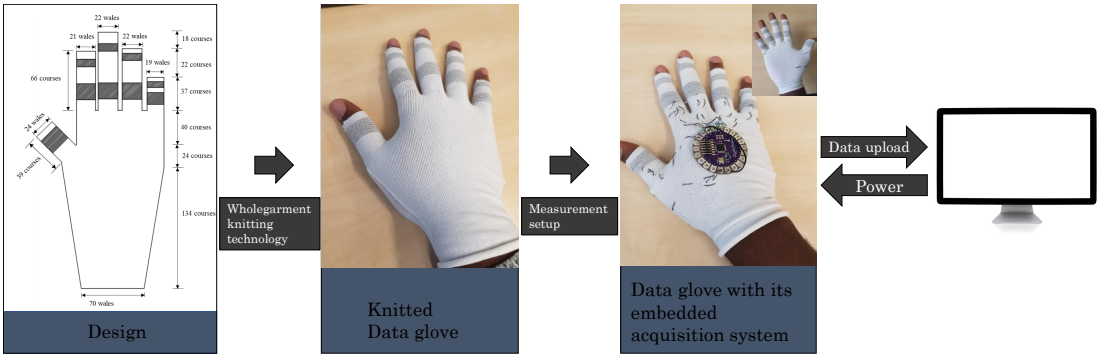

Figure 4.4: Block diagram illustrating the design and implementation of the weft knit Data glove.

sewing. Particularly, the sensors at the PIP (proximal interphalangeal) joints are connected to the analog inputs of the microprocessor by sewing conductive thread in front of the glove. Furthermore, the sensors were also connected to the negative pin of the microprocessor at the back of the glove to prevent a short circuit between the positive and negative threads. These analog inputs have individual ADCs that convert analog voltages between 0 and 3.3volts to digital values between 0 and 1023. This allows the microprocessor to read the data of all fingers in parallel. The microprocessor was programmed to transmit data from the sensor at a frequency of 20 Hertz. However, the analog output of weft knit strain sensors is electrical resistance, therefore a voltage divider circuit is required

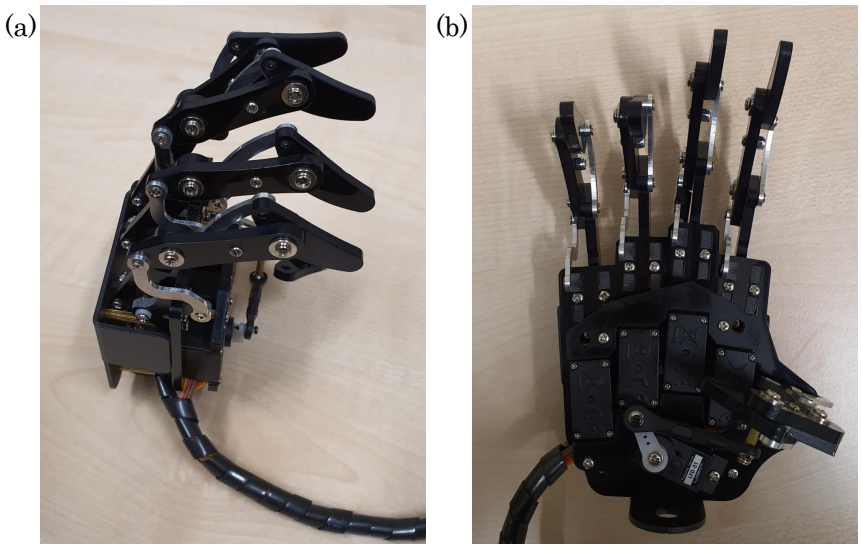

Figure 4.5: Robotic hand used for glove evaluation. (a) Side view (b) Front view illustrating its motors.

to convert the sensor's resistance to voltage. The sensor voltage is obtained as:

$$V_{sensor} = V_{input} \cdot \frac{R_{sensor}}{R_{fixed} + R_{sensor}}, \tag{4.17}$$

where V_{sensor} is the calculated sensor's voltage, V_{input} is the input voltage, R_{fixed} is a fixed resistor value and R_{sensor} is the variable resistance of the weft knit strain sensor. Furthermore, the computer also provides power to the microprocessor although a coin-cell battery can be embedded in the glove to enable it store data for upload at a later date.

4.3.2 Glove Evaluation

The robotic hand shown in Figure 4.5 was applied as an emulation tool in evaluating the glove's sensor. Its joint angle was set accurately without constraints such as fatigue and stability that may plague human participants when instructed to maintain a posture for a considerable period. The robot was obtained commercially and consists of stepper motors that control the joints at each finger. All evaluations were performed with the proximal interphalangeal joint of the middle finger of the robot.

Flexion and Extension

The first experiment consists of the opening (extension) and closing (flexion) of the hand. This test simulates one of the prominent hand motions and depicts the repeatability of the sensor. The robot was programmed to perform this at a frequency of one oscillation every 9 seconds.

Drift

Weft knit strain sensors are known to observe phenomena such as hysteresis and drift that negatively impact the sensor's output [37]. Drift occurs when the sensor's output stray away from the original measurement when the extension of the sensor is constant.

A second experiment was performed to visualise the drift in the sensor and illustrate the use of machine learning in reducing the impact of this phenomenon in a classification scenario. In this scenario, the sensor's output was recorded when the joint was held at 0°, 15°, 30°, 45°, 60° and 75° for 90 seconds. The first 15 seconds and the last 15 seconds were eliminated to remove the noise caused by the impact of switching to the next angle. Subsequently, classical machine learning algorithms such as Support vector machines (SVM), Linear Regression and naïve Bayes were used to classify the sensor's output.

4.4 Results and Discussion

4.4.1 Model Validation

The average experimental and simulation results of the strain test are illustrated in Figure 4.6. The sensor exhibits an exponential relationship between its resistance and extension. The piezoresistivity plot of the sensor can be divided into three phases. In the first two phases, the sensor resistance decreases linearly as the sensor is extended but the slope of decrease varies between the two phases. In the third phase, the sensor's resistance is relatively constant. This occurs because at this level of extension, the contact resistances between certain conductive loops

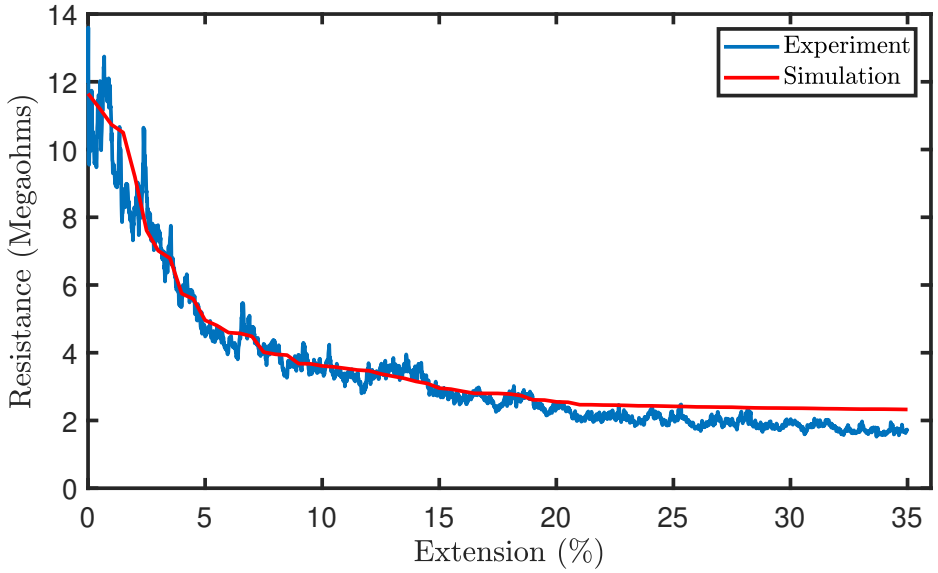

Figure 4.6: Experimental and simulation results of strain test.

in the sensor are negligible. The first linear phase occurs between 0% and 6% extension, the second linear phase occurs between 6% and 25%, and the third phase occurs after 25% extension. Our simulation results largely agree with the experimental results. Particularly, the average percentage error between the simulation and experimental for the entire range of extension was 11.47%. However, the error was lower when excluding the third phase. The average percentage error in the linear phases was 7.33% while the average percentage error in the third phase was 21.66%. The increase in the error in the third phase ensued because of the difficulty in simulating the specific loops whose contact resistances are negligible when the sensor is extended beyond 25%. Particularly, our simulation assumes uniform behaviour across all knit loops in the sensor but in reality, this is not the case especially as the sensor approaches its breaking point.

In addition, we illustrate the relationship between the derived contact resistance and the simulated equivalent resistance at each level of strain in Figure 4.7. We observed that the change in contact resistance between the conductive loops is directly proportional to the change in the equivalent resistance of the sensor. Moreover, the R^2 value of its linear fit was calculated to be 0.9742, thereby showing a high linearity of the relationship between the contact resistance

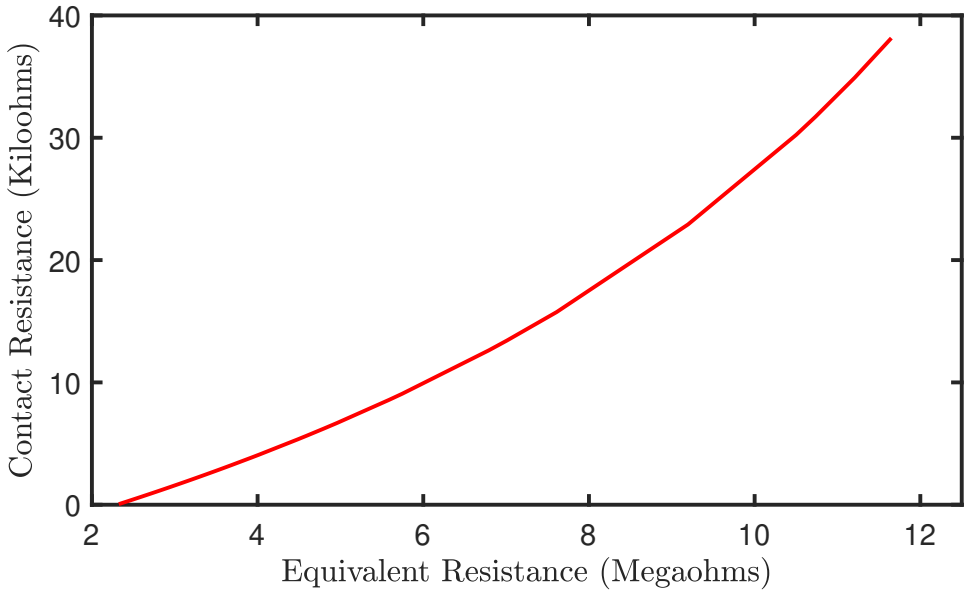

Figure 4.7: Relationship between the contact resistance between the conductive loops and the equivalent resistance of the sensor.

and the equivalent resistance. This is important because it can simplify future simulations of the electromechanical behaviour of weft knit strain sensors. Furthermore, this relationship explains the contact between the loops as the sensor is stretched. From equation 4.15, we observe that the contact pressure is inversely proportional to the contact resistance. Therefore, since the equivalent resistance is directly proportional to the contact resistance, we assume that the equivalent resistance is inversely proportional to the contact pressure. Furthermore, by observing the relationship between the equivalent resistance and the extension of the sensor in Fig 4.6, we derive that the contact pressure between the conductive loops increases exponentially as the sensor is extended.

4.4.2 Glove Evaluation

Flexion and Extension

Figure 4.8 shows the result of the flexion and extension at the robot's joint. It was observed that the sensor's output was noisy particularly at the peaks and

troughs of the signal. Therefore, a Savitzky-Golay filter (polynomial order of 5 and window length of 85) was applied on the output. Savitzky-Golay was selected because of its advantage in removing noise while still preserving the shape of the signal. In addition, it has been deployed in the filtering of the output of weft knit strain sensors [33]. The selection of its configuration was chosen empirically by varying the polynomial order and its window length till an optimal result was observed. The filter removes most of the noise that was present in the raw signal and illustrates the repeatability of the sinusoidal oscillations in the sensor's output. However, there are still minor distortions in the filtered signal. These distortions represent the hysteresis and drift common in weft knit strain sensors.

Drift

The sensor's output at each angle threshold in the drifting experiment is shown in Figure 4.9. This figure provides a preliminary visualisation of the experiment's results. The mean and median values illustrate the skew of the data. We observed that the output of the sensor reduced as the angle increased for most of the experiment. However, changes in the angles at the beginning and end of the experiment opposed this observation. This was expected as prior experimental results from the tensile test had shown instability and non-linearity in the sensor's output at the beginning and end of its extension respectively.

A detailed visualisation of the data is illustrated in Figure 4.10 with an histogram plot and its probability distribution fit. As illustrated in the histogram plots, the sensor's output fluctuates despite the fixed angle of the robot's joint. However, we observe that the most of the data were within a limited range during these fluctuations. Particularly, we observe that the data at each angle were mostly distributed into two classes. Therefore, we implemented a mixed Gaussian distribution (MGD) using expected maximisation (EM) algorithm [116] to provide an accurate fit of the data. We also limited the number of classes to two based on our empirical observations to prevent overfitting. From the MGD fits, we observed that one class was significantly smaller than the other class in terms of the density. We hypothesise that the smaller class is noise and the bigger class

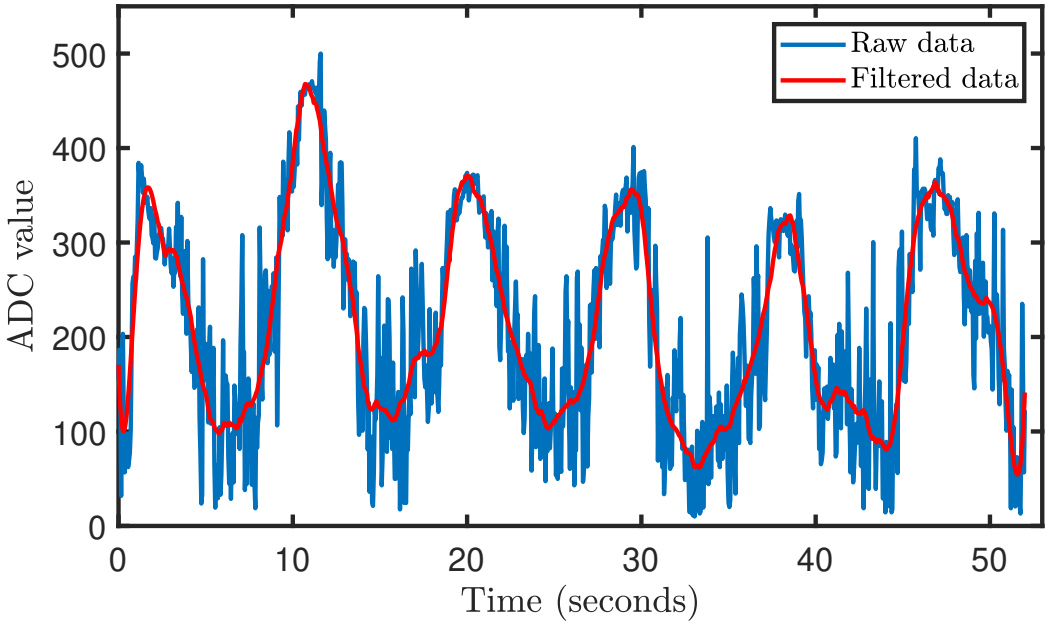

Figure 4.8: Flexion and extension experimental result.

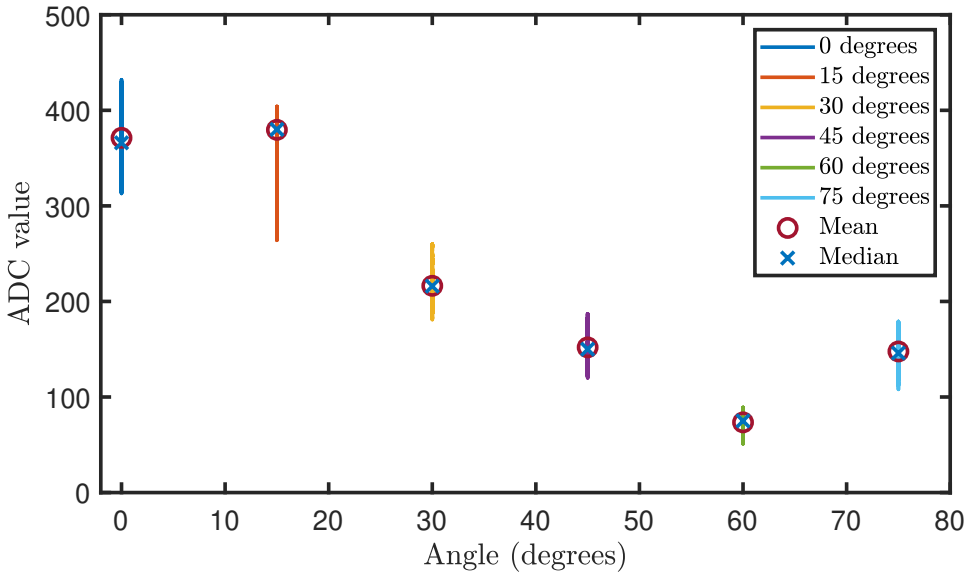

Figure 4.9: Data plot of drift experimental result. Mean and median are shown to illustrate skew of data.

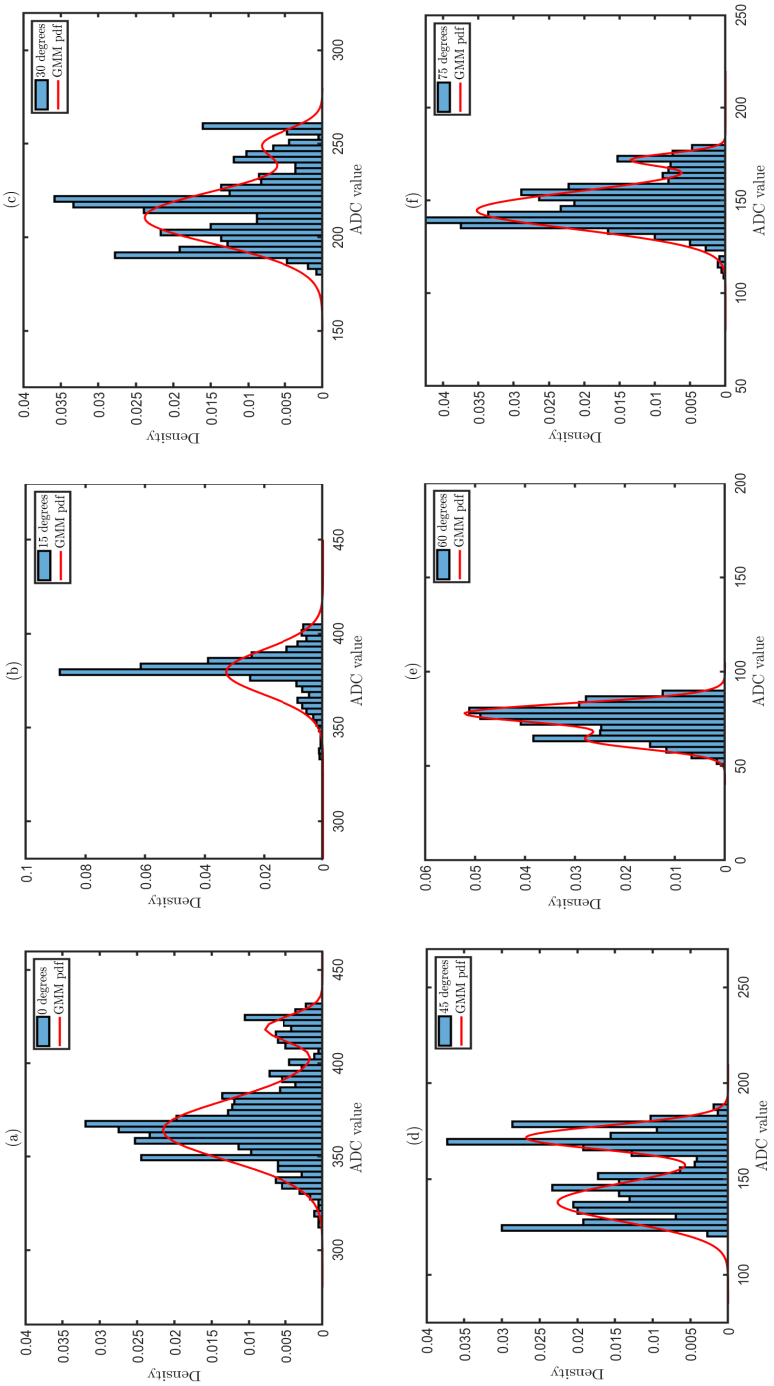

Figure 4.10: Histogram plots and respective mixed gaussian distribution fits of the sensor's output at (a) 0° (b) 15° (c) 30° (d) 45° (e) 60° (f) 75°

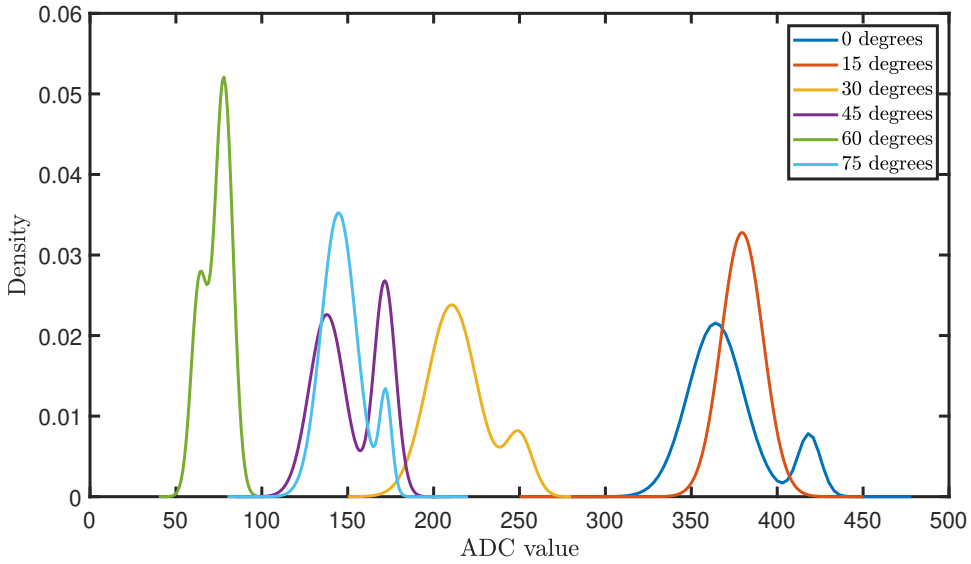

Figure 4.11: Mixed gaussian distribution fits of the sensor's output at various angles.

is the real signal. However, we did not eliminate the noise to prevent biasing the results of the classifiers.

Furthermore, we plot the MGD fits of all angles in Figure 4.11. This depicts a comprehensive view of the effect of drift on the sensor's output. We observed that drift causes the distribution fits of some angles to overlap each other. Particularly, the drift in the sensor's output at 0° and 75° may reduce the accuracy of a linear classifier. Therefore, although drift occurs at every angle in the experiment, the impact on classification is worse when considering the instability and non-linearity of the sensor's output at specific sections of its extension.

Subsequently, we evaluate the performance of three classifiers in accurately classifying the sensor's data. These classifiers are SVM, Linear Regression and naïve Bayes algorithms [117, 118]. Particularly, each classifier is evaluated on its performance in classifying the data of a specific angle from all other angles. The performance metric for evaluating the classifiers is the area under the receiver operating curve. Firstly, a confusion matrix comprising of the true positive rate (TPR) and the false positive rate (FPR) of the classifier is computed. The TPR is the proportion of correctly identified data values while the FPR is the proportion

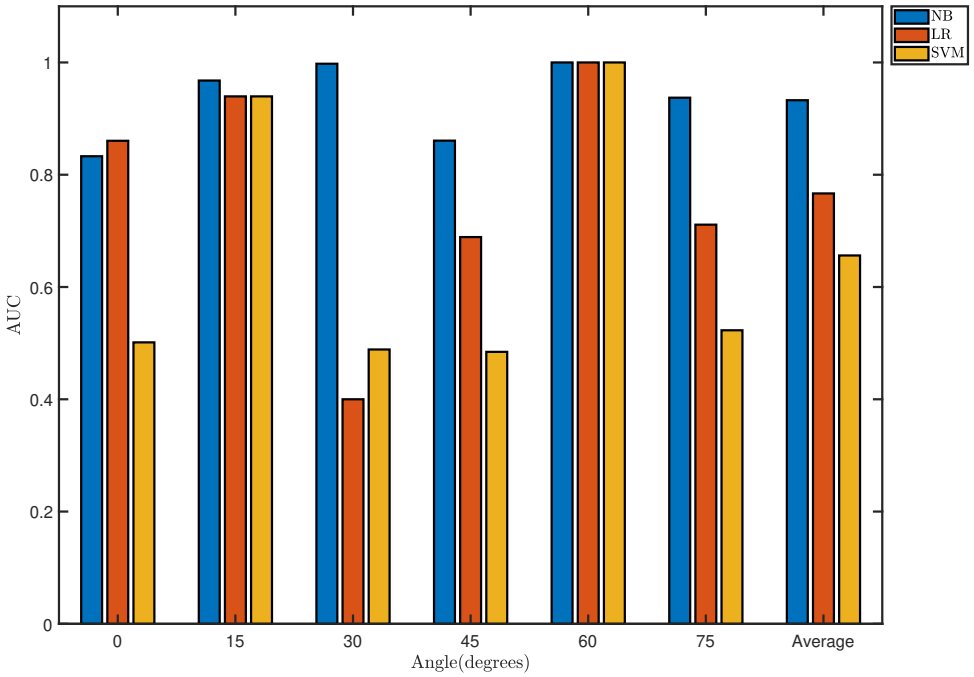

Figure 4.12: Area under the ROC for the different classifiers at the various angles.

of incorrectly identified data values. The TPR and FPR for each classifier is plotted as a receiver operating curve (ROC). The area under the ROC (AUC) is then calculated using the trapezoidal rule.

The classification results are shown in Figure 4.13 and Figure 4.12. We observed that naïve Bayes classifier performed better than other classifiers with an average AUC of 0.9327 while linear regression and SVM had an average AUC of 0.7667 and 0.6557 respectively. Linear regression under-performed because as observed in the visualisation of the data, the overlap of data from different angles complicate the linear classification of the data. Moreover, this also explains why SVM under-performed because of the difficulty of its linear kernel in classifying the data. It is likely that if a non-linear kernel such as the Gaussian kernel is implemented, it would improve its performance. However, naïve Bayes classifier performed adequately because it assumed the independence of each feature in deriving the probability of the feature vectors.

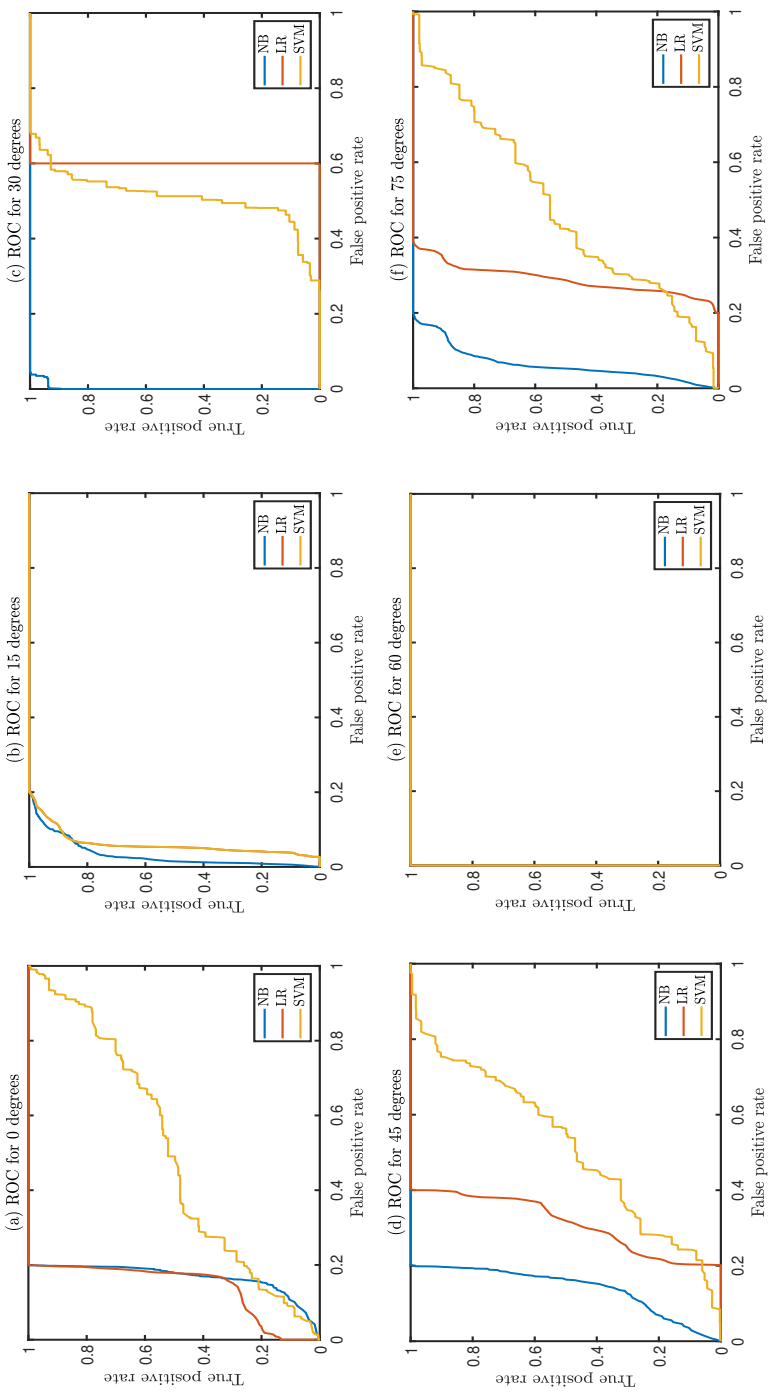

Figure 4.13: Receiver operating curve for the classifiers at the different angles. NB, LR and SVM represent naïve Bayes, Linear regression and Support vector machine classifiers respectively.

4.5 Conclusion

In this chapter, we have proposed a wholly textile data glove capable of measuring the joint angles of the interphalangeal joints. We achieved this by creating its novel weft knit strain sensors and its textile support structure in a single fabrication process. Additionally, we presented the electromechanical model of its sensors and verified it experimentally. Moreover, we evaluate the repeatability of the glove in a flexion and extension experiment. The results show that when a filter is applied to remove the noise, the consistency of the glove is verified. Furthermore, we evaluate three machine learning algorithms in classifying the output of the data. We observe that the drift in the sensor limits the performance of linear classification algorithms. However, the performance of naïve Bayes classifier illustrates that a non-linear classifier can perform excellently in classifying the glove's output.

Future work will investigate the performance of deep learning algorithms in a real-world classification scenario such as grasp or gesture recognition.

Chapter 5

Grasp Classification with Weft-knit Data Glove using Convolutional Neural Networks

Deep learning algorithms have been shown to classify data more accurately than classical machine learning algorithms. In this chapter, we apply a deep learning algorithm, a convolutional neural network (CNN), to classify data acquired from human participants using the data glove in two grasp classification scenarios. In addition, we compare the classification accuracy of CNN with classical machine learning algorithms applied on the data set. The results show that the simple CNN algorithm outperforms these classical machine learning algorithms.

5.1 Introduction

The use of weft knit strain sensors in wearable devices provides a substantial potential in designing textile wearable devices that are light weight, flexible and accurate [14]. Wearable devices that comprise of weft knit strain sensors include a knee sleeve and a respiration belt [13, 76]. In Chapter 4, we designed a lightweight textile data glove whose sensors and support structure are wholly textile. The entire glove is fabricated in a single manufacturing process thus eliminating the need for an external attachment between the support structure and the strain sensors. We achieved this by weft knitting conductive yarn and an elastomeric

yarn into weft knit strain sensors and weft knitting the rest of the glove with the elastomeric yarn using WholeGarment^{TM} technology. Consequently, our data glove provides the feel and appearance of normal clothing while being capable of sensing strain.

Classification of the acquired data into comprehensible information is vital for the increased adoption of wearable devices as it is impractical for physiotherapists to understand the raw data. The use of machine learning in conjunction with a data glove to classify acquired data into various sign languages is quite popular [119, 120, 121]. However, only a few studies have utilised machine learning techniques in classifying the grasps performed with a data glove. Particularly, Bernardin et al. [122] employed HMM to classify gestures made with a sensor fusion of tactile sensors and Cyberglove. The gestures were classified using Kamakura taxonomy into four major categories: power, intermediate, precision and thumbless grips. Classification accuracy was an average of 85.25% for the single-user system and 91.5% for the multiple-user system. In addition, Heumer et al. [123] compared 28 different classifiers categorised into Lazy, function approximators, Tree-based and Rules-based and Bayes classifiers in the classification of grasps performed using a Cyberglove. It was observed that on average, function approximating classifiers performed best with a minimum and maximum accuracy of 81.41% and 86.8% respectively. Although, the results of these classical machine learning algorithms are quite promising, they are limited by the selection of their hand-crafted features. The performances of these algorithms are limited because they rely on the manual selection of features that best represent the data.

In contrast, deep neural networks (DNN) extract optimal features directly from the data by its layer-by-layer processing and in-model feature transformation. This has enabled DNN to outperform classical machine learning techniques in various applications such as computer vision, speech recognition and disease detection [124, 125, 126, 127, 128, 129, 130]. Convolutional neural networks (CNNs) are the most popular DNN algorithms. Typically, they comprise of stacked convolutional filters, activation and pooling layers that enable its optimal selection of discriminative features in a time-series data. CNN algorithms have been very successful across several fields particularly in the field of rehabilitation using electrocardiography (ECG) and electromyography (EMG) data [131, 132, 133, 134].

Furthermore, CNN algorithms have been employed in grasp classification, albeit using a camera-based method. Notably, images of 500 objects were classified into four categories: pinch, tripod, palmar wrist neutral and palmar wrist pronated. In an offline test, the CNN algorithm performed at an accuracy of 85% for seen objects and an accuracy of 75% for unseen objects [135]. Seen objects were objects used for the algorithm's validation that were included in the training data while unseen objects were validation objects that were not included in the training data and were therefore novel to the algorithm.

In addition, CNNs have been utilised successfully in other glove-based gesture classification. The taxonomies in these studies include sign languages and custom taxonomies[136, 137, 138]. In particular, CNN was used to classify hand poses acquired with a data glove [139]. The classification accuracy was computed to be 89.4%. However, the study was limited to only one participant.

Although CNN algorithms have performed excellently across several classification applications, to the best of our knowledge, they have not been implemented in grasp classification using a data glove. Therefore, in this chapter, we propose applying CNN in classifying grasps performed with the weft knit data glove. We compare the results with popular classical machine learning algorithms. Our results show that the simple CNN architecture outperforms the classical machine learning algorithms.

5.2 Materials and Methods

5.2.1 Data Glove

In this study, we utilise the data glove illustrated in Chapter 4. As shown in Figure 5.1, it is a wholly knitted textile glove with no external attachment between the support structure and the strain sensors. This was achieved by knitting the sensors and the support structure in a single fabrication process using WholeGarment^{TM} technology. Data is transmitted by sewing conductive thread from the sensors in the data glove to the analog-digital converters (ADC) located in the microprocessor (Arduino Lilypad). A voltage divider circuit enables the

ADC to convert the resistance of the weft knit strain sensors to digital values between 0 and 1023. The microprocessor is connected to a computer (Intel I7-8750H, 16GB RAM, Nvidia GTX1060) for offline processing on MATLAB R2019. The USB port of the computer also powers the microprocessor. Furthermore, positive and negative connections are prevented from creating a short circuit by sewing the negative connections at the back of the glove and positive connections at the front of the glove. The measurement setup is depicted in Figure 5.1(b) and (c).

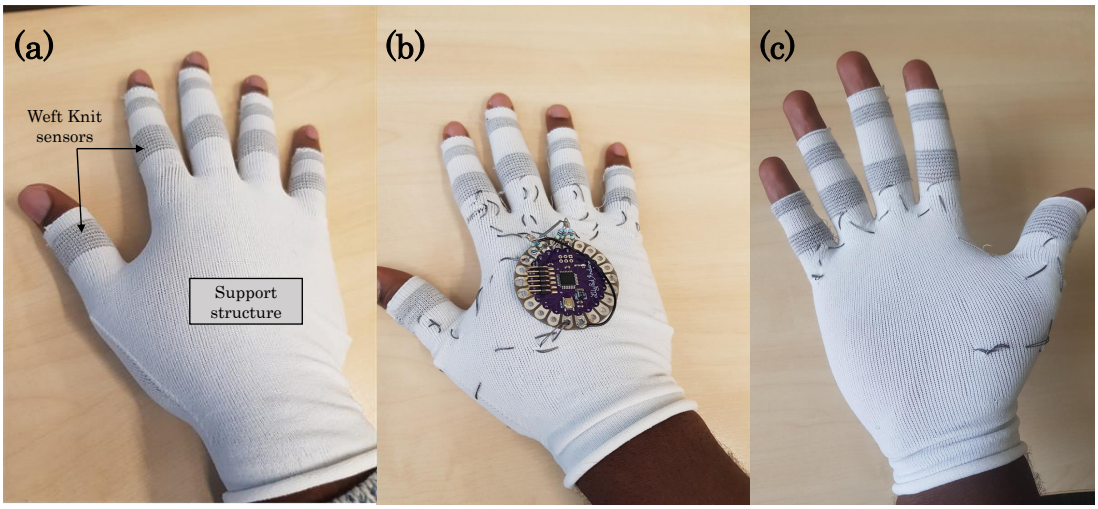

Figure 5.1: (a) Fabricated weft knit data glove, (b) Front view of the data glove and its embedded measurement setup, and (c) Back view illustrating connection with conductive thread.

5.2.2 Experimental Setup

This study was approved by the Faculty Research Ethics Committee of University of Leeds, UK (reference: MEEC 19-006). There were five healthy participants in this study including three males and two females. All participants signed an informed consent form. The ethical approval of this study and the consent form is shown in Appendix A.

The Schlesinger taxonomy [140, 141] was used in this study for selecting the grasp types. This taxonomy is widely known to be the earliest study to accurately

Table 5.1: Objects used in the experiment and their grasp types

Grasp Type	Objects
Cylindrical	Water bottle, flask, coffee cup, can, plastic bottle.
Hook	Mug, bag strap, headphones, kettle, back pack.
Lateral	Key, CD, ruler, id card, spoon.
Palmar	breadboard, phone, match box, multimeter, plastic case.
Spherical	Lemon, orange, apple, mouse, onion.
Tip	Pen, pencil, chopstick, stylus, ball pen.

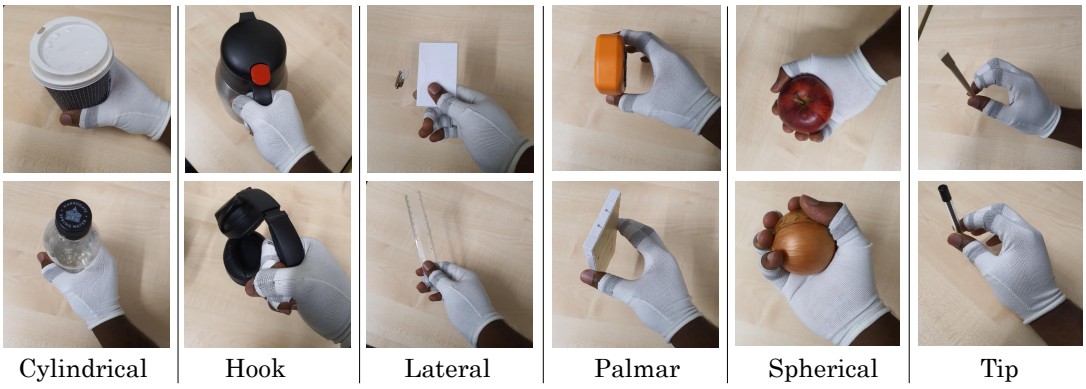

Figure 5.2: Grasp types of objects used in the study (Schlesinger taxonomy).

categorise the different grasps of a human hand [142]. We selected this taxonomy as a research constraint that acts as a base in which more patient-tailored taxonomies can be built upon.

For each grasp type shown in Figure 5.2, 5 objects were selected for the experiment. These objects and their corresponding grasp type are enumerated in Table 5.1. The participants performed five grasps per object thereby providing a total of 750 samples (5 participants x 5 grasps x 30 objects). Each grasp was for 30 seconds and participants were allowed to take breaks during the experiment to prevent fatigue.

5.2.3 Data Pre-processing

Data was recorded by the glove at a frequency of 20 hertz from the five sensors located at the distal interphalangeal joints. For each 30 seconds grasp of an object, 3000 (600 x 5 sensors) data values were recorded. This data obtained in the time series represents the signal features. As CNN requires a 3d image as an input, each grasp is represented as a 600x5x1 array. A short transition time was implemented between each new grasp to facilitate the collection of data. This transition time was later removed from the data to ensure that only the grasping period was recorded from the glove. In addition, this eliminated the complexities that involve the starting position of the grasping hand.

We perform no feature extraction or filtering of the data for CNN or the classical machine learning algorithms as this study aims to show the performance of algorithms in classifying raw data from weft knit strain sensors. Particularly, as research on classification using weft knit strain sensors is still nascent, it would be impractical to extract features manually.

5.2.4 CNN Algorithm

Convolutional Neural Networks are feed forward deep neural networks consisting of stacks of convolutional and pooling layers and then one or more fully connected layers [143, 144]. The convolutional layers employ convolution in extracting the features from the input data. Particularly, feature maps are generated by convolving the input signal with filters (kernels) consisting of neurons with learnable weights and biases. The convolution operation of the g-th feature map on the f-th convolutional layer located at position (a, b) can be described as:

$$v_{f,g}^{a,b} = \sigma\left(b_{f,g} + \sum_{i} \sum_{x=0}^{X_f-1} \sum_{y=0}^{Y_f-1} w_{f,g,i}^{x,y} v_{f-1,i}^{a+x,b+y}\right), \tag{5.1}$$

where $b_{f,g}$ is the feature map's bias, $w_{f,g,i}^{x,y}$ is from the weight matrix, X and Y are the kernel's height and width respectively, and $\sigma(\cdot)$ is a non-linear activation function such as Rectified Linear Unit (RELU), Sigmod or Tanh. In our architecture we use a RELU non-linear function and it can be represented as:

$$\sigma(k) = \max(0, k). \tag{5.2}$$

A pooling layer is added between convolutional layers to increase the invariance of the feature maps to minor changes in the input. It achieves this by aggregating the neighbouring outputs as a representative of the spatial region. In earlier studies, average pooling was the standard. However, maximum pooling has become the benchmark in state-of-the-art CNN approaches [143]. Similar to traditional neural networks, the fully-connected (FC) layer(s) classifies the input signal based on the extracted features obtained from previous layers.

5.2.5 CNN Architecture

An ablation study was performed to determine the optimal CNN configuration. Four parameters (i.e. the number of convolutional blocks, the number and size of convolutional filters, and the dropout layer's probability) were varied to create 16 CNN configurations. These parameters are known to significantly impact the performance of a CNN [145]. The configurations and their parameters are shown in Table 5.2. All other parameters were constant for all configurations. In particular, each convolutional block had a rectified unit layer (RELU) acting as a nonlinear activation function, a downsampling pooling layer with filters of size 2x1 and a dropout layer to reduce overfitting. The last convolutional block was connected to a fully-connected layer with 6 hidden units representing the 6 grasp types, a softmax layer which employs a cross entropy loss function and a classification layer. Moreover, the networks were trained at a dynamic learning rate using stochastic gradient descent. The initial learning rates were 0.001 and were reduced by 95% after every 10 epochs. The batch sizes were fixed at 16 and the number of epochs was 36.

These configurations were utilised in classifying the data in two experiments. In the first experiment, one grasp was used as the validation data while the remaining 4 grasps were used as the training data i.e (80% training data and 20% validation data). Thereafter, cross validation was performed by repeating the experiment 5 times where each grasp was utilised as the validation data. In the second experiment, the CNN configurations were trained with 4 out of 5 objects with the remaining object as the validation data i.e (80% training data and 20%

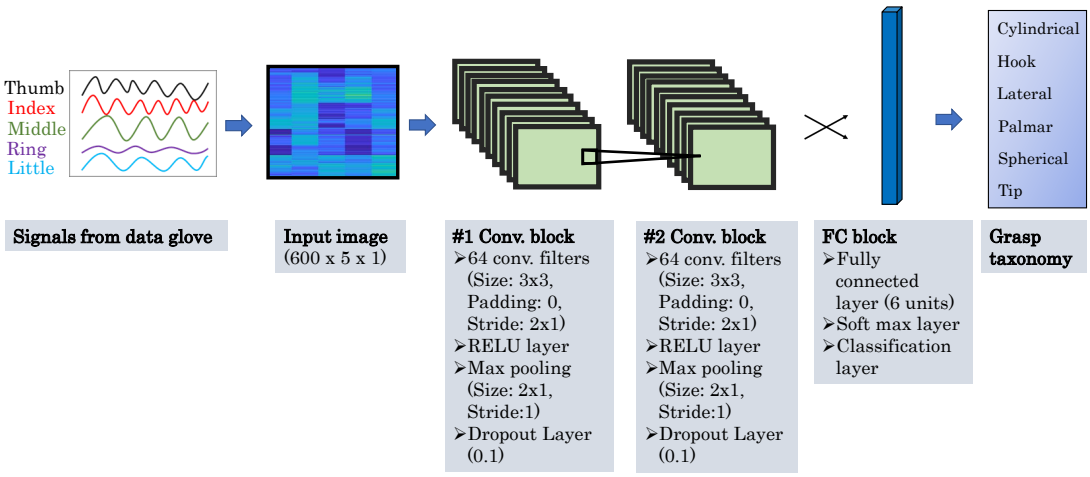

Figure 5.3: CNN architecture (C15) for grasp classification.

validation data). Cross validation was also performed by repeating the experiment 5 times where each object was used as the validation data. The average accuracy of each CNN classifier in both experiments was calculated. These experiments were performed on Participant 1's data with the aim of utilising the best CNN configuration in terms of classification accuracy on an expanded experiment comprising of all participants.

The results of this study are also shown in Table 5.2. It was observed that CNN configurations with two convolution blocks had a higher accuracy than similar configurations with only one convolutional block. However, the higher accuracy occurred at a computation cost as observed in the increased run times seen in configurations with two convolutional blocks. In particular, configurations with two convolutional blocks had run times that were on average 1.5 seconds longer than similar configurations. However, the aim of this ablation study was to select the optimal CNN configuration in terms of its accuracy. Therefore, classifier C15 illustrated in Figure 5.3 was seen to achieve the highest average classification accuracy and was selected as the optimal CNN configuration. Moreover, in comparison with configurations with two convolutional blocks, the computation time of C15 was relatively low. No further optimisation of C15 was performed in its implementation on the expanded experiment. This study was important in ensuring that the optimal parameters were selected for the CNN algorithm.

Table 5.2: CNN configurations and their respective parameters.

Config.	**Conv. Filter size**	**Number of Conv. Filters**	**Number of Conv. blocks**	**Dropout Proba-bility**	**Accuracy**	**Run time**
C1	3x2	32	1	0.1	81.00	4.5s
C2	3x2	32	1	0.2	82.67	4.4s
C3	3x2	32	2	0.1	83.67	6.0s
C4	3x2	32	2	0.2	82.00	6.1s
C5	3x2	64	1	0.1	79.67	5.0s
C6	3x2	64	1	0.2	76.33	5.0s
C7	3x2	64	2	0.1	83.67	6.7s
C8	3x2	64	2	0.2	81.00	6.9s
C9	3x3	32	1	0.1	78.67	4.7s
C10	3x3	32	1	0.2	80.67	5.0s
C11	3x3	32	2	0.1	83.67	6.3s
C12	3x3	32	2	0.2	82.00	6.1s
C13	3x3	64	1	0.1	81.00	5.1s
C14	3x3	64	1	0.2	78.33	5.1s
C15	3x3	64	2	0.1	**86.00**	6.2s
C16	3x3	64	2	0.2	82.34	6.3s

5.2.6 Classification Scenarios

In this study, we evaluate the performance of the selected CNN (C15) and other algorithms on the following classification scenarios. These scenarios are:

Object Seen

This scenario exemplifies applications where the validation objects are known. That is, the objects in the validation data are part of the training data. Traditionally, classifiers will achieve high accuracy in this scenario but because weft knit strain sensors experience hysteresis and drift, the performance of the classifiers will be adversely affected. In this scenario, the classifiers were trained with 4 out of 5 grasps of an object and validated with the last grasp of the object (i.e.

120 images for training and 30 images for validation per participant). Cross validation was performed by repeating this experiment 5 times where each grasp of an object was selected as the validation data and computing the average accuracy. Furthermore, this was repeated for all participants and the average accuracy was recorded.

Object Unseen

This scenario illustrates applications where the objects grasped by the patient are unknown. It ensures that the therapist is provided with some information about the grasp type despite the object being held by the patient is not part of the training data set. In these experiments, the classifiers were trained with 4 out of the 5 objects in each grasp type and were validated with the last object (120 images for training and 30 images for validation per participant). Similar to the object seen experiment, cross validation was performed by repeating the experiment 5 times where each object was selected as the validation data and the average accuracy was computed. In addition, the experiment was repeated for all participants.

5.2.7 Comparative Machine Learning Techniques

In this study, popular machine learning techniques were implemented to compare their performance with the CNN in the various applications. These techniques include k-nearest neighbours (k-nn), Support Vector machine (SVM) and Decision Trees (trees) [108, 146, 147, 148, 149]. The default parameters in Matlab R2019's Machine Learning Toolbox were selected for the various configurations of these techniques. As there are no classification studies with weft knit strain sensors, these parameters were chosen from a popular and reliable toolbox to provide a verifiable comparative study.

k-nearest neighbours (k-nn)

k-nn is a probabilistic pattern recognition technique that classifies a signal output based on the most common class of its k nearest neighbours in the training data [150]. The most common class (also referred to as the similarity function) can

be computed as a distance or correlation metric. In this study, we select the Euclidean distance as the similarity function as it is the most commonly used metric in k-nn. The number of k-neighbours was varied to be 1, 10 and 100 for fine, medium and coarse k-nn techniques respectively. The probability density function $p(\mathbf{M}, c_j)$ of the output data $\mathbf{M}$ belonging to a class c_j with jth training categories can be computed as:

$$p(\mathbf{M}, c_j) = \sum_{n_z \epsilon knn} d(\mathbf{M}, n_z) V(n_z, c_j), \tag{5.3}$$

where n_z is a neighbour in the training set, $V(n_z, c_j)$. The Euclidean distance $d(\mathbf{M}, n_z)$ of output data $\mathbf{M}$ and neighbour n_z can be calculated as:

$$d(\mathbf{M}, n_z) = \sqrt{\sum_{z=1}^{k} (\mathbf{M}_z - n_z)^2}. \tag{5.4}$$

Gaussian SVM

Traditionally, support vector machines (SVM) is a supervised learning method used for performing linear classification. However, the data obtained during experiment cannot be separated using linear hyperplanes because of the close resemblance of some grasp types and the hysteresis and drift that occur in a weft knit strain sensor [151]. In order to use SVMs for non-linear classification, we apply Gaussian kernels which can map the data into an unlimited dimension space. Three variations of Gaussian SVM were implemented by selecting 7.9, 32, and 130 on the kernel scale for fine, medium and coarse Gaussian SVM respectively. The decision function for Gaussian SVM classification of pattern data $\mathbf{u}$ can be represented as:

$$f(\mathbf{u}) = \text{sign}\left(\sum_{k=1}^{h} \lambda_k c_k \exp\left(\frac{-\|\mathbf{u}_k - \mathbf{u}\|^2}{2\sigma^2}\right) + t \right), \tag{5.5}$$

where c_k is the class label for the k-th support vector $\mathbf{u}_k$, λ_k is the Lagrange multiplier, and t is the bias.

Decision Tree

Decision tree is a supervised learning technique that aims to split classification into a set of decisions that determine the class of the signal [152]. The output of the algorithm is a tree whose decision nodes have multiple branches and its leaf nodes deciding the classes. Three configurations of the Decision tree algorithm were implemented by varying the maximum number of splits as 100, 20 and 4 for fine, medium and coarse Decision tree respectively.

5.3 Results

5.3.1 Object Seen

Figure 5.4 illustrates the accuracy of the classifiers when the object to be grasped is known. CNN outperforms all the classical classifiers with an average accuracy of 88.27%. This accuracy is slightly lower than results obtained by commercial data gloves in other classification scenarios. This is caused by the drift that occurs in weft knit strain sensors. Drift causes the output of the sensor to stray despite the absence of change in its extension.

Figure 5.5 illustrates the confusion matrix of the average results of all participants in the object seen scenario. The confusion matrix shows that grasps of Hook, Lateral, Spherical and Tip are classified excellently at 87.2%, 92.8%, 92% and 92.8% respectively. In contrast, the average classification accuracy of Cylindirical and Palmar grasps were significantly lower at 80% and 84.8% respectively.

Figure 5.6 depicts a detailed view of the average classifier class performance on each participant. CNN outperforms all classifier classes for each participant in terms of its mean accuracy. In particular, it outperforms other classifier classes by an average of 21% in terms of its mean classification accuracy. Moreover, CNN achieves an accuracy of 99.33% for Participant 5 (P5) because the glove was manufactured to fit the hand size of this participant.

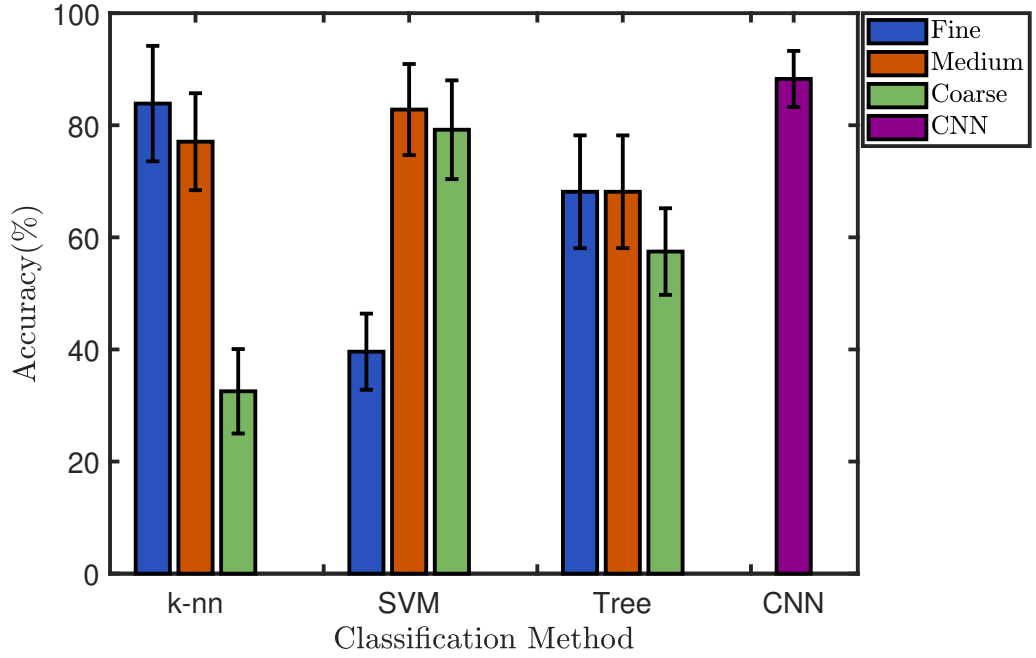

Figure 5.4: Object seen. Bars represent mean accuracy of the classifier and error-bars illustrate the standard deviation.

Figure 5.5: Confusion matrix depicting the average results of the object seen scenario.

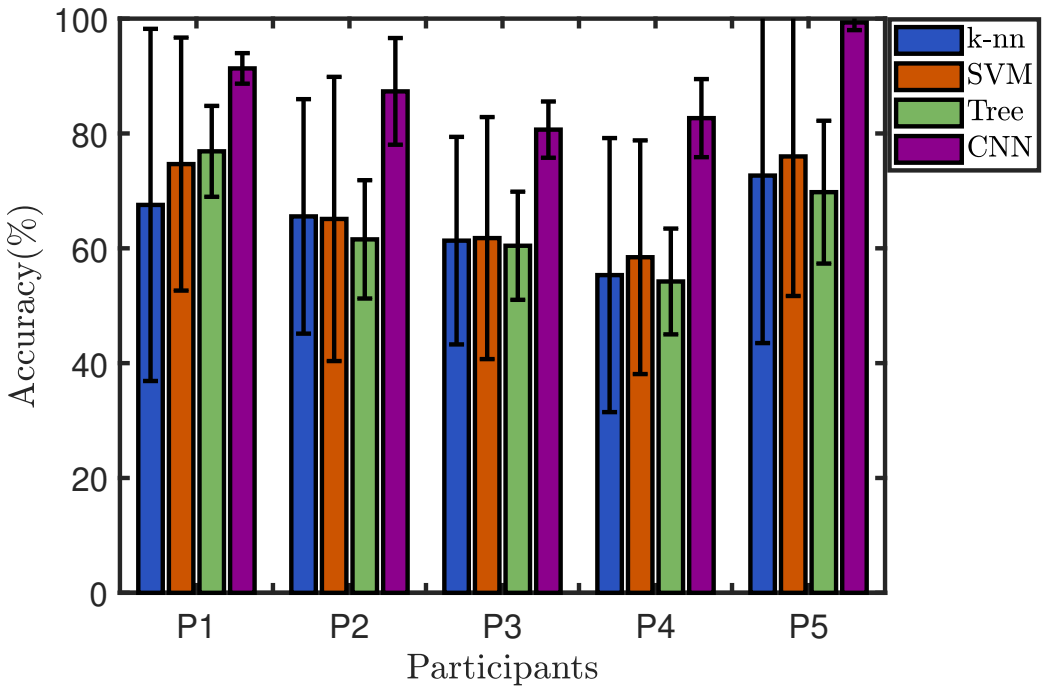

Figure 5.6: Detailed results of object seen. Bars represent mean accuracy of the classifier class performance for each participant and error-bars illustrate the standard deviation.

5.3.2 Object Unseen

Figure 5.7 depicts the accuracy of the classifiers when the validation object is unknown. This exemplifies applications where the glove may be used to grasp objects not within the training data. It was observed that the accuracy of the classifiers in this scenario were lower than the accuracy seen in object seen scenario. This was expected as it is common in glove-based gesture classification because the validation objects are not part of the training data (i.e., they are unknown). Nonetheless, CNN outperforms the classical machine learning methods with an average accuracy of 75.73%.

Figure 5.8 illustrates an expanded view of the performance of each classifier class on the participants. CNN outperforms other classifier classes in each participant in terms of its mean accuracy. Particularly, for P5, it outperforms the next best classifier class by 23.8%.

Table 5.3: Accuracy of CNN classifier for each participant in the two classification scenarios

Participants	**Object seen**		**Object unseen**	
	Mean	**Std.**	**Mean**	**Std.**
P1	91.33	2.66	76.00	4.90
P2	87.33	9.29	74.00	13.40
P3	80.67	4.90	69.33	12.54
P4	82.67	6.80	66.67	8.69
P5	99.33	1.33	92.67	9.98
Average	**88.27**	**5.00**	**75.73**	**9.90**

Figure 5.9 depicts the confusion matrix of the average results of all participants in the object unseen scenario. Similar to the results obtained in the object seen scenario, the algorithm struggled with classifying Cylindrical and Palmar objects with classification accuracy of 63.2% and 68.8% respectively. In contrast, higher classification accuracy were achieved in Hook, Lateral, Spherical and Tip objects with accuracy of 72.8%, 84%, 79.2% and 86.4% respectively.

5.4 Discussion

In the last decade, the implementation of convolutional neural networks in several applications has been very popular. These applications include image and text classification, disease recognition and gait classification. In these applications, CNN has outperformed popular machine learning algorithms because of its ability to automatically extract features from the data set. In contrast, machine learning algorithms require manual feature extraction techniques such principal component analysis or dimensionality reduction to produce accurate classification accuracy. However, despite its popularity, there has been no research on its application to grasp classification from data obtained with a piezoresistive data glove. Therefore, this study aims to bridge that gap by implementing a CNN architecture that outperforms classical machine learning algorithms in this application.

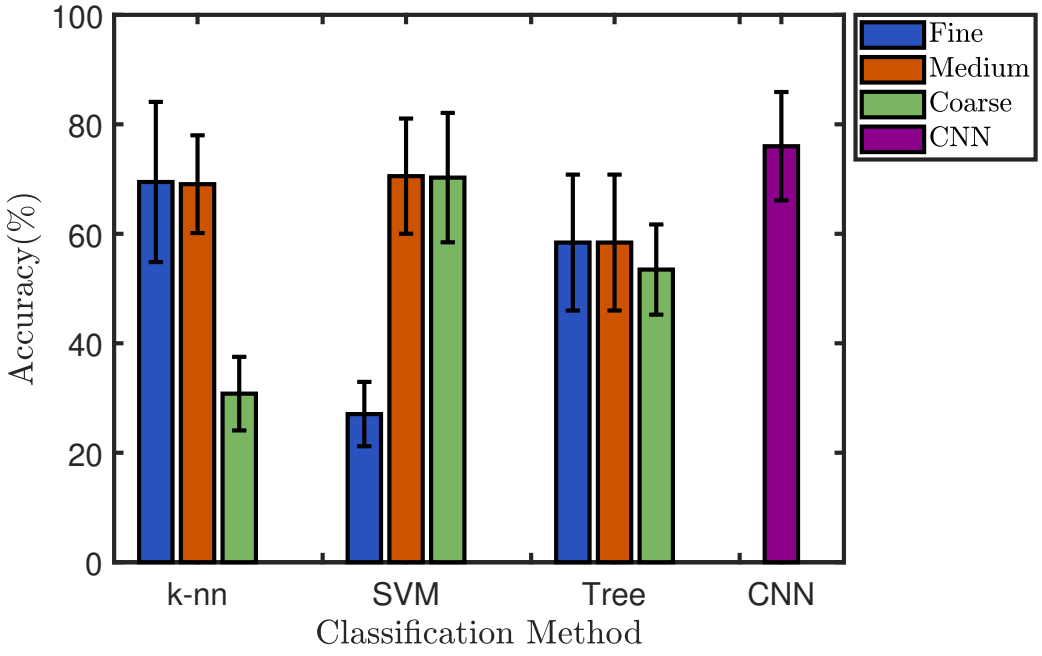

Figure 5.7: Object unseen. Bars represent mean accuracy of the classifier and error-bars illustrate the standard deviation.

Our results show that a simple CNN architecture outperforms k-nn, Gaussian SVM and Decision Tree algorithms in both classification scenarios. Moreover, the simplicity of our CNN architecture is intentional. Particularly, the absence of research illustrating the implementation of CNNs in this application caused us to investigate the performance of a simple architecture before applying more complex CNN architectures.

In addition, the results in Table 5.3 illustrate that the accuracy of all algorithms are higher for P5 (participant 5) than for other participants. This transpired because the data glove was created to fit the hand size of this participant. This illustrates the potential of textile wearables, as the one-size-fits-all constraints can be eliminated by fabricating these devices alongside the conventional size measurements (for example: XS-extra small, S-small, M-medium, L-large etc.) that have been used in the clothing industry for several decades. Therefore, by utilising weft knit strain sensors, higher classification accuracy can be achieved by creating perfectly fitting wearables based on the user's physical dimensions.

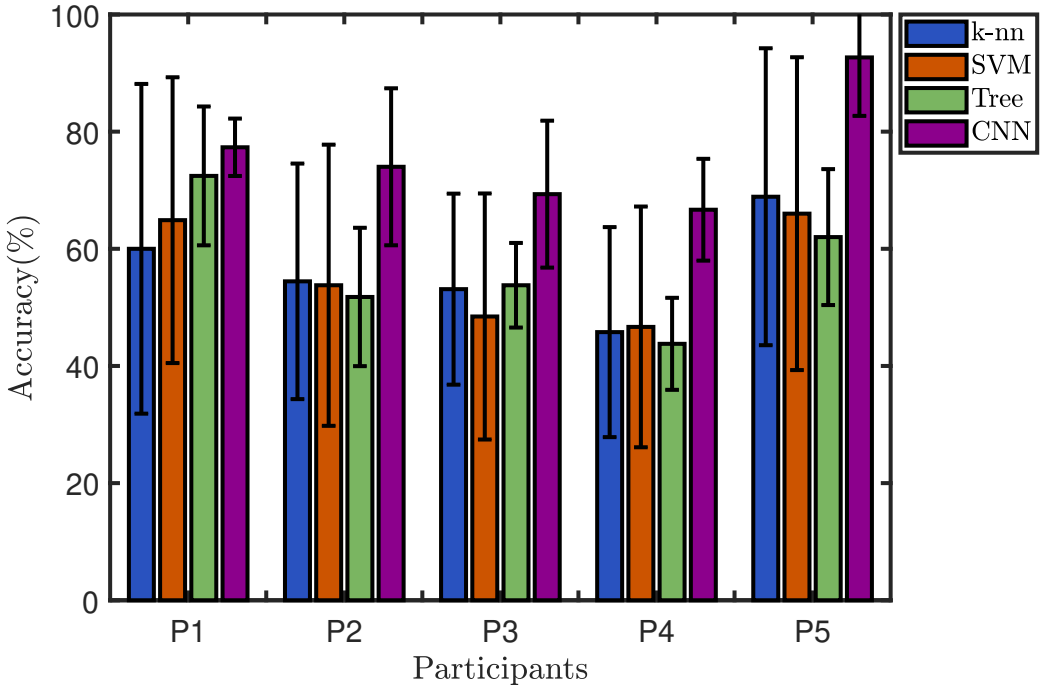

Figure 5.8: Detailed results of object unseen. Bars represent mean accuracy of the classifier class performance for each participant and error-bars illustrate the standard deviation.

Furthermore, the results of this study in Table 5.4 show that the average accuracy of most classifiers reduced in the second classification scenario. This scenario depicted an application of the glove where the grasp type of the object is unknown. Consequently, the validation data set comprises objects not in the training data set. Therefore, it is a more difficult classification problem for the algorithms. However, despite this difficulty, CNN still outperforms other classifiers.

Although, CNN outperforms other classifiers, its average accuracy among the participants is less than 90%. However, we have shown that for participants for whom the glove is specifically designed for, then the average accuracy was much higher (>99% for seen objects and >92% for unseen objects) regardless of whether the validation object was part of the training set. This is remarkable for classification using weft knit strain sensors as they are still technologically immature and struggle with hysteresis and drift. This is a fertile area for further

Figure 5.9: Confusion matrix depicting the average results of the object unseen scenario.

Table 5.4: Accuracy of the classifiers in the two classification scenarios. The best classifier is highlighted with a bold font.

Classifier	**Object seen**		**Object unseen**	
	Mean	**Std.**	**Mean**	**Std.**
Fine k-nn	83.87	10.30	69.47	14.63
Medium k-nn	77.07	8.65	69.07	8.93
Coarse k-nn	32.53	7.53	30.80	6.72
Fine SVM	39.60	6.79	27.07	5.88
Medium SVM	82.80	8.13	70.53	10.52
Coarse SVM	79.20	8.81	70.27	11.82
Fine tree	68.13	10.06	58.40	12.42
Medium tree	68.13	10.06	58.40	12.42
Coarse tree	57.47	7.72	53.47	8.24
CNN	**88.27**	5.00	**75.73**	9.90

research as more deep learning architectures such as LSTM (long short-term memory) or CNN-LSTM can be applied in the classification of their raw data.

Recently, a study illustrated the use of LSTM on grasp classification using a knitted glove [153]. It will be interesting to compare the performance of CNN to LSTM in grasp classification from data acquired with a knitted data glove. Although the memory properties of LSTM should provide an advantage over CNN [138], CNN has also been seen to outperform LSTM [136]. Therefore, it will be interesting to see if more complex deep learning algorithms improve the accuracy of grasp classification using data gloves. Higher performances (>95% average accuracy) in this application may rapidly increase the commercial adoption of data gloves in rehabilitation.

In addition, a data glove can measure the progress of stroke patients by calculating their range of motion and the force produced by the finger muscles. Progress in the patient's rehabilitation can be observed if there are significant increases in the range of motion and the muscular force. The weft knit data glove can be used to measure their range of joints by utilising the exponential correlation between the change in resistance of the sensor and the angle shown in Chapter 4. In addition, the speed at which the change in resistance occurs can be correlated with the muscular force at the fingers. Although, this application is outside the scope of the thesis, it provides a good research area that may also aid the commercial adoption of this device in rehabilitation.

5.5 Conclusion

In this chapter, we have pioneered the use of convolutional neural networks on grasp classification using a piezoresistive data glove. Using our fabricated weft-knit data glove, we observed that our simple CNN architecture outperformed classical machine learning techniques in the two classification scenarios. Notably, the average classification accuracy of our CNN was 88.27% and 75.73% in the object seen and object unseen scenarios respectively. Future work will involve the application of more robust deep learning approaches to improve the classification accuracy.

Chapter 6

Effect of Miss and Tuck Stitches on a Weft Knit Strain Sensor

Miss stitches reduce the width and length of a fabric while tuck stitches increase the width of a fabric but decrease its length. These structural changes should affect the contact points in the sensor and consequently, the piezoresistivity of the sensor. Therefore, this chapter investigates the impact of incorporating miss and tuck stitches on the piezoresistivity of a weft knit strain sensor. Particularly, the electromechanical models of a tuck stitch and a miss stitch in a weft knit strain sensor are proposed. These models were used to develop loop configurations of sensors consisting of various percentages of miss or tuck stitches. Finally, the developed loop configurations were simulated and verified experimentally in a tensile test. The results show that changes in the percentage of tuck or miss stitches significantly affect the piezoresistivity of the sensor.

6.1 Introduction

In the last decade, the application of knit fabrics has expanded from the traditional textile applications to their use in the creation of wearable electronics. From the use of warp knit to create textile antennas to the use of weft knit to create strain sensors, the application of knitting to create conventional electronics is being adopted rapidly [10, 13]. In particular, conductive weft knitted fabrics

have been utilised as strain sensors because of their elastic structure and piezoresistivity [14]. The piezoresistivity of the sensor is the behaviour of the sensor's electrical resistance when load is applied or the sensor is extended.

In recent past, several studies have investigated the impact of loop architecture on the piezoresistivity of the sensor. Notably, the impact of knitting parameters on a weft knit strain sensor's piezoresistivity was intensively studied by Atalay et al. [37, 38]. The sensors were created by knitting double covered elastomeric and silver-coated conductive nylon yarns in an interlock knit. Particularly, courses of the conductive nylon yarns were embedded on a host fabric. The host fabric was knitted in an interlock structure with elastomeric yarn. This sensor configuration was selected empirically by the authors for its high gauge factor and linearity. Subsequently, the effect of changes in i) the input tension and linear density of the elastomeric yarn, and ii) the input tension of the conductive yarn were explored. It was observed that a decrease in the elastomeric yarn's input tension or its linear density caused the electrical resistance to increase significantly. This was because they affect the number of contact points which in turn affects the contact resistance. Moreover, the results showed that sensors knitted with a lower elastomeric yarn input tension exhibited a longer linear working range. Furthermore, the study illustrated that increases in the input tension of the conductive yarn caused an increase in the electrical resistance of the sensor. This occurred because an increase in the conductive yarn's input tension reduced the stitch length. Due to the interlock structure of the host fabric, a reduced stitch length decreases the contact areas between the conductive loops. Consequently, the reduced contact areas increased the electrical resistance of the sensor. This phenomenon is consistent with Holm's contact theory [73].

In a subsequent study, the effect of the addition of elastomer was investigated by Atalay et al. [15]. Two samples of sensors were manufactured in a plain knit. A sample of sensors was knitted with conductive yarn while the other sample of sensors was knitted in a structure that comprised of elastomer and conductive yarn. It was observed that the sample knitted with only conductive yarn showed an inversely proportional relationship between its change in resistance and its extension, while the second sample with an elastic structure showed a directly proportional relationship between its change in resistance and its extension. This

difference in piezoresistive behaviour occurred because their electric circuits are fundamentally different. A major factor in the piezoresistive behaviour of a weft knit strain sensor is the contact resistance that occurs between two conductors. Particularly, in the sensor without the elastomer, contact resistance occurs at the intermeshing of one conductive loop with another conductive loop. Conversely, in the sensor with the elastomer, the interlocking of a conductive loop with a non-conductive loop does not create a contact resistance. However, contact resistance still occurs in the sensor with the elastomer because the elastomer increases the tightness of the fabric such that the legs of the same conductive yarn loop make contact.

In summary, changes in the knitting parameters have affected the piezoresistivity of a weft knit strain sensor. However, all the previous studies mentioned have been implemented using only a knitted loop stitch. In contrast, there are two other types of stitches, and they are the miss and tuck stitches. These three stitches are shown in Figure 6.1. The tuck stitch occurs when a needle accrues more than one stitch thus tucking the extra stitch behind the first stitch. The extra stitch is the tuck stitch and it changes the structure of the fabric because its legs are not connected to the head of a previous loop. A miss stitch materialises when a needle does not a collect a yarn, thus allowing the yarn to float behind the needle and connecting the loops on either side of it [57]. These stitches can be combined with a knitted loop stitch to create different sensor configurations that may have different piezoresistive behaviour.

Therefore, in this study, we aim to investigate the effect of miss and tuck stitches on the piezoresistivity of a weft knit strain sensor. Particularly, we achieve this by proposing for the first time, detailed electro-mechanical models of miss and tuck stitches. These models are then simulated for loop configurations comprising of varying percentage of miss stitches or tuck stitches to observe their impact on the sensor's piezoresistive behaviour. In particular, we ensure that the effect of either miss or tuck stitches are observed separately by ensuring that the loop configurations have only miss stitches or tuck stitches. Thereafter, the predicted behaviour is validated experimentally by tensile testing sensors knitted with the same loop configurations.

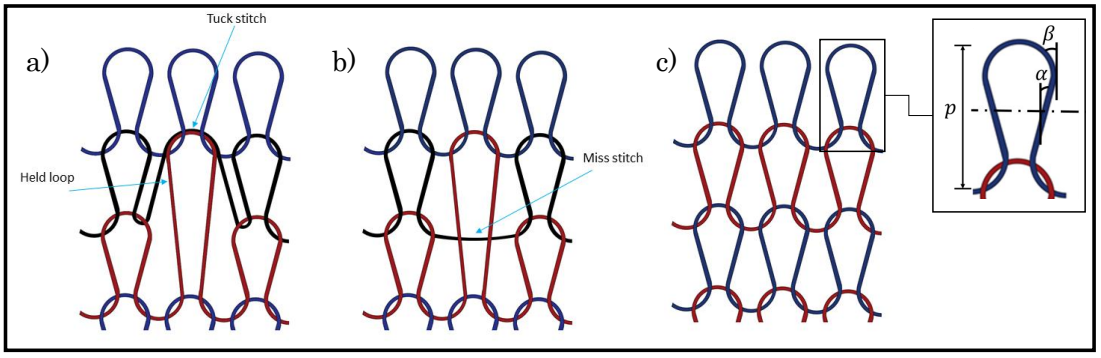

Figure 6.1: Types of loop stitches. a) Tuck loop stitch, b) Miss stitch, c) Knitted loop stitch. The held loop is the knitted loop stitch tucked by a tuck stitch. p is the course spacing, α and β are the loop and interlocking angles respectively.

6.2 Related Work

The effect of miss and tuck stitches on a weft knit strain sensor was described in the patent application [154]. Notably, the author describes a series of experiments where the effect of miss and tuck stitches were studied on determining the optimal configuration for different applications. For these experiments, 4 samples of sensors were created by knitting conductive yarn in different percentages of miss and tuck stitches combined with a constant percentage of knitted loop stitches. A control sample was also knitted with only knitted loop stitches. The constant percentage of knitted loop stitches in each sample was 50%. The percentage ratio of miss stitches to tuck stitches (M2T) were (5:45), (10:40), (45:5) and (40:10).

The first experiment was implemented to determine the optimal structure for use in a resistive strain sensor. The parameters measured were the mean electrical resistance (MER), the dynamic range i.e. maximum extension and the effect of fabric thickness and optical porosity on the MER. The observations drawn from the experiment were:

1. The samples with M2T of (40:10) and (10:40) showed the largest dynamic range. This is excellent for strain applications because the sensor can absorb the strain due to its flexibility.

2. The variation of resistance values was more stable in the four samples than in the control sample. This allows for more accurate measurements in strain sensing applications. The samples with the most stable resistance values were samples with M2T of (10:40) and (45:5).

3. Samples with a higher fabric thickness had a lower MER while samples with a lower optical porosity had a lower MER. A lower MER is needed for an optimal regulation of the contact resistance and this is achieved because a higher fabric thickness and lower optical porosity increase the contact area between the yarns. It was observed that all four samples had a lower MER compared to the control sample with samples with M2T of (10:40) and (45:5) being the lowest.

Therefore, a strain sensor would be optimised if it is made with samples that show a large dynamic range and less variation in MER; and have a high fabric thickness and a low optical porosity. The sample which fits this criterion is the sample with 10% miss stitches and 40% tuck stitches.

The second experiment involved placing two specific weights (150gm and 400gm) on the samples and measuring the resistance of the sensor. This was then plotted with the baseline resistance before any weights were added. The plots show the linear fits of the resistances of the samples at the various weights (0, 150 and 400gm) with varying negative gradients. The sensor with the highest coefficient of determination, R^2, was chosen as the optimal sample. The samples with the highest tuck stitches (M2T of (10:40) and (5:45)) were seen to have the highest R^2 value. It was assumed that this occurred because the tuck stitches increased the contact area and thus could regulate the contact resistance.

The third experiment involved human subjects of different weights placing their weights on the samples by standing with only one foot on the samples. The aim was to demonstrate the response of the sensor to the pressure from human concentrated weight in order to simulate what will happen in an application such as socks that measure pressure of the feet. The experiment was only performed on samples with M2T of (5:45) and (10:40). The resistance was measured relative to the weight of each subject at different positions in the sensor and plotted alongside the baseline resistance. The locations chosen to measure the resistance

on the sensor were the points adjacent to the ankle and ball of the foot. The plot of the resistance relative to the weight provided a logarithmic response unlike the linear response that was obtained in the previous experiment. The optimal fabric was chosen on the basis of its gradient as a small gradient is favoured because it illustrates a larger response to weight applied. The sensor with 10% miss stitches and 40% tuck stitches was found to have the smaller gradient and was chosen as the optimal sensor.

Other experiments used a larger variation of M2Ts in the samples and in one of them, samples were tested to deduce how resistance behaves relative to pressure applied in the wale and course directions. It was observed that when pressure was applied in the course direction, there was no visible change in resistance. But in the wale direction, there was a visible change in the resistance when pressure was exerted. The author also notes that the sensors with 10% miss stitches and 40% tuck stitches exhibit a solid inverse linear relationship between the resistance and load. This was attributed to the high percentage of tuck stitches as it increases the number of contact points. Another experiment sought to find out the relationship between the resistance of sensors with miss and tuck stitches and temperature changes. It was observed that sensor displayed a linear relationship between its resistance and changes in its surrounding temperature. It was also observed that the samples with a higher number of tuck stitches had a better linear fit than other samples.

The experiments in this patent aim to ascertain if the addition of miss and tuck stitches will optimise the resistance of the fabric for specific applications. This patent does an excellent job in illustrating how miss and tuck stitches can optimise a sensor for different applications. However, the conclusions are purely empirical and there is no theoretical model that describes the impact of the addition of miss and tuck stitches. Additionally, the rationale behind the choice of percentage of miss and tuck stitches in each loop configuration is not illustrated. Furthermore, combining miss and tuck stitches makes it more difficult to understand their separate impact on the piezoresistive behaviour of the sensor.

In contrast, the effect of miss and tuck stitches on a conductive weft knit fabric were investigated separately [155]. Samples were knitted with knit stitches and different percentages of either miss or tuck stitches. Subsequently, their resistance

was measured and it was observed that the increases in the percentage of tuck or miss stitches caused a decrease in the resistance of the sensor. However, this study is only experimental as there is no theoretical model to explain the cause of the impact. In addition, this study was limited to the impact of miss and tuck stitches on the initial resistance of the sensor. It did not investigate the impact of miss and tuck stitches on the sensor's piezoresistivity.

Furthermore, the impact of consecutive miss stitches on the overall resistance of a conductive weft knit fabric was also investigated by Liu et al. [156]. Samples of the fabric were knitted in a plain base structure with a course containing one knitted loop and varying numbers of consecutive miss stitches. It was observed that as the number of consecutive miss stitches increased, the resistance of the fabric decreased. This effect materialised because of the reduced contact resistance caused by the miss stitches. However, this study only investigates the impact on the initial resistance of the sensor and not its behaviour when the sensor is extended.

This chapter addresses the research gap neglected in previous studies. Notably, we investigate the effect of miss and tuck stitches on a weft knit strain sensor separately. Furthermore, unlike previous studies, we do not limit our study to only the initial resistance of the sensor. We also investigate the piezoresistivity of the sensors as they are extended. Particularly, the mean resistance, the linear and quadratic R^2 values of the sensor's piezoresistivity. In addition, we do not restrict this study to only experimental observations. In contrast, we propose electromechanical models that explain the behaviour of the sensors.

6.3 Materials and Methods

6.3.1 Electromechanical Model of a Tuck stitch

This section describes a novel resistive model of a tuck stitch in a weft knit strain sensor. The basic assumptions used to formulate this model are:

- The conductive yarn used is a perfect intrinsic conductor.

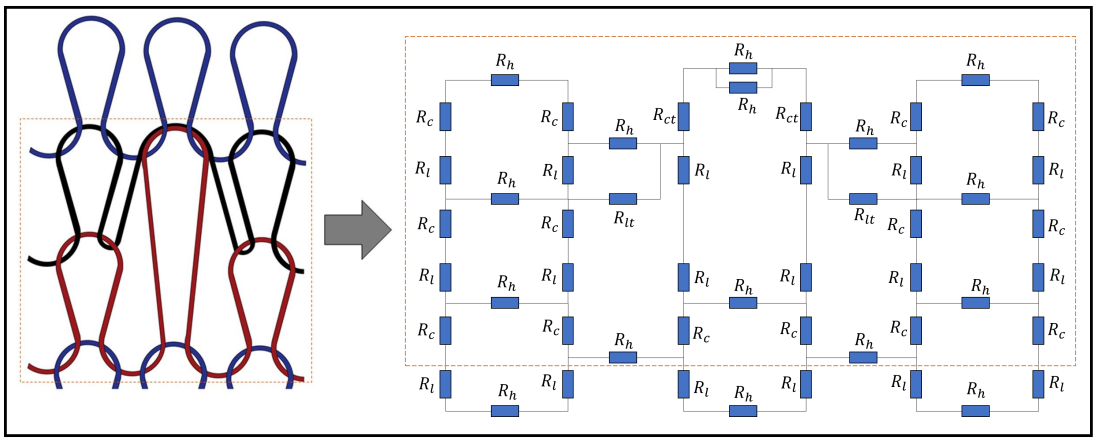

Figure 6.2: Resistive model of a tuck stitch in a weft knit strain sensor.

- The lengths of the head of a tuck stitch and the head of its held knitted loop stitch are equal.
- The head and sinker of a knitted loop stitch are of equal lengths.

Figure 6.2 illustrates the theoretical model of a tuck stitch knitted with conductive yarn. In this model, we postulate that a tuck stitch adds length resistances as a result of its legs and heads. Furthermore, we claim that it changes the contact resistance between the loops because of the contact pressure it adds to the fabric, especially at the location of the tuck stitches. Particularly, plain knit fabrics with tuck stitches are known to be less extensible than plain knit fabrics without tuck stitches because the tucked loops add an extra layer of pressure at the junctions where the intermeshing of loops occur [57]. Therefore, by representing its geometrical parameters with equivalent resistive values, we model the tuck stitch as a resistive circuit.

Using Postle model [16], we consider the loop leg, L_l, as a bent beam and derive its length as:

$$L_l = \frac{p}{\sqrt{2(\sin\alpha + \sin\beta)}} f(k,\gamma), \tag{6.1}$$

where $f(k,\gamma)$ is the difference between the complete and incomplete integrals and can be calculated as:

$$f(k,\gamma) = \int_0^{\frac{\pi}{2}} \frac{d\gamma}{\sqrt{1-k^2\sin^2\gamma}} - \int_0^{\gamma} \frac{d\gamma}{\sqrt{1-k^2\sin^2\gamma}}, \tag{6.2}$$

and parameters k and γ are calculated as:

$$k = \sin\left(\frac{\pi}{4} + \frac{\alpha}{2}\right), \tag{6.3}$$

$$\gamma = \sin^{-1}\left(\frac{1}{k\sqrt{2}}\left(\cos\frac{\beta}{2} - \sin\frac{\beta}{2}\right)\right). \tag{6.4}$$

The length of the loop head, L_h, is also calculated using Postle model. By considering it to be two equal segments of a circle we derive it as:

$$L_h = \frac{p(\frac{\pi}{2} - \beta)}{2(\sin\alpha + \sin\beta)}, \tag{6.5}$$

The resistance of the held loop's legs and header is then calculated as:

$$R_l = \frac{\rho L_l}{A_r}, \tag{6.6}$$

$$R_h = \frac{\rho L_h}{A_r}, \tag{6.7}$$

where A_r is the cross-sectional area of the conductive yarn.

As mentioned in the earlier assumption, we model the length of tuck stitch head to be equal to the length of the held loop head. Therefore, the resistances of tuck and held loop heads are the same. Consequently, a parallel connection of resistors is formed. The combination of this resistances at the head of the tuck stitch is calculated as:

$$R_{ht} = \frac{R_h}{2}. \tag{6.8}$$

Using Kurbak model [157], the total length of a tuck stitch, L_{tt} can be calculated:

$$L_{tt} = L_t - 4d, \tag{6.9}$$

where d is the diameter of the yarn. Furthermore, from the Munden model [68], the length of a stitch is:

$$L_{tt} = 2(L_{ht} + L_{lt}), \tag{6.10}$$

Therefore since the loop length of the held loop head is equal to the tuck loop head, the length of the tuck loop leg is:

$$L_{lt} = L_l - 2d, \tag{6.11}$$

and its resistance is

$$R_{lt} = \frac{\rho L_{lt}}{Ar}. \tag{6.12}$$

The contact resistance in the tucked loop is determined by assuming that the contact pressure is twice the contact pressure at a knit loop because both the tuck yarn and the held yarn interlock the previous loop. Therefore by combining this assumption with Holm's contact theory, the contact resistance at a tuck yarn, R_{ct}, is derived as:

$$R_{ct} = \frac{\rho}{2}\sqrt{\frac{\pi H}{2nP_r}}, \tag{6.13}$$

where P_r is the contact pressure between the loops, n is the number of contact points, H is the material hardness and ρ is the resistivity.

Therefore, the contact resistance at a tuck loop can be related to the contact resistance at a knit loop as:

$$R_{ct} = 0.707 * R_c. \tag{6.14}$$

6.3.2 Electromechanical Model of a Miss stitch

A novel resistive model of a weft knit strain sensor with a miss stitches is illustrated in Figure 6.3. To model this sensor, it was assumed that the miss stitch is split across 3 equal lengths as it floats from one interlocked loop to another.

In modelling a miss stitch, the contact resistance present in a knitted loop is removed because there are no interlocking loops. However, the resistance of a miss stitch can be modelled as a length resistance. Therefore, we propose that the length of a miss stitch is the sum of all wale spacings of all loops it floats across. Therefore, for a miss stitch that floats across one loop, its length, L_m, can be described as:

$$L_m = W_s, \tag{6.15}$$

where W_s is the average wale spacing of the fabric.

Furthermore, based on the assumption that length of a miss stitch is split equally in three lengths as it extends from one interlocked loop to another, we introduce a parameter R_m to represent the resistance of one-third of the miss stitch. Therefore, the resistance parameter, R_m was calculated as:

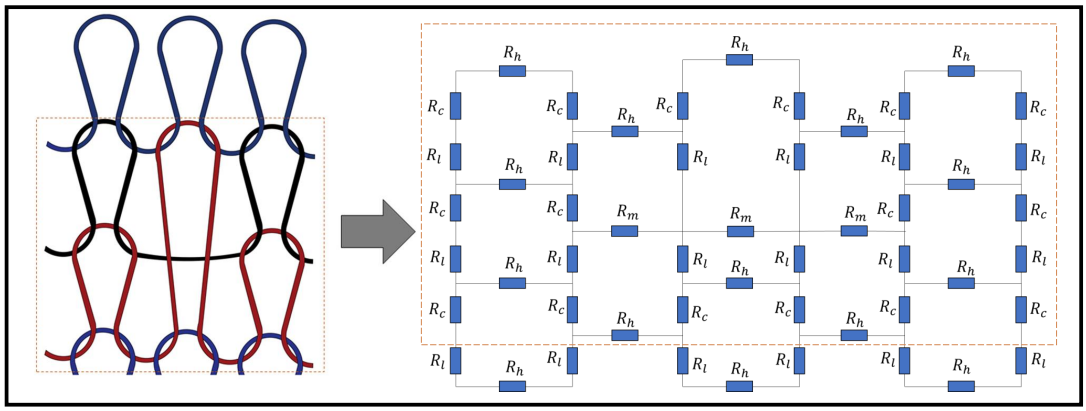

Figure 6.3: Resistive model of a miss stitch in a weft knit strain sensor

$$R_m = \frac{\rho W_s}{3Ar}. \tag{6.16}$$

6.3.3 Circuit Analysis

A circuit analysis is undertaken to determine the equivalent resistance of a weft knit strain sensor with tuck stitches or miss stitches. To achieve this, two sensors with 3 wales and 3 courses are illustrated in Figure 6.4, where a miss stitch and a tuck stitch are located in the middle of the sensors. Kirchoff current and voltage laws were employed to derive the equivalent resistance in the sensors.

To derive the equivalent resistance in the sensor with the miss stitch, we add a voltage source and use the hypothetical currents $(I_{m1} - I_{m14})$ to determine the equivalent resistance.

$$\begin{aligned}(I_{m1} - I_{m2})(R_h + R_l) + (I_{m1} - I_{m5})R_h + \\ (I_{m1} - I_{m7})(2R_l + R_h) + (I_{m1} - I_{m10})R_h + \\ (I_{m1} - I_{m12})(R_h + R_l) = 0,\end{aligned} \tag{6.17}$$

$$\begin{aligned}(I_{m2} - I_{m1})(R_h + R_l) + I_{m2}(R_c + R_l) + \\ (I_{m2} - I_{m3})R_h + (I_{m2} - I_{m5})R_c = 0,\end{aligned} \tag{6.18}$$

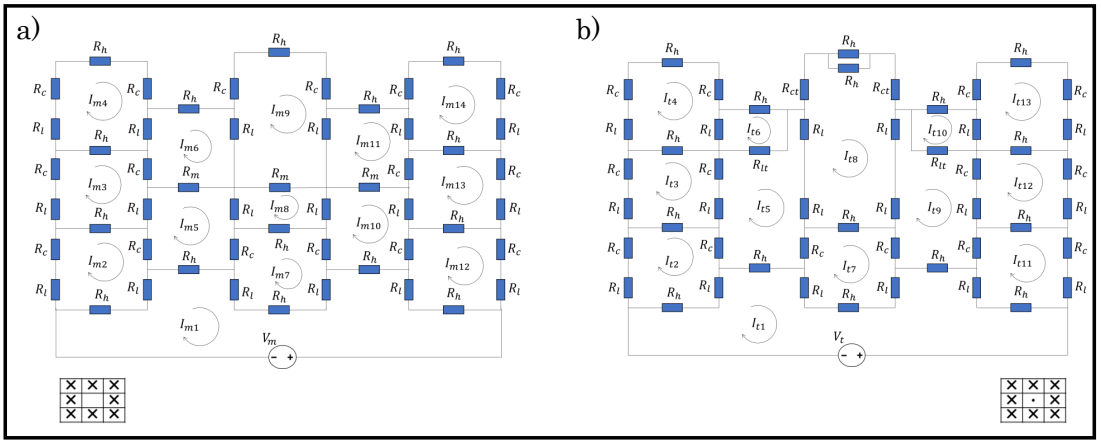

Figure 6.4: Resistive circuits of a) a Miss stitch, and b) a tuck stitch in a weft knit strain sensor

$$(I_{m3} - I_{m5})R_l + (I_{m3} - I_{m2})R_h + I_{m3}(R_c + R_l) + (I_{m3} - I_{m4})R_h + (I_{m3} - I_{m6})R_c = 0, \tag{6.19}$$

$$(I_{m4} - I_{m6})R_l + (I_{m4} - I_{m3})R_h + I_{m4}(2R_c + R_l + R_h) = 0, \tag{6.20}$$

$$(I_{m5} - I_{m6})R_m + (I_{m5} - I_{m8})R_l + (I_{m5} - I_{m7})R_c + (I_{m5} - I_{m1})R_h + (I_{m5} - I_{m2})R_c + (I_{m5} - I_{m3})R_l = 0, \tag{6.21}$$

$$I_{m6}(R_h) + (I_{m6} - I_{m9})R_l + (I_{m6} - I_{m5})R_m + (I_{m6} - I_{m3})R_c + (I_{m6} - I_{m4})R_l = 0, \tag{6.22}$$

$$(I_{m7} - I_{m1})(R_h + 2R_l) + (I_{m7} - I_{m5})R_c + (I_{m7} - I_{m8})R_h + (I_{m7} - I_{m10})R_c = 0, \tag{6.23}$$

$$(I_{m8} - I_{m7})R_h + (I_{m8} - I_{m5})R_l + (I_{m8} - I_{m9})R_m + (I_{m8} - I_{m10})R_l = 0, \tag{6.24}$$

$$(I_{m9} - I_{m11})R_l + (I_{m9} - I_{m8})R_m + (I_{m9} - I_{m6})R_l + I_{m9}(R_h + 2R_c) = 0, \tag{6.25}$$

$$(I_{m10} - I_{m13})R_l + (I_{m10} - I_{m12})R_c + (I_{m10} - I_{m1})R_h + (I_{10} - I_{m7})R_c + (I_{m10} - I_{m8})R_l + (I_{m10} - I_{m11})R_m = 0, \tag{6.26}$$

$$\begin{aligned} I_{m11}(R_h) + (I_{m11} - I_{m14})R_l + \\ (I_{m11} - I_{m13})R_c + (I_{m11} - I_{m10})R_m + \\ (I_{m11} - I_{m9})R_l = 0, \end{aligned} \tag{6.27}$$

$$\begin{aligned} (I_{m12} - I_{m1})(R_h + R_l) + (I_{m12} - I_{m10})R_c + \\ (I_{m12} - I_{m13})R_h + I_{m12}(R_c + R_l) = 0, \end{aligned} \tag{6.28}$$

$$\begin{aligned} (I_{m13} - I_{m10})R_l + (I_{m13} - I_{m11})R_c + \\ (I_{m13} - I_{m14})R_h + I_{m13}(R_c + R_l) + \\ (I_{m13} - I_{m12})R_h = 0, \end{aligned} \tag{6.29}$$

$$\begin{aligned} (I_{m14} - I_{m11})R_l + I_{m4}(2R_c + R_l + R_h) + \\ (I_{m14} - I_{m13})R_h = 0. \end{aligned} \tag{6.30}$$

The hypothetical currents were calculated as

$$\mathbf{i} = \mathbf{R}^{-1}\mathbf{v}, \tag{6.31}$$

where,

$$\mathbf{i} = \begin{bmatrix} I_{m1} \\ I_{m2} \\ \dots \\ I_{m14} \end{bmatrix}, \mathbf{v} = \begin{bmatrix} V_m \\ 0 \\ \dots \\ 0 \end{bmatrix}$$

and

$$\mathbf{R} = \begin{bmatrix} 5R_h + 4R_l & \dots & 0 & 0 & \dots & 0 \\ -(R_h + R_l) & \dots & 0 & 0 & \dots & 0 \\ \dots & \dots & \dots & \dots & \dots & \dots \\ 0 & \dots & 0 & -R_l & \dots & 0 \\ -2R_l + R_h & \dots & -R_h & 0 & \dots & 0 \\ 0 & \dots & R_m + R_h + 2R_l & -R_m & \dots & 0 \\ 0 & \dots & -R_m & 2R_l + 2R_c + R_m + R_h & \dots & 0 \\ \dots & \dots & \dots & \dots & \dots & \dots \\ 0 & \dots & 0 & 0 & \dots & 2(R_c + R_h + R_l) \end{bmatrix}. \tag{6.32}$$

The equivalent resistance was then calculated as:

$$R_{m(eq)} = \frac{V_m}{I_{m1}}. \tag{6.33}$$

To derive the equivalent resistance in the sensor with the tuck stitch, we employ the same methodology in determining the equivalent resistance. The

hypothetical currents I_{tn} were derived using (6.31) but resulted in a different resistance matrix. The resistance matrix derived for the sensor with a tuck stitch was calculated as:

$$\mathbf{R} = \begin{bmatrix} 5R_h + 4R_l & \dots & -R_h & \dots & 0 & \dots & 0 \\ -(R_h + R_l) & \dots & -R_c & \dots & 0 & \dots & 0 \\ \dots & \dots & \dots & \dots & \dots & \dots & \dots \\ -R_h & \dots & 3R_l + 3R_c + R_h + R_{lt} & \dots & -2R_l & \dots & 0 \\ 0 & \dots & -R_{lt} & \dots & 0 & \dots & 0 \\ -(2R_l + R_h) & \dots & -R_c & \dots & -R_h & \dots & 0 \\ 0 & \dots & -2R_l & \dots & 4R_l + 2R_{ct} + 1.5R_h & \dots & 0 \\ \dots & \dots & \dots & \dots & \dots & \dots & \dots \\ 0 & \dots & 0 & \dots & 0 & \dots & 2(R_c + R_h + R_l) \end{bmatrix}, \tag{6.34}$$

and the equivalent resistance was calculated as:

$$R_{t(eq)} = \frac{V_t}{I_{t1}}. \tag{6.35}$$

6.3.4 Determination of Contact Resistance

The conductive yarn used in the simulation and fabrication of the sensor is a multifilament yarn consisting of 20% stainless steel and 80% polyester filaments. Consequently, the stainless steel component ensures that the sensor complies to Holm's contact theory which postulates that the contact resistance between two conductors can be calculated as:

$$R_c = \frac{\rho}{2}\sqrt{\frac{\pi H}{nP_r}}, \tag{6.36}$$

where, R_c is the contact resistance, ρ is the electrical resistivity, H is the hardness of the material used, n is the number of contact points and P_r is the contact pressure between the conducting materials.

Typically, the material hardness and the electrical resistivity are constant based on the properties of conductive yarn used, while the number of contact points is subject to the sensor's design. Therefore, the changes to the contact resistance is dependent on changes to the contact pressure between the loops. The changes in the contact pressure occur as a result of changes to the strain applied on the sensor, thus causing the weft knit strain sensor to exhibit piezoresistivity. However, the contact pressure between the interlocking loops has proven difficult to measure or predict. Therefore, researchers have found alternative methods to

determine the contact resistance accurately by measuring the contacting force [13].

However, Zhang et al. [14] proposed from empirical observations that the correlation between the contact resistance, R_c, and equivalent resistance, R_{eq}, of the sensor can be derived as:

$$R_{eq} = R_c \cdot K, \tag{6.37}$$

where K is a variable coefficient based on the sensor's structural design.

From equations 6.31 and 6.33, we derive that

$$\mathbf{R}_{1,1}^{-1} = R_{eq}, \tag{6.38}$$

where $\mathbf{R}_{1,1}^{-1}$ is the first element of the inverse matrix of the resistance matrix $\mathbf{R}$ of the sensor. Therefore,

$$\mathbf{R}_{1,1}^{-1} = D \cdot R_c. \tag{6.39}$$

where D is the coefficient of R_c in $\mathbf{R}_{1,1}^{-1}$.

However, this method is computationally intensive. Therefore, we propose a less computationally intensive method in Algorithm 3. Algorithm 3 is a control algorithm that calculates the contact resistance from the equivalent resistance with an initial random positive value as D. Subsequently, a control feedback is used to calculate the optimised value of D. A threshold was set to stop the algorithm when the percentage change in the input contact resistance to its previous value was less than 3%. This was selected empirically as the accuracy of the model was not significantly improved below this threshold.

6.3.5 Simulation Parameters

To determine the effect of miss and tuck stitches on a plain weft knit strain sensor, different loop configurations of a sensor with varying percentages of tuck stitches and miss stitches within the sensor were designed. The loop configurations depicted in Table 6.2 and Table 6.3 were then simulated using the postulated models. The unit circuit diagram of the loop configurations are shown in Figures 6.5 and 6.6. It can be observed in the circuit diagram of sensors with 6.25% and 8.33% tuck stitches that the length resistances of the sinker loops of the held

Algorithm 3 Contact Resistance solution

Initialise:
$R_{sim} \leftarrow 0$
$D \leftarrow 0 < D < \text{inf}$
Loop:
$R_c = R_{exp}/D$
Input R_c into modelled circuit to determine R_{sim}
if $|R_{sim(n)} - R_{sim(n-1)}| > (0.03 \cdot R_{sim(n)})$ **then**
    $D = R_{sim(n)}/R_c$
    goto *Loop*
else
    Return R_c
end if
▷ R_{sim} and R_{exp} are the simulated and experimental equivalent resistances respectively

loop were neglected. It was initially assumed that their lengths were equal to the lengths of the sinker loop of other knit stitches. However, it was observed that this assumption negatively affected the expected results. In contrast, neglecting it improved significantly the simulation results of the model in terms of its correlation with experimental results. A feasible explanation for this occurrence is that the lengths of the sinker loops of the held loop are negligible because they have transferred to the lengths of the loop legs of the held loop thus resulting in the longer loop legs of a held loop than other knitted loop stitches.

Moreover, the loop configurations were designed to prevent consecutive tuck or miss stitches either in the course or wale direction to reduce the complexity in modelling. These loop configurations were simulated with LTspice using the numerical variables shown in Table 6.1.

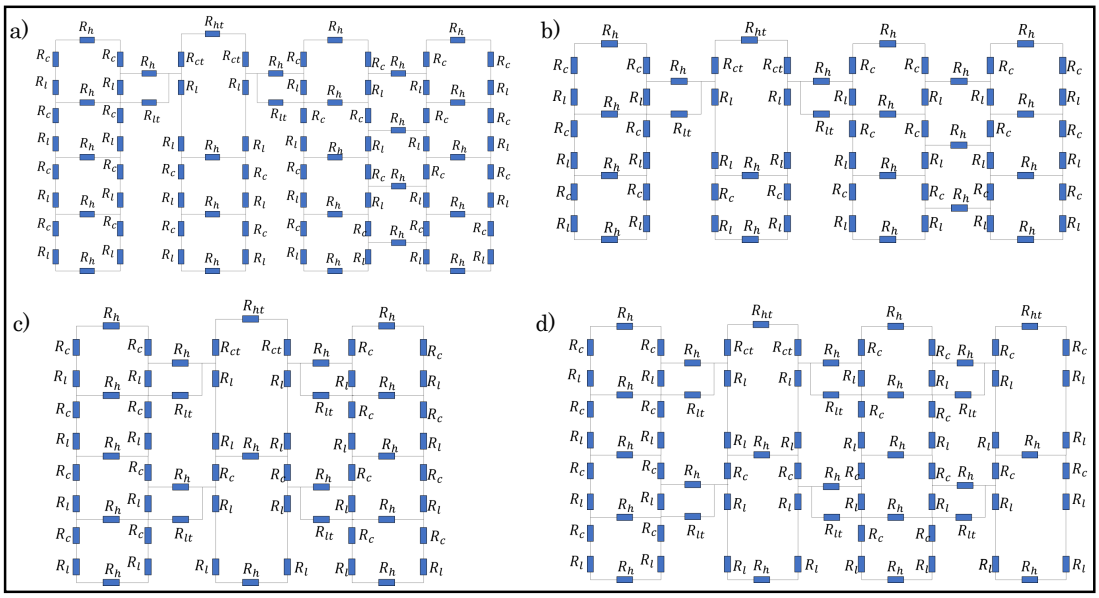

Figure 6.5: Unit circuit diagram of samples with tuck stitches. a) 6.25% tuck stitches b) 8.33% tuck stitches c) 16.67% tuck stitches d) 25% tuck stitches.

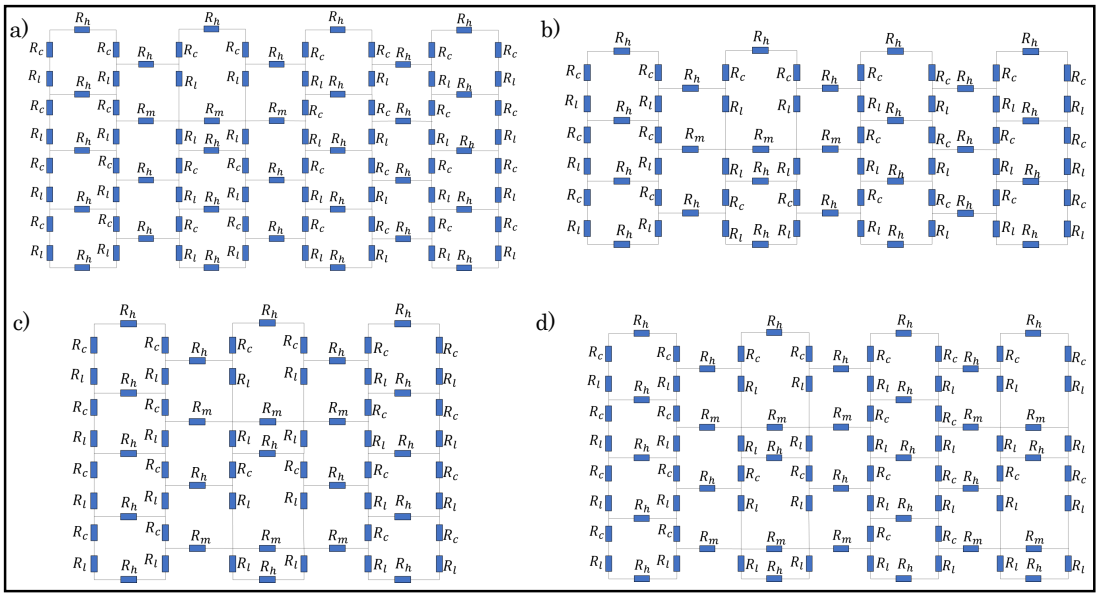

Figure 6.6: Unit circuit diagram of samples with miss stitches. a) 6.25% miss stitches b) 8.33% miss stitches c) 16.67% miss stitches d) 25% miss stitches.

Table 6.1: Numerical Parameters for Simulation.

Parameters	Values
Number of courses	72
Number of wales	72
$\alpha(^\circ)$	24.75
$\beta(^\circ)$	10.85
Course spacing (mm)	3
Wale spacing (mm)	2
$\rho(ohms.mm)$	300
Yarn's Diameter (mm)	0.4

6.3.6 Experimental Validation

Sample Preparation.

Eight samples of weft knit strain sensors were knitted using a Shima Seiki Mach2s 12-gauge knitting machine with the loop configurations shown in Tables 6.2 and 6.3. All sensors were knitted with conductive yarn as a 72 courses by 72 wales plain knit fabric with a digital cam setting of 30. The cam setting is a dimensionless value representing the stitch length that will be attempted by the knitting machine. The conductive yarn used in knitting the samples was a Schoeller multifilament conductive yarn commercially available from Uppingham Yarns Ltd. According to its specification sheet, it can be stretched up to 5.5% extension and its yarn count and linear density were $2/50Nm$ and 400 dtex respectively. Notably, as seen in Table 6.1, our simulation parameter for resistivity was chosen as $300\Omega mm$ after a preliminary measurement of a relaxed sample of the yarn. Furthermore, the yarn consists of 80% polyester and 20% stainless steel filaments which provide an advantage of being an intrinsic conductor as opposed to yarns coated with conductive ink. Particularly, a multifilament conductive yarn is more environmentally stable than a coated conductive yarn because the conductive inks used in coating yarns are very sensitive to environmental changes such as temperature [78].

The knitted samples are illustrated in Figures 6.7 and 6.8 and their respective parameters are shown in Table 6.4. Tuck stitches reduce the length of a fabric and

Table 6.2: Loop Configuration for Tuck stitches simulation. "**X**" represents a knitted loop stitch and "•" represents a tuck stitch.

% of Tuck stitches	Loop configuration
6.25%	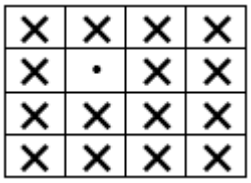
8.33%	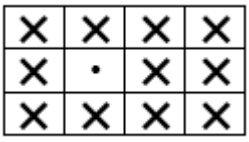
16.67%	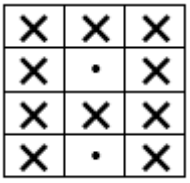
25%	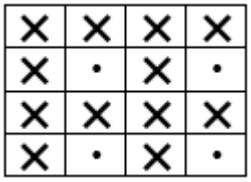

increase the width of a fabric. This is illustrated in Table 6.4 where the reduced length and increased width caused a larger number of courses/cm and a smaller number of wales/cm as the percentage of tuck stitches in the sensor increased. The reduced length and increased width occur because the tension of tuck stitches pull down their held loops, thereby decreasing their length but expanding their width [57]. In contrast, miss stitches reduce the width of the fabric because the wales are more drawn together by the miss stitches. As depicted in the changes in the wales/cm, this phenomenon is observed in all sensor configurations with miss stitches except the sensor comprising of 6.25% miss stitches. The exception is likely a result of the location of the miss stitches. In addition, miss stitches also reduce the length of the fabric as illustrated by the increase in courses/cm of the sensors as the percentage of miss stitch increased. This occurred because

Table 6.3: Loop Configuration for Miss stitches simulation. "**X**" represents a knitted loop stitch and " " represents a miss stitch.

% of Miss stitches	Loop Configuration
6.25%	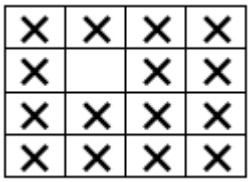
8.33%	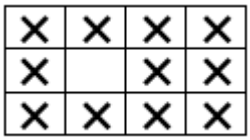
16.67%	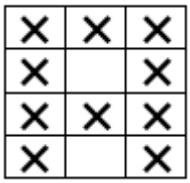
25%	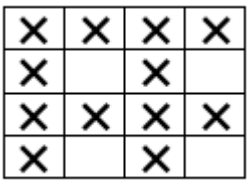

in a miss stitch, the loop height is replaced by the diameter of the yarn which in most cases, is considerably smaller than the loop height.

Experimental Procedure.

The samples were dry relaxed for 48 hours to remove any existing strains from the knitting process. Thereafter, a tensile test was performed using an Instron3369 tensile machine. Particularly, the steel clamps were lined with insulated rubber pads to prevent any conductance between the tensile machine and the sensors. The testing procedure consisted of stretching the sensors in the course-wise direction at a speed of 10 millimeter per minute till the sensors were extended to 25% extension while the sensor's resistance was measured by a digital multimeter

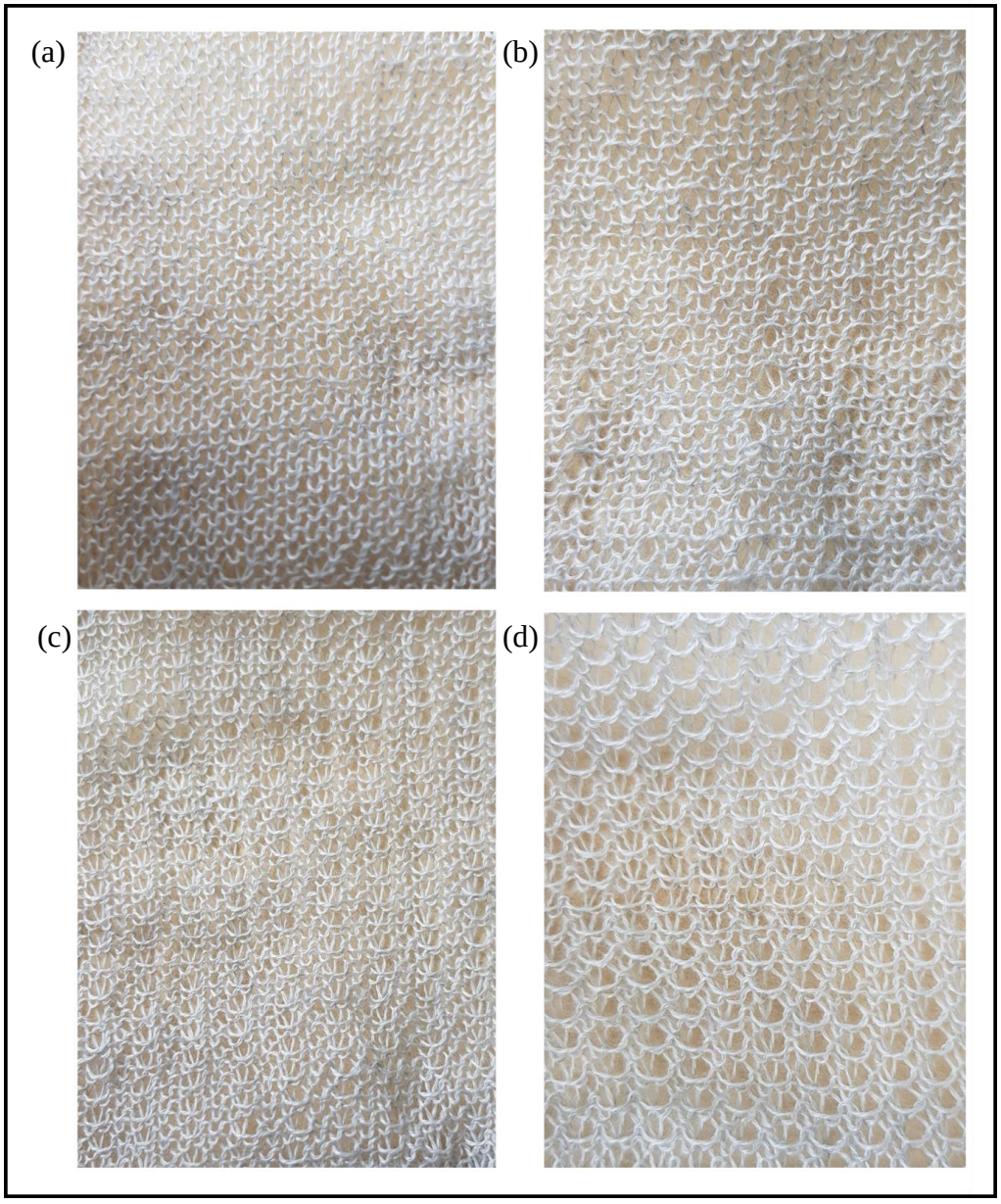

Figure 6.7: Knitted samples with miss stitches. a) 6.25% miss stitches b) 8.33% miss stitches c) 16.67% miss stitches d) 25% miss stitches.

Table 6.4: Fabric parameters of the knitted sensors.

Configuration	Wales/cm	Courses/cm	Stitch density
6.25% Miss	5.00	5.39	26.95
8.33% Miss	4.56	5.43	24.76
16.67% Miss	4.97	5.50	27.34
25% Miss	5.04	6.05	30.49
6.25% Tuck	4.11	5.48	22.52
8.33% Tuck	4.07	5.63	22.91
16.67% Tuck	3.60	6.49	23.64
25% Tuck	3.16	7.24	22.88

(TENMA 72-7770a).

6.4 Results and Discussion

6.4.1 Effect of Tuck Stitches on a Weft Knit Strain Sensor

The raw experimental results of the tensile experiment with sensors consisting of tuck stitches is shown in part (a) of Figure 6.9. A Savitzky-Golay filter of polynomial order N = 5 and window length of 9 was applied to reduce the analog noise from the data. The filtered data is illustrated in part (b) of Figure 6.9.

Observing these results, it is difficult to ascertain if the sensor piezoresistive behaviour can be characterised as a polynomial of the 1st-order (linear) or a polynomial of the 2nd-order (quadratic). Therefore, we plot the R^2 value, coefficient of determination, of both polynomial fits for each configuration of tuck stitches in the sensor. As shown in figure 6.11, the R^2 values of both polynomial fits were both higher than 0.8 but the results show that the quadratic polynomial is a better fit. However, we observe that as the percentage of tuck stitches in the sensor increases, the R^2 value of the 1st-order polynomial fit increases. In simple terms, this means that the increase in tuck stitches led to a more linear piezoresistive behaviour in the sensor. Particularly, the sensor with 25% tuck stitches exhibited a higher R^2 value in its linear fit than the quadratic fit. This effect occurred because as illustrated in equation 6.14, the addition of tuck stitches increases the

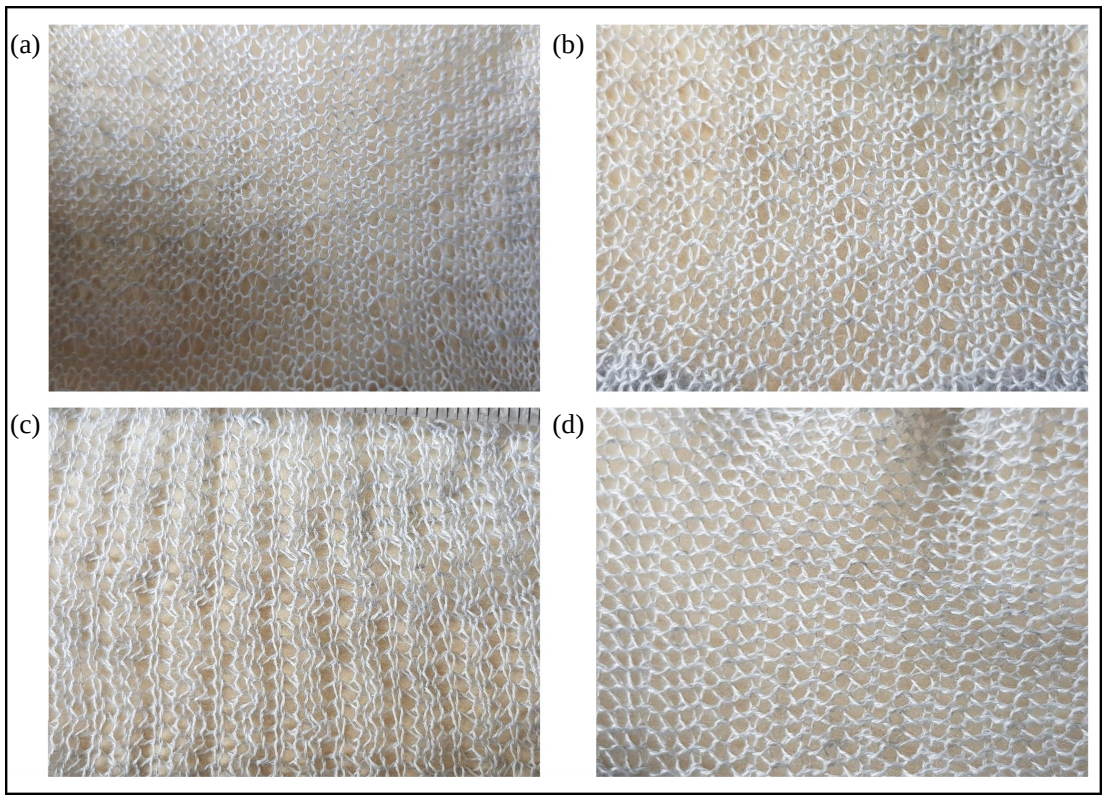

Figure 6.8: Knitted samples with tuck stitches. a) 6.25% tuck stitches b) 8.33% tuck stitches c) 16.67% tuck stitches d) 25% tuck stitches.

contact pressure at the contact points. Increased pressure at the contact point has been observed to cause a higher linear piezoresistive behaviour in weft knit strain sensors [37]. This phenomenon occurs because the larger initial contact pressure increases the extension range for the intermesh between the loops to disintegrate during extension thereby preserving the linear decrease of the contact area as the sensor is extended. Furthermore, it can be observed that our simulation results closely agree with the experimental results.

The initial and mean resistances are shown in Figure 6.12. It was observed that increases in the tuck stitches led to a decrease in the initial resistance of the sensor. This occurred because an increase in the percentage of tuck stitches causes an increased initial contact pressure. As mentioned earlier, this increase in contact pressure reduces the contact and equivalent resistances. The mean

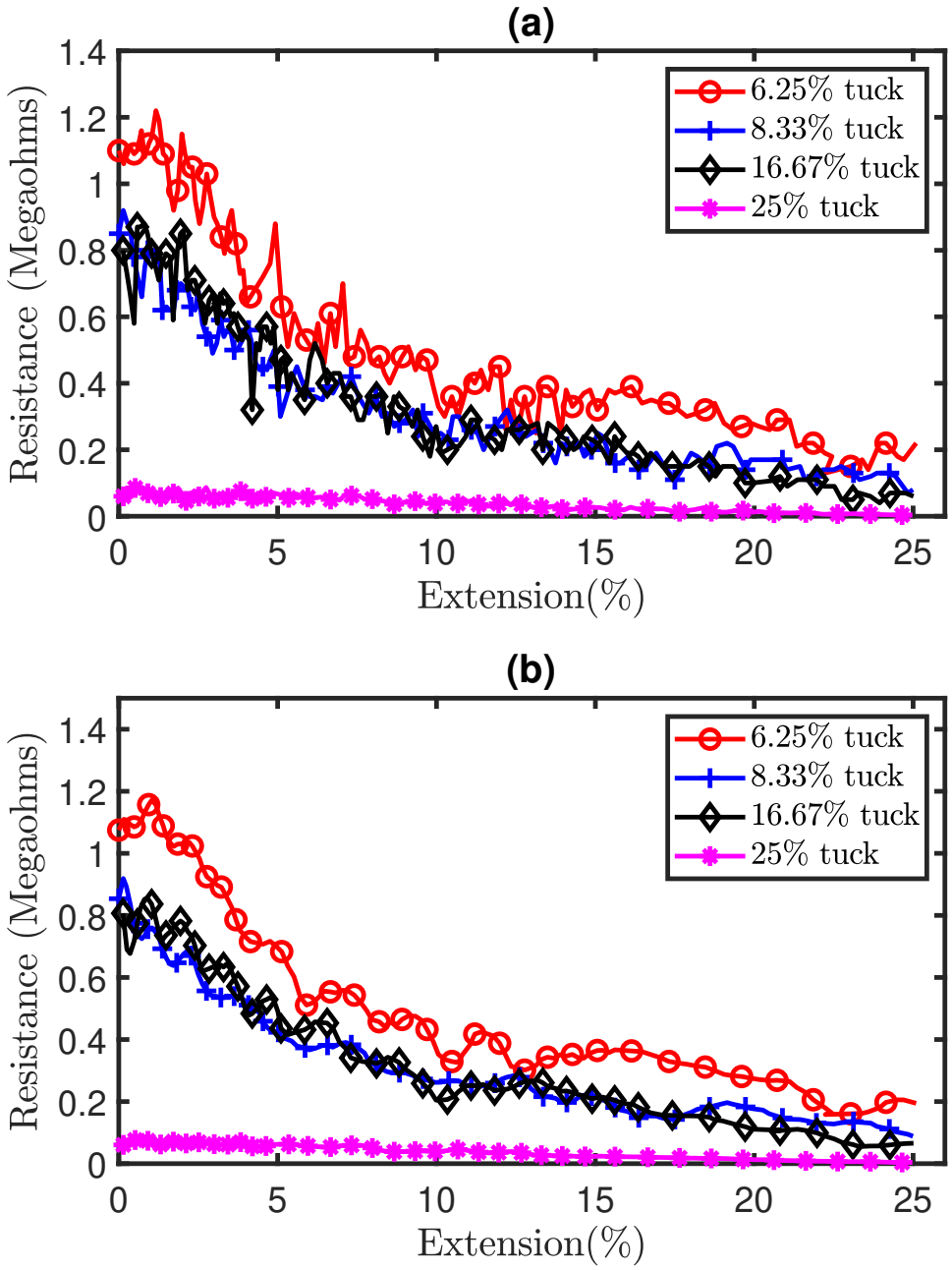

Figure 6.9: Experimental results of tensile test on sensors with tuck stitches. a) Pre-filtered results, b) Post-filtered results.

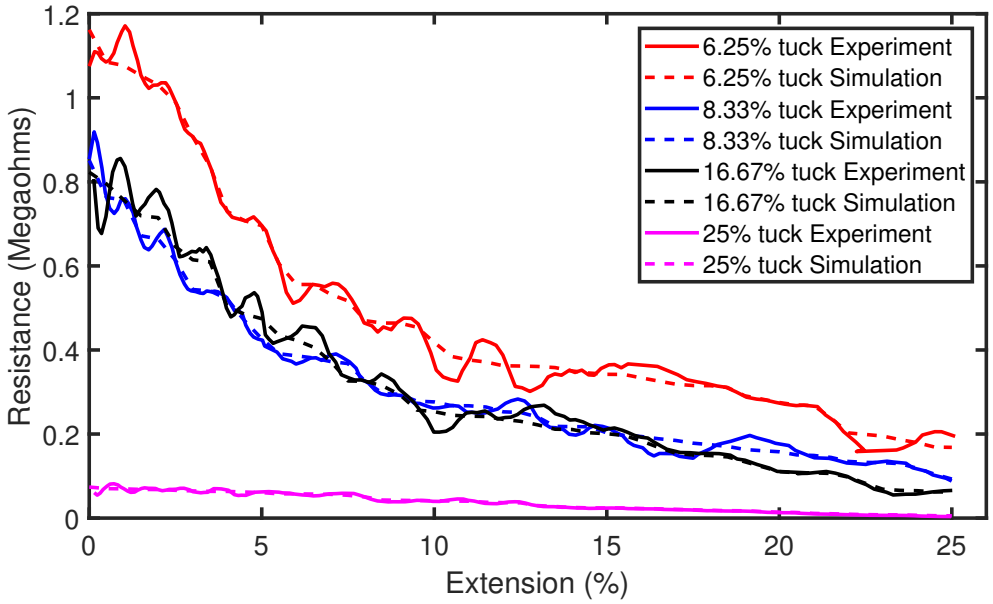

Figure 6.10: Comparison of simulation and experimental results for sensors with tuck stitches.

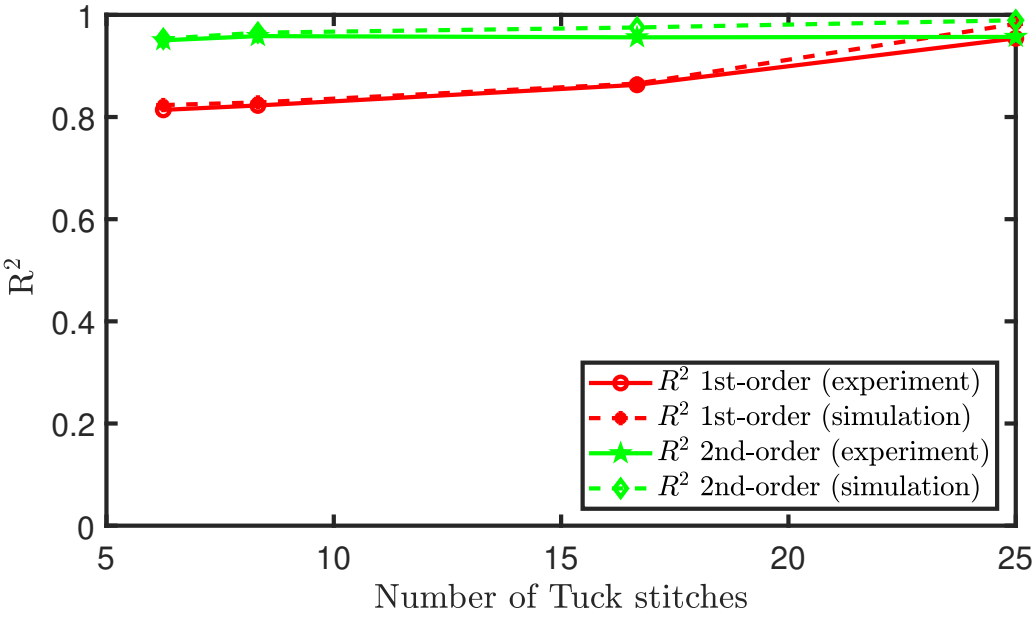

Figure 6.11: Polynomial fit of the piezoresistive behaviour of sensors with tuck stitches.

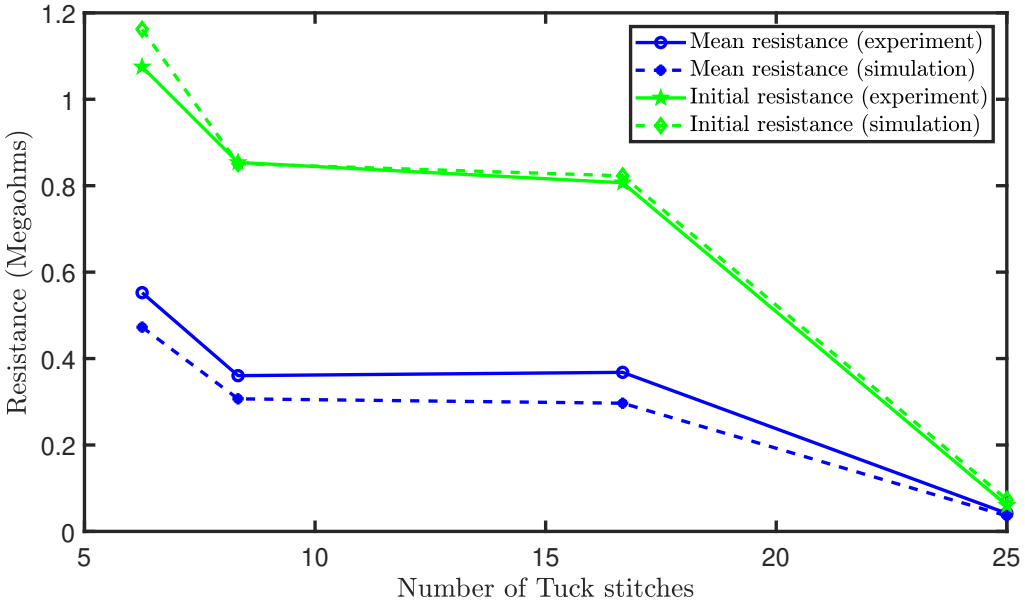

Figure 6.12: Initial and mean resistances of sensors with tuck stitches.

resistance across the extension is also depicted in Figure 6.12. There was a reduction in the mean resistance as the percentage of tuck stitches in the sensor increases with the exception of the sensor with 16.67% tuck stitches where the mean resistance slightly increased. It is believed that this exception is as a result of the limitations of the loop configuration and that a different loop configuration with the same percentage of tuck stitches will have a lower mean resistance during extension than sensors with lower percentage of tuck stitches. In addition, Figure 6.10 shows that our simulation results generally agree with these experimental results.

6.4.2 Effect of Miss Stitches on a Weft Knit Strain Sensor

The experimental results of the tensile test on sensors with miss stitches is shown in part (a) of Figure 6.13. The Savitzky-Golay filter of polynomial order N = 5 and window length of 9 was also applied on the data to remove analog noise and the filtered results are shown in part (b) of Figure 6.13.

Similar to the methodology used in analysing the experimental results of sensors consisting of tuck stitches, we plot the R^2 values, coefficient of determination,

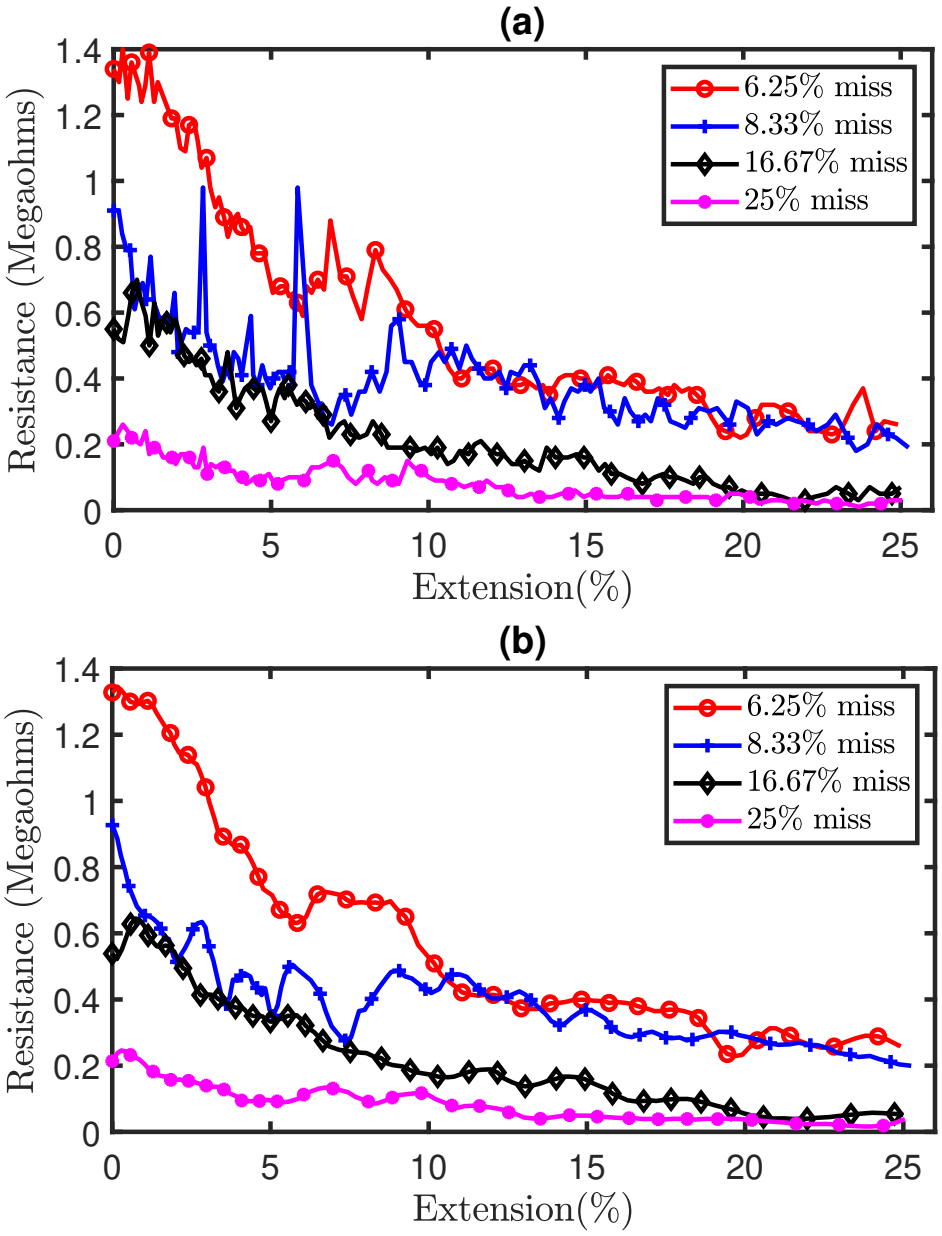

Figure 6.13: Experimental results of tensile test on sensors with miss stitches. a) Pre-filtered results, b) Post-filtered results.

of both polynomial fits for each configuration of miss stitches in the sensor. We observe in Figure 6.15 that these plots exhibit a similar shape but the polynomial fit of the 2nd-order is better than the fit of the 1st order in terms of the R^2 value for every loop configuration consisting of miss stitches. However, we were unable to draw any consistent relationship between the changes in the miss stitches and the changes in the R^2 values of the sensors. This erratic behaviour is not well-modelled by our simulation results because the presence of miss stitches cause the behaviour to be largely dependent on the floating stitch of the conductive yarn and not the weft knit structure of the sensor.

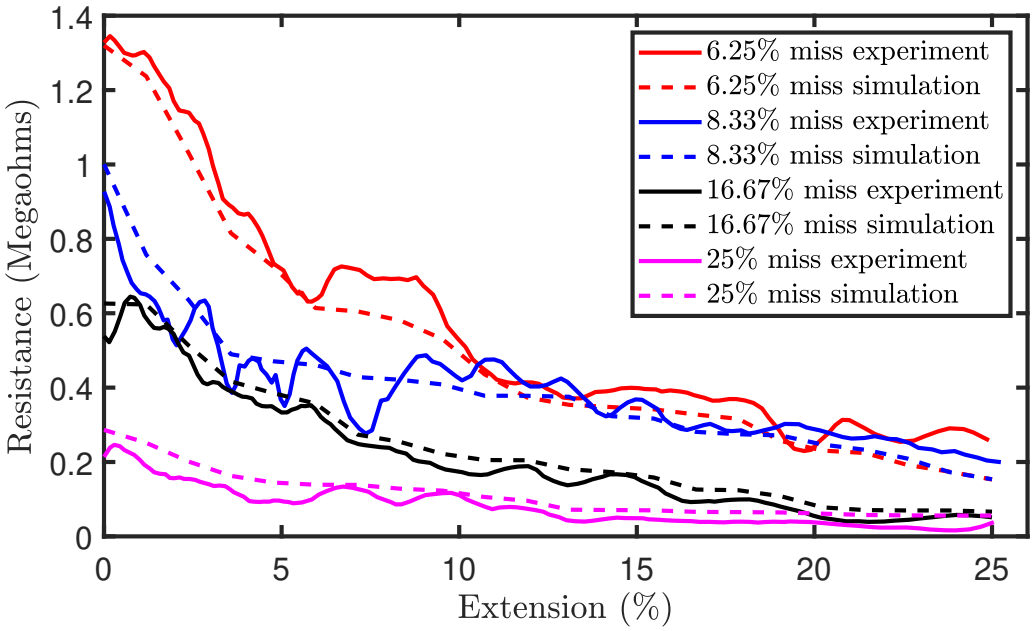

Figure 6.14: Comparison of simulation and experimental results for sensors with miss stitches.

Figure 6.16 depict the initial and mean resistance of the sensors during the experiment. It was shown that the initial resistance and the mean resistance reduces as the percentage of miss stitches increased. This occurred because miss stitches do not interlock with other loops leading to a lack of contact resistances at the locations of the missed stitches. Therefore, the increase in miss stitches reduces the contact resistances present in the sensor and thus the equivalent resistance of the sensor. In terms of the initial and mean resistances, our simulation

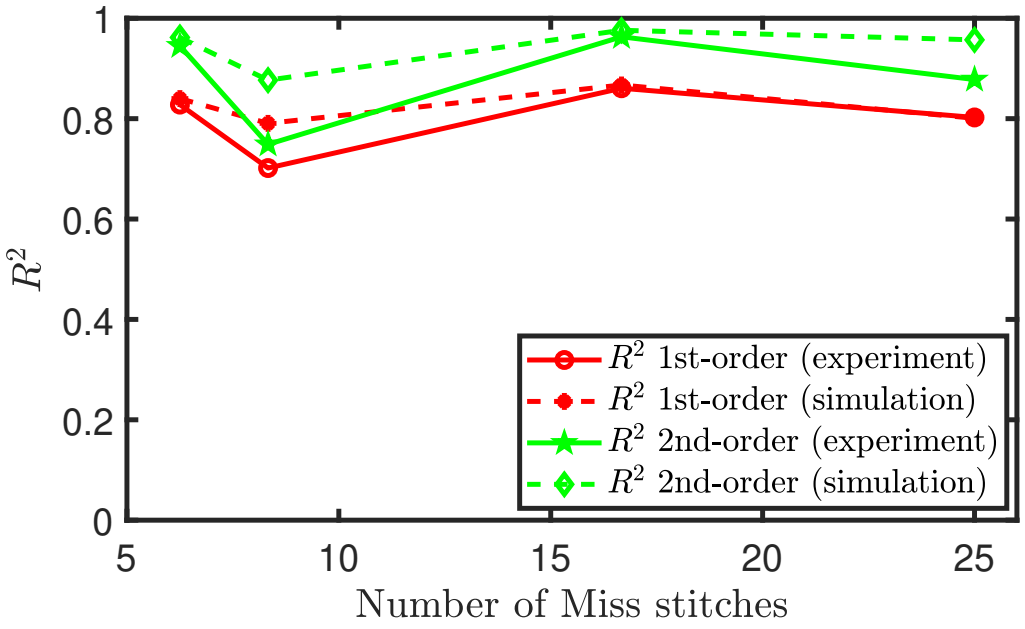

Figure 6.15: Polynomial fit of the piezoresistive behaviour of sensors with miss stitches.

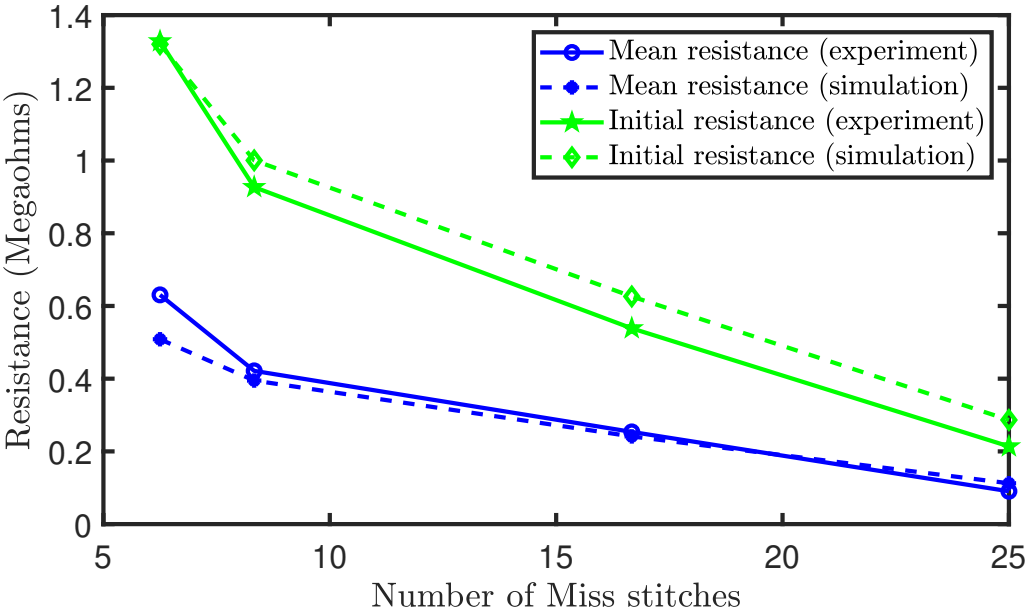

Figure 6.16: Initial and mean resistances of sensors with miss stitches.

results generally agree with the experimental results. Figure 6.14 illustrates the simulated and experimental results. The difference in the magnitude of the effect of miss stitches on the sensor between the simulation and experimental results is as a result of the limitations of the modelling assumptions in comparison to real working conditions.

6.5 Conclusion

In this chapter, we have proposed two electromechanical models depicting a miss stitch and a tuck stitch in weft knit strain sensors. Subsequently, we expanded these models to simulate various loop configurations consisting of varying percentages of tuck or miss stitches in a weft knit strain sensor. The simulated results were then validated by tensile testing sensors knitted with the same simulated loop configurations and numerical parameters. It was observed that increases in the percentage of miss stitches or tuck stitches in a weft knit strain sensor decreased the initial resistance, mean and median resistances. However, the sensor consisting of 16.67% tuck stitches did not agree with the simulated result in terms of the decrease of the mean and median resistance. It is believed that this occurred as a result of the limitations of the selected loop configuration.

Additionally, we observed that a quadratic polynomial best characterises the piezo-resistive behaviour of a weft knit strain sensor consisting of miss or tuck stitches. However, it was observed that increases in percentage of tuck stitches in the sensor increased the R^2 value of the linear fit of its piezoresistivity. This is usually seen as a strong determinant of a weft knit strain sensor's accuracy. In contrast, increases in the percentage of miss stitches did not lead to a consistent change in the R^2 value of the sensor's piezoresistivity.

This chapter will provide researchers with fundamental knowledge on how to effectively model weft knit strain sensors with tuck or miss stitches. Moreover, the observations from the simulated and experimental results will direct the design and application of tuck or miss stitches on a weft knit strain sensor.

Chapter 7

Conclusion and Future Work

In this chapter, I present the main results and the most relevant contributions of this thesis. In addition, I discuss potential extensions of the work undertaken in this thesis.

7.1 Summary and Conclusions

In chapter 3, a novel electromechanical model of a plain knit sensor is presented. This model was designed to simulate the piezoresistivity of a plain knit sensor. Notably, it was based on the loop and interlocking angles of the knitted stitches in the sensor. The model was presented for sensors that are knitted with only non-elastic conductive yarn. Furthermore, it was based on the assumption that the conductive yarn is a perfect intrinsic conductor and that the contact pressure between each intermeshed stitch is constant throughout the sensor. In addition, the model assumes that the interlocking and loop angles are limited by width and length jamming. The interlocking and loop angles were used in calculating the length of the legs, head and sinker of the stitches. Moreover, the length of the head and sinker of the loops were assumed to be equal. These computed lengths were utilised to calculate the length resistances in the model. The contact resistance for each intermeshed loop was derived using a novel algorithm from the total (/equivalent) resistance of the sensor during the experimental tensile test. The model was validated by a tensile test performed on sensors knitted with the

simulation parameters. The simulation results generally agreed with the experimental results. Particularly, the average percentage error between 2% strain and 14.6% strain was 10.4% and the overall percentage error across the tensile range was 16.63% which is significantly smaller than previous studies. Furthermore, a parametric study was performed to simulate the influence of changes in the loop or interlocking angles on the piezoresistivity of the sensor. It was observed that changes in the loop angle caused a 2.27% change in the initial resistance of the sensor while changes in the interlocking angle caused a change of up to 25.5% and 22.2% in the initial and mean resistance of the sensor respectively.

In chapter 4, the model presented in chapter 3 was expanded to simulate the behaviour of a sensor knitted with 50% non-elastic conductive yarn and 50% elastic non-conductive yarn. This configuration was selected to increase the extensibility of the sensor. The simulation results were very similar to the experimental results with an average percentage error of 11.47% which was significantly smaller than the error obtained in the previous configuration. The new sensor configuration was then employed in designing a knitted data glove. Particularly, the sensors were placed at the distal and proximal interphalangeal joints and the entire glove was knitted in a single fabrication process using WholeGarment technology. This ensured that the glove was lightweight and wholly textile with no external attachments between the support structure and the sensors. The glove's sensors were validated using a robotic hand to simulate the opening and closing of a human fist. The results illustrated the repeatability of the sensor especially when a simple filter is applied to remove some of the analog noise. In addition, a classification scenario was developed to investigate the effect of drift on the sensor. The robotic hand was used to hold the sensor for a minute at specific angles between 0° and 75° which is the typical range of an interphalangeal joint in the human hand. Subsequently, three classical machine learning classifiers were employed in classifying the data. The results showed that the drift in the sensor's output reduces the accuracy of linear classifiers.

In chapter 5, a deep learning approach was evaluated on a real-world classification scenario using the data glove and human participants. Notably, this is a pioneering study on the use of deep learning and a piezoresistive data glove. Moreover, this study pioneers the use of deep learning on any human motion

capture system that comprises of weft knit strain sensors. In this study, I evaluated convolutional neural networks (CNN) in a grasp classification application. In this application, human participants were asked to grasp objects of different shapes while wearing the data glove. The CNN algorithm was then employed to accurately classify the data accurately. I evaluated the algorithm in two scenarios. Firstly, when the validation object was part of the training data set and secondly, when the validation object was not part of the training data set. I observed that although the validation object was part of the training data set in the first scenario, the drift in the sensor's output contributed to a lower accuracy than expected. In addition, I observed that the accuracy of the algorithm in the second scenario was lower than the first scenario, particularly because it was a more difficult classification task as the validation object was not part of the training data set. Furthermore, I explored the performance of the algorithm for each of the participants and I observed that the accuracy of the algorithm was much higher in Participant 5 than in other participants. This occurred because the glove was designed for the hand size of this participant. However, the elasticity of the glove still ensured that the performance of the algorithm was also relatively high in classifying the data of other participants. Furthermore, this observation reinforces the advantage of weft knit strain sensors in human motion capture applications, as they can be designed for different human sizes and are not constrained to the one-size-fits-all design of other strain sensors. In addition, the performance of the CNN algorithm was compared to popular machine learning techniques. It was observed that our simple CNN architecture performed better than comparable machine learning techniques.

In chapter 6, I investigated the effect of miss and tuck stitches on the piezoresistivity of a weft knit strain sensor. Firstly, using the mature electromechanical model developed in Chapters 3 and 4, I developed an electromechanical model for a 3x3 (3 courses and 3 wales) plain knit sensor consisting of a tuck stitch and another 3x3 sensor consisting of a miss stitch. Subsequently, this model was expanded to several models of 72x72 (72 courses and 72 wales) sensors consisting of 6.25%, 8.33%, 16.67% and 25% miss stitches and 6.25%, 8.33%, 16.67% and 25% tuck stitches. These various configurations of sensors were knitted and put through a tensile test. The simulation and experimental results generally agreed

for most of the configurations. Furthermore, it was observed that increases in miss stitches or tuck stitches reduced the initial and mean resistances of the sensors. Notably, it was observed that increases in the amount of tuck stitches increase the linearity of the sensor's piezoresistivity. The increase in linearity as a result of an increase in percentage of tuck stitches occurs because of the increase in contact pressure in the tuck loop. This observation is very significant because high linearity is a characteristic of an accurate strain sensor. Moreover, it can be used in guiding the design of weft knit strain sensors that increase the performance of linear classifiers and reduce the need for complex algorithms in classification scenarios.

In summary, the chapters in these thesis can be decribed as the following:

- In Chapter 3, the modelling of a basic configuration of a weft knit sensor is presented and evaluated.
- In Chapter 4, a more flexible sensor is proposed and used in creating a data glove. The data glove is then evaluated using a robotic hand and linear machine learning algorithms.
- In Chapter 5, the data glove is evaluated with human participants and non-linear machine learning algorithms.
- In Chapter 6, different configurations of weft knit sensors are modelled and evaluated experimentally.

7.2 Future Work

7.2.1 Wireless Data Glove

A wireless prototype of the weft knit data glove was the winner of the Digital Innovation Challenge 2019. We utilised traditional electronic components to provide wireless transmission and portable power supply. In a subsequent study, we will replace these components with a textile antenna to wireless transmit data and utilise wireless backscatter technology to passively power the glove. This will bring us closer to our goal of providing a wholly-textile commercial data glove.

7.2.2 Influence of Knitting Parameters

In this thesis, I have investigated the influence of loop angles, interlocking angles, miss stitches, tuck stitches on the piezoresistivity of the sensor. However, there are still a number of knitting parameters and structures that were not investigated due to the limited scope of this research. Particularly, the piezoresistivity of other base structures such as Purl and Rib base structures have hardly been studied. Moreover, hybrid weft knit strain sensors comprising of multiple base structures have not been investigated in any form. Research into these structures may lead to a more optimal weft knit strain sensor.

7.2.3 Impact of Human Parameters

The impact of human parameters such as sweat and body temperature on weft knit strain sensors have not been studied. In order to develop a commercial wearable device that utilises weft knit strain sensors, the investigation of the impact of these factors on weft knit strain sensors is crucial as they determine the feasibility of regular human use of the device.

7.2.4 Other Deep Learning Approaches

In Chapter 5, I utilised a simple deep learning algorithm to accurately classify data from human participants. However, there are more complex CNN architectures and other deep learning approaches that have performed better than our architecture in other research fields such as in medical imaging and sEMG. Therefore, it would be interesting to investigate the performances of these techniques on different data glove classification applications.

Appendix A

Ethical Review (MEEC 19-006)

Due to the experiments carried out with human participants in Chapter 5, an ethical review application was submitted. The ethical review application and its approval are shown below. In addition, the participant consent and information forms are also illustrated below.

A.1 Ethical Review Approval

The Secretariat
University of Leeds
Leeds, LS2 9JT
Tel: 0113 3431642
Email: MEECResearchEthics@leeds.ac.uk

UNIVERSITY OF LEEDS

Engineering and Physical Sciences joint Faculty Research Ethics Committee (EPS FREC)

Mr Emmanuel Ayodele
PhD Candidate (PGR Student)
School of Electronic and Electrical Engineering (IRASS)
Room 2.73, Faculty of Engineering
University of Leeds
LEEDS LS2 9JT

24th October 2019

Dear Emmanuel

Title of study **Activity Classification via Weft Knit Data Glove**
Ethics reference **MEEC 19-006**

I am pleased to inform you that the application listed above has been reviewed by the MaPS and Engineering joint Faculty Research Ethics Committee (MEEC FREC) and following receipt of your response to the Committee's initial comments, I can confirm a favourable ethical opinion as of the date of this letter. The following documentation was considered:

Document	*Version*	*Date*
Ethical_Review_Form_Emmanuel_Ayodele_version_1.1_23 08 19	1.1	23/08/2019
Participant_consent_form_Emmanuel_Ayodele_Version1.3_24 10 19	1.3	24/10/2019
Participant_information_sheet_Emmanuel_Ayodele_Version 1.4_24 10 19	1.4	24/10/2019
Recruitment_email_Emmanuel_Ayodele_version1.1_23 08 19	1.1	23/08/2019
GateKeeper permission_Emmanuel_Ayodele_Version1.1_23 08 19	1.1	23/08/2019

Please notify the committee if you intend to make any amendments to the information in your ethics application as submitted at date of this approval as all changes must receive ethical approval prior to implementation. The amendment form is available at http://ris.leeds.ac.uk/EthicsAmendment.

Please note: You are expected to keep a record of all your approved documentation and other documents relating to the study, including any risk assessments. This should be kept in your study file, which should be readily available for audit purposes. You will be given a two week notice period if your project is to be audited. There is a checklist listing examples of documents to be kept which is available at http://ris.leeds.ac.uk/EthicsAudits.

We welcome feedback on your experience of the ethical review process and suggestions for improvement. Please email any comments to MEECResearchEthics@leeds.ac.uk.

Yours sincerely

Rachel E de Souza, Research Ethics & Governance Administrator, The Secretariat
On behalf of Dr Ray Holt, Acting Chair, MEEC FREC

CC Student supervisor

A.2 Participant Consent Form

School of Electronic and Electrical Engineering, Faculty of Engineering

UNIVERSITY OF LEEDS

Consent to take part in "Activity Classification via Weft Knit Data Glove."

	Please add your initials next to the statements you agree with
I confirm that I have read and understand the information sheet/ letter dated _____ explaining the above research project and I have had the opportunity to ask questions about the project.	
I agree for the data collected from me to be stored on a secure University of Leeds server for back up in a pseudonymised form.	
I consent for my anonymised data to be used for future research.	
I understand that relevant sections of the data collected during the study, may be looked at by auditors from the University of Leeds or from regulatory authorities where it is relevant to my taking part in this research. I give permission for these individuals to have access to my records.	
I consent to the disclosure of experiment data and results in institutional repository, academic meetings, journals and other publication types.	
I agree to take part in the above research project.	

Name of participant	
Withdrawal of the experiment data (To be kept blank unless acquired data is to be withdrawn. A signature is then required).	
Name of lead researcher	
Signature of the lead researcher	
Signature of participant	
Date*	

*To be signed and dated in the presence of the participant.

Once this has been signed by all parties the participant should receive a copy of the signed and dated participant consent form, the letter/ pre-written script/ information sheet and any other written information provided to the participants. A copy of the signed and dated consent will be kept in a secure location. The code number of the participant will be stored in a separate password protected document on a secure University of Leeds server.

Project title: Activity Classification via Weft Knit Data Glove.	*Document type*	*Version #*	*Date*
	Consent form template	1.3	24/10/2019

A.3 Application for Ethical Approval

UNIVERSITY OF LEEDS RESEARCH ETHICS COMMITTEE APPLICATION FORM [1]

UNIVERSITY OF LEEDS

Please read each question carefully, taking note of instructions and completing all parts. If a question is not applicable please indicate so. The superscripted numbers (eg[8]) refer to sections of the guidance notes, available at http://ris.leeds.ac.uk/UoLEthicsApplication. Where a question asks for information which you have previously provided in answer to another question, please just refer to your earlier answer rather than repeating information.
Information about research ethics training courses: http://ris.leeds.ac.uk/EthicsTraining.

To help us process your application enter the following reference numbers, if known and if applicable:

Ethics reference number:	**MEEC 19-006**
Student number and/ or grant reference:	**200991840**

PART A: Summary

A.1 Which Faculty Research Ethics Committee would you like to consider this application?[2]

- ○ Arts, Humanities and Cultures (AHC)
- ○ Biological Sciences (BIOSCI)
- ○ Social Sciences/ Environment/ LUBS (AREA)
- ◉ MaPS and Engineering (MEEC)
- ○ Medicine and Health (Please specify a subcommittee):
  - ○ School of Dentistry (DREC)
  - ○ School of Healthcare (SHREC)
  - ○ School of Medicine (SoMREC)
  - ○ School of Psychology (SoPREC)

A.2 Title of the research[3]

Activity Classification via Weft Knit Data Glove.

A.3 Principal investigator's contact details[4]	
Name *(Title, first name, surname)*	Mr Emmanuel Ayodele
Position	PhD Candidate (PGR Student)
Department/ School/ Institute	School of Electronic and Electrical Engineering (IRASS)
Faculty	Faculty of Engineering
Work address *(including postcode)*	2.73, School of Electronic and Electrical Engineering, University of Leeds. Ls2 9JT.
Telephone number	+44(0)7931776779
University of Leeds email address	El15eoa@leeds.ac.uk

A.4 Purpose of the research:[5] (Tick as appropriate)

- [x] Research
- [ ] Educational qualification: ***Please specify:*** _____
- [ ] Educational Research & Evaluation[6]
- [ ] Medical Audit or Health Service Evaluation[7]
- [ ] Other

A.5 Select from the list below to describe your research: (You may select more than one)

- [x] Research on or with human participants
- [ ] Research which has potential adverse environmental impact.[8] ***If yes, please give details:***

  _____

- [x] Research working with data of human participants
  - [x] New data collected by qualitative methods
  - [x] New data collected by quantitative methods
  - [ ] New data collected from observing individuals or populations
  - [x] Routinely collected data or secondary data
  - [ ] Research working with aggregated or population data
  - [ ] Research using already published data or data in the public domain
- [ ] Research working with human tissue samples (*Please inform the relevant Persons Designate if the research will involve human tissue)*[9]

A.6 Will the research involve NHS staff recruited as potential research participants (by virtue of their professional role) or NHS premises/ facilities?

- [ ] Yes
- [x] No

If yes, ethical approval must be sought from the University of Leeds. Note that approval from the NHS Health Research Authority may also be needed, please contact FMHUniEthics@leeds.ac.uk for advice.

A.7 Will the research involve any of the following:[10] (You may select more than one)

If your project is classified as research rather than service evaluation or audit and involves any of the following an application must be made to the NHS Health Research Authority via IRAS www.myresearchproject.org.uk as NHS ethics approval will be required. ***There is no need to complete any more of this form****. Further information is available at http://ris.leeds.ac.uk/NHSethicalreview and at http://ris.leeds.ac.uk/HRAapproval.*
You may also contact ***governance-ethics@leeds.ac.uk*** *for advice.*

- [ ] Patients and users of the NHS (including NHS patients treated in the private sector)[11]
- [ ] Individuals identified as potential participants because of their status as relatives or carers of patients and users of the NHS
- [ ] Research involving adults in Scotland, Wales or England who lack the capacity to consent for themselves[12]
- [ ] A prison or a young offender institution in England and Wales (and is health related)[14]
- [ ] Clinical trial of a medicinal product or medical device[15]
- [ ] Access to data, organs or other bodily material of past and present NHS patients[9]
- [ ] Use of human tissue (including non-NHS sources) where the collection is not covered by a Human

Tissue Authority licence[9]

☐ Foetal material and IVF involving NHS patients

☐ The recently deceased under NHS care

☑ None of the above

You must inform the Research Ethics Administrator of your NHS REC reference and approval date once approval has been obtained.

The HRA decision tool to help determine the type of approval required is available at http://www.hra-decisiontools.org.uk/ethics. If the University of Leeds is not the Lead Institution, or approval has been granted elsewhere (e.g. NHS) then you should contact the local Research Ethics Committee for guidance. The UoL Ethics Committee needs to be assured that any relevant local ethical issues have been addressed.

A.8 Will the participants be from any of the following groups? (Tick as appropriate)

☐ Children under 16[16] ***Specify age group:*** _____

☐ Adults with learning disabilities[12]

☐ Adults with other forms of mental incapacity or mental illness

☐ Adults in emergency situations

☐ Prisoners or young offenders[14]

☑ Those who could be considered to have a particularly dependent relationship with the investigator, eg members of staff, students[17]

☐ Other vulnerable groups

☐ No participants from any of the above groups

Please justify the inclusion of the above groups, explaining why the research cannot be conducted on non-vulnerable groups.

Fellow PhD researchers are preferred as participants as they generally understand the importance of research and are likely to participate because of interest without any financial benefit. Additionally, it is believed that the average phd researcher falls under the age group necessary for the study.

It is the researcher's responsibility to check whether a DBS check (or equivalent) is required and to obtain one if it is needed. See also http://ris.leeds.ac.uk/healthandsafetyadvice and http://www.homeoffice.gov.uk/agencies-public-bodies/dbs.

A.9 Give a short summary of the research[18]

*This section must be completed in **language comprehensible to the lay person**. Do not simply reproduce or refer to the protocol, although the protocol can also be submitted to provide any technical information that you think the ethics committee may require. This section should cover the main parts of the proposal.*

Remote progress measurement can help to drastically reduce the cost of rehabilitation of patients who cannot afford to employ therapists for home visits to follow-up on their progress. It also allows therapist and other healthcare professionals to remotely monitor the progress of several patients within the travel time it takes to meet one patient.

In this project, we have developed a novel internet of things (IoT) data glove that can measure the joint angles of fingers in the hand. However, it will be more useful if the data obtained can be classified into respective activities (i.e. what the patient is doing) such as making a fist, holding a pen etc. Therefore, several healthy participants are asked to perform non-strenuous grasping activity of holding different objects such as a pen, key, computer mouse etc. while wearing the glove. The obtained data is then used to train a classifier (algorithm) such that when the glove is worn by a new participant, it can accurately say what they are holding. This algorithm can then be applied in the future to determine specifically what activity the patient can perform to his/her therapist/doctor. The doctor/therapist can evaluate from the results how much progress the patient has made.

It is worth noting, that we have disabled the IoT capability of the glove for the experiment to ensure that the data of the participant is fully within our control and is not subject to the risk associated with involving 3rd parties.

A.10 What are the main ethical issues with the research and how will these be addressed?[19]
Indicate any issues on which you would welcome advice from the ethics committee.
Although, I as a phd student have no authority over other phd students that will participate in this research, I acknowledge that some of the participants are fellow colleagues who might not want to say no as they might need me in their own experiments in the future. Therefore, I am using a gatekeeper outside of the research team to approach them via a mass email. Furthermore, the information sheet makes it clear that participants reserve the right to say no.

There may be concerns about the data glove in terms of health and safety. However, the data glove is extremely light (lighter than current commercial gloves) because it is wholly textile. Furthermore, the transmission setup (i.e. that connects the glove to the pc) is made up of commercial wearable devices with no recorded safety issues. Therefore, the data glove has no potential health and safety issues.

PART B: About the research team

B.1 To be completed by students only[20]	
Qualification working towards (eg Masters, PhD)	PhD
Supervisor's name (Title, first name, surname)	Dr Syed Ali Raza Zaidi
Department/ School/ Institute	School of Electronic and Electrical Engineering Institute of Robotics, Autonomous Systems and Sensing
Faculty	Faculty of Engineering
Work address (including postcode)	1.70, School of Electronic and Electrical Engineering, University of Leeds. Ls2 JT.
Supervisor's telephone number	+44(0)113 343 5241
Supervisor's email address	S.A.Zaidi@leeds.ac.uk
Module name and number (if applicable)	

B.2 Other members of the research team (eg co-investigators, co-supervisors) [21]	
Name *(Title, first name, surname)*	Dr Zhiqiang Zhang
Position	University Academic Fellow
Department/ School/ Institute	School of Electronic and Electrical Engineering Institute of Robotics, Autonomous Systems and Sensing
Faculty	Faculty of Engineering
Work address *(including postcode)*	1.69 School of Electronic and Electrical Engineering, University of Leeds. Ls2 JT.
Telephone number	+44(0)113 343 0289
Email address	Z.Zhang3@leeds.ac.uk

Name (Title, first name, surname)	Jane Scott
Position	Senior Teaching Fellow
Department/ School/ Institute	School of Design
Faculty	Faculty Of Arts, Humanities And Cultures
Work address (including postcode)	1.03, Clothworkers South, University of Leeds, Ls2 9JT.
Telephone number	+44(0)113 343 3777

Email address	J.C.Scott@leeds.ac.uk

Name (Title, first name, surname)	Dr Des McLernon
Position	Reader
Department/ School/ Institute	School of Electronic and Electrical Engineering Institute of Robotics, Autonomous Systems and Sensing
Faculty	Faculty of Engineering
Work address (including postcode)	2.66 School of Electronic and Electrical Engineering, University of Leeds. Ls2 JT.
Telephone number	+44(0)113 343 2050
Email address	D.C.McLernon@leeds.ac.uk

Part C: The research

C.1 What are the aims of the study?[22] (Must be in language comprehensible to a lay person.)

The aim of this study is to collect data from the participants performing simple grasping activities and use this data to train the algorithm in our novel glove so that the glove can say what activities are performed by any user. Therefore, when a patient wears the glove in the future, the therapist can know what the patient is doing without being there.

C.2 Describe the design of the research. Qualitative methods as well as quantitative methods should be included. (Must be in language comprehensible to a lay person.)

It is important that the study can provide information about the aims that it intends to address. If a study cannot answer the questions/ add to the knowledge base that it intends to, due to the way that it is designed, then wasting participants' time could be an ethical issue.

10 participants will be selected for the study. The data collected in the experiments will be divided into training and testing. The training set will be used to "teach" the algorithm in the glove while the testing set will be used to test the accuracy of the algorithm in predicting what activities where performed by the testing set.

C.3 What will participants be asked to do in the study?[23] *(e.g. number of visits, time, travel required, interviews)*

Each participant will be asked to grasp objects of different shapes. The 6 shapes are, cylindrical, hook, lateral, palmar, spherical and tip. There will be 3 objects in each shape category. Example of objects include a key, a computer mouse, an ID card etc. These objects are very light and it is expected that the entire experiments for each person will take less than 30 minutes. The experiments will be scheduled in batches of 1 so as not to waste the time of the participants waiting for one person to finish. Additionally, this ensures that the identity of each participant is not disclosed to other participants.

C.4 Does the research involve an international collaborator or research conducted overseas?[24]

☐ Yes ☑ No

If yes, describe any ethical review procedures that you will need to comply with in that country:

Describe the measures you have taken to comply with these:

Include copies of any ethical approval letters/ certificates with your application.

C.5 Proposed study dates and duration

Research start date (DD/MM/YY): 1/10/2019 Research end date (DD/MM/YY): 1/12/2019

Fieldwork start date (DD/MM/YY): _____ Fieldwork end date (DD/MM/YY): _____

C.6. Where will the research be undertaken? (i.e. in the street, on UoL premises, in schools)[25]

The research will be conducted in the Intelligent Robotics lab 1.53 in the school of electronic and electrical engineering.

RECRUITMENT & CONSENT PROCESSES

C.7 How will potential participants in the study be identified, approached and recruited?[26]
How will you ensure an appropriately convened sample group in order to meet the aims of the research? Give details for subgroups separately, if appropriate. How will any potential pitfalls, for example dual roles or potential for coercion, be addressed?

Potential participants are those who have no serious injuries in their hand or fingers. Additionally, they should be between 20 and 35 as statistically, people in this age range are known to have fully developed bones and have not been impacted by diseases such as stroke or rheumatoid arthritis which might affect joints in the hand.

As the department of electrical and electronic engineering has a lot of research students between the age of 20 and 35 and understand the importance of research and its impact on the society, they form the ideal candidates to participate in this study. As gender, race, religion and sexual orientation are irrelevant in this study, we will not be accessing any sources of identifiable personal information. However, since age and disability are excluding factors in this study, we will ensure that those who fall outside the requirements don't bother applying so that we don't obtain any personal information from them. We achieve this by clearly stating our exclusion criteria in our mass email and information sheet.

A mass email will be sent out to PhD students in the department of electrical and electronic engineering by a gatekeeper. We have selected the school administrator (Clair Atkinson) as the gate keeper. She has the authority to send out mass emails to PhD candidates in the school. We have also attached the mass email to be sent as a supporting document.

C.8 Will you be excluding any groups of people, and if so what is the rationale for that?[27]
Excluding certain groups of people, intentionally or unintentionally may be unethical in some circumstances. It may be wholly appropriate to exclude groups of people in other cases

Only participants with healthy joints in their hand can participate in this study. Healthy participants will form a good baseline to study the accuracy of the algorithm in classifying activities while participants with injuries will skew the results. We have added an age criteria excluding those younger than 20 because their bones are not fully developed and we have excluded people older than 35 as they are more likely to have diseases that may impact the joints in their hand.

C.9 How many participants will be recruited and how was the number decided upon?[28]
It is important to ensure that enough participants are recruited to be able to answer the aims of the research.

The number of participants was selected based on the prevalence in recent published papers. Data will be collected from 10 healthy participants. A dataset of 10 healthy participants is large enough to train the algorithm to classify new data into accurate activities.

Remember to include all advertising material (posters, emails etc) as part of your application

C10 Will the research involve any element of deception?[29]
If yes, please describe why this is necessary and whether participants will be informed at the end of the study.

No!

C.11 Will informed consent be obtained from the research participants?[30]

☑ Yes ☐ No

If yes, give details of how it will be done. Give details of any particular steps to provide information (in addition to a written information sheet) e.g. videos, interactive material. If you are not going to be obtaining informed consent you will need to justify this.

Participants will be informed about the aims, procedure and impact of the study in the information sheet that will be attached in the mass email. If they are interested in participating, they will be asked to sign a consent form. The consent form illustrates a written consent to participate in the study.
Furthermore, I will answer any questions they may have and explain verbally the procedure once again before the experiment begins.

If participants are to be recruited from any of potentially vulnerable groups, give details of extra steps taken to assure their protection. Describe any arrangements to be made for obtaining consent from a legal representative.

Since, potential participants are fellow PGR students, a gate keeper has been chosen to approach potential participants to prevent any form of coercion from the research team. We have also made it explicitly clear in the information sheet that potential participants have the right to say no.

Will research participants be provided with a copy of the Privacy Notice for Research? If not, explain why not.
Guidance is available at https://dataprotection.leeds.ac.uk/information-for-researchers.

☑ Yes ☐ No

***Copies of any written consent form, written information and all other explanatory material should accompany this application**. The information sheet should make explicit that participants can withdraw from the research at any time, if the research design permits. Remember to use meaningful file names and version control to make it easier to keep track of your documents.*
Sample information sheets and consent forms are available from the University ethical review webpage at http://ris.leeds.ac.uk/InvolvingResearchParticipants.

C.12 Describe whether participants will be able to withdraw from the study, and up to what point (eg if data is to be anonymised). If withdrawal is not possible, explain why not.
Any limits to withdrawal, eg once the results have been written up or published, should be made clear to participants in advance, preferably by specifying a date after which withdrawal would not be possible. Make sure that the information provided to participants (eg information sheets, consent forms) is consistent with the answer to C12.

Participants can withdraw from the study at ANY time they wish to do so. There is a section on the consent form that needs to be filled if participants want to withdraw their data. When this section is filled alongside a signature from the participant, the data is destroyed/deleted in the presence of the participant.

C.13 How long will the participant have to decide whether to take part in the research?[31]
It may be appropriate to recruit participants on the spot for low risk research; however consideration is usually necessary for riskier projects.

A deadline of a week will be given in the mass email. Although, this project is a low risk, we are giving sufficient time to allow enough participants to signify interest in the project.

C.14 What arrangements have been made for participants who might have difficulties understanding verbal explanations or written information, or who have particular communication needs that should be taken into account to facilitate their involvement in the research?[32] *Different populations will have different information needs, different communication abilities and different levels of understanding of the research topic. Reasonable efforts should be made to include potential participants who could otherwise be prevented from participating due to disabilities or language barriers.*

As the preferred target group are PhD researchers in the school of electrical and electronic engineering, it is expected that their written and oral communication skills will be sufficient to understand the aim, objectives and procedures of the study. However, if there are any participants who find it difficult to understand some sentences, google translate will be used to translate the sentences to their native languages.

C.15 Will individual or group interviews/ questionnaires discuss any topics or issues that might be sensitive, embarrassing or upsetting, or is it possible that criminal or other disclosures requiring action could take place during the study (e.g. during interviews or group discussions)?[33] *The information sheet should explain under what circumstances action may be taken.*

☐ Yes ☐ No *If yes, give details of procedures in place to deal with these issues.*

C.16 Will individual research participants receive any payments, fees, reimbursement of expenses or any other incentives or benefits for taking part in this research?[34]

☐ Yes ☐ No

If Yes, please describe the amount, number and size of incentives and on what basis this was decided.

RISKS OF THE STUDY

C.17 What are the potential benefits and/ or risks for research participants in both the short and medium-term?[35]

Potential risks for the participants include light fatigue due to performing grasping activities for less than 30 minutes. However, we mitigate this by advising/ensuring that participants perform a light warm up of their fingers before the experiments and we will take breaks if we notice or the user says that they are tired. We will advise the user to inform the research team if they need a break at any point in the experiment.

There are also potential risks to the storage of the data but we have mitigated these scenarios in later sections of this application.

C.18 Does the research involve any risks to the researchers themselves, or people not directly involved in the research? *Eg lone working*[36]

☐ Yes ☑ No

If yes, please describe: _____

Is a risk assessment necessary for this research?
If you are unsure whether a risk assessment is required visit http://ris.leeds.ac.uk/HealthAndSafetyAdvice or contact your Faculty Health and Safety Manager for advice.

☐ Yes ☑ No If yes, please include a copy of your risk assessment form with your application.

RESEARCH DATA

C.19 Explain what measures will be put in place to protect personal data. E.g. anonymisation procedures, secure storage and coding of data. Any potential for re-identification should be made clear to participants in advance.[37] *Please note that research data which appears in reports or other publications is not confidential, even if it is fully anonymised. For a fuller explanation see http://ris.leeds.ac.uk/ConfidentialityAnonymisation. Further guidance is available at http://ris.leeds.ac.uk/ResearchDataManagement.*

The identity of the participants is pseudonymized using code numbers. The data of each participant is identified with a chosen code number. The code number is written on the consent form and is only known by the participant and the research team. This method was selected so that the data of each participant can be recognised if the participant wants to withdraw their data. It is worth noting that the data itself does not have any recognisable traits that can be linked to the participant.

The data and the consent form are stored in separate folders on the researcher's University pc and the university assigned OneDrive backup. Furthermore, different folders are used for different participants i.e. each participant will have 2 folders, one for their data and one for their consent form. These folders will be secured with strong and unique passwords.

Non-members of the research team will not have access to the PC or OneDrive account and thus their data or consent forms.

Additionally, during experiments. Non-members of the research team are not allowed into the labs.

Data or consent forms will not be stored on the personal devices of the research team.

C.20 How will you make your research data available to others in line with: the University's, funding bodies' and publishers' policies on making the results of publically funded research publically available. Explain the extent to which anonymity will be maintained. *(max 200 words)* Refer to http://ris.leeds.ac.uk/ConfidentialityAnonymisation and http://ris.leeds.ac.uk/ResearchDataManagement for guidance.

This research is privately funded so there is no need to share the research data to funding bodies. However, if the research data is made available to others such as the university or journals, it will be made available only with the code numbers and not the real identity of the participants. As earlier mentioned, it is impossible to identify participants directly or indirectly from the data collected.

C.21 Will the research involve any of the following activities at any stage (including identification of potential research participants)? (Tick as appropriate)

- ☐ Examination of personal records by those who would not normally have access
- ☐ Access to research data on individuals by people from outside the research team
- ☐ Electronic surveys, please specify survey tool: _____ (further guidance)
- ☐ Other electronic transfer of data
- ☐ Use of personal addresses, postcodes, faxes, e-mails or telephone numbers
- ☐ Use of audio/ visual recording devices (NB this should usually be mentioned in the information for participants)
- ☐ FLASH memory or other portable storage devices

Storage of personal data on, or including, any of the following:

- ☑ University approved cloud computing services
- ☐ Other cloud computing services
- ☐ Manual files
- ☐ Private company computers
- ☐ Laptop computers
- ☐ Home or other personal computers (not recommended; data should be stored on a University of Leeds server such as your M: or N: drive where it is secure and backed up regularly: http://ris.leeds.ac.uk/ResearchDataManagement.)

Unclassified and Confidential University data must be kept on the University servers or in approved cloud services such as Office 365 (SharePoint or OneDrive). The N: Drive or Office 365 should be used for the storage of data that needs to be shared. If Highly Confidential information is kept in these shared storage areas it must be encrypted. Highly Confidential data that is not to be shared should be kept on the M: Drive. The use of non-University approved cloud services for the storage of any University data, including that which is unclassified, is forbidden without formal approval from IT. Further guidance is available via http://ris.leeds.ac.uk/ResearchDataManagement.

C.22 How do you intend to share the research data? (Indicate with an 'X) *Refer to http://library.leeds.ac.uk/research-data-deposit for guidance.*

- ☐ Exporting data outside the European Union
- ☐ Sharing data with other organisations
- ☐ Publication of direct quotations from respondents
- ☐ Publication of data that might allow identification of individuals to be identified
- ☑ Submitting to a journal to support a publication
- ☑ Depositing in a self-archiving system or an institutional repository
- ☐ Dissemination via a project or institutional website
- ☐ Informal peer-to-peer exchange
- ☐ Depositing in a specialist data centre or archive
- ☐ Other, please state: _____.
- ☐ No plans to report or disseminate the data

C.23 How do you intend to report and disseminate the results of the study? (Indicate with an 'X) Refer to http://ris.leeds.ac.uk/ResearchDissemination and http://ris.leeds.ac.uk/Publication for guidance.

- [x] Conference presentation
- [x] Peer reviewed journals
- [x] Publication as an eThesis in the Institutional repository
- [ ] Publication on website
- [ ] Other publication or report, please state: _____
- [ ] Submission to regulatory authorities
- [ ] Other, please state: _____.
- [ ] No plans to report or disseminate the results

C.24 For how long will data from the study be stored? Please explain why this length of time has been chosen.[38] Refer to the RCUK Common Principles on Data Policy and http://ris.leeds.ac.uk/info/71/good_research_practice/106/research_data_guidance/5.
***Students**: It would be reasonable to retain data for at least 2 years after publication or three years after the end of data collection, whichever is longer.*

__3_____ years, _____0___ months.

As this is a PhD study, the data will be retained for 3 years after the end of the data collection and will be discarded securely afterwards. This time period allows for any investigation into any allegation of academic fraud. The data will be discarded by utilising the university's IT department tool in deleting sensitive data.

CONFLICTS OF INTEREST

C.25 Will any of the researchers or their institutions receive any other benefits or incentives for taking part in this research over and above normal salary or the costs of undertaking the research?[39]

- [ ] **Yes**
- [x] **No**

If yes, indicate how much and on what basis this has been decided

_____

C.26 Is there scope for any other conflict of interest?[40] *For example, could the research findings affect the any ongoing relationship between any of the individuals or organisations involved and the researcher(s)? Will the research funder have control of publication of research findings? Refer to http://ris.leeds.ac.uk/ConflictsOfInterest.*

- [ ] Yes
- [x] No

If so, please describe this potential conflict of interest, and outline what measures will be taken to address any ethical issues that might arise from the research.

C.27 Does the research involve external funding? (Tick as appropriate)

- [ ] Yes
- [x] No

If yes, what is the source of this funding? _____

NB: If this research will be financially supported by the US Department of Health and Human Services or any of its divisions, agencies or programmes please ensure the additional funder requirements are complied with. Further guidance is available at http://ris.leeds.ac.uk/FWAcompliance and you may also contact your FRIO for advice.

PART D: Declarations

Declaration by Principal Investigators

1. The information in this form is accurate to the best of my knowledge and belief and I take full responsibility for it.
2. I undertake to abide by the University's ethical and health & safety guidelines, and the ethical principles underlying good practice guidelines appropriate to my discipline.
3. If the research is approved I undertake to adhere to the study protocol, the terms of this application and any conditions set out by the Research Ethics Committee (REC).
4. I undertake to seek an ethical opinion from the REC before implementing substantial amendments to the protocol.
5. I undertake to submit progress reports if required.
6. I am aware of my responsibility to be up to date and comply with the requirements of the law and relevant guidelines relating to security and confidentiality of patient or other personal data, including the need to register when necessary with the University's Data Protection Controller (further information available via http://ris.leeds.ac.uk/ResearchDataManagement).
7. I understand that research records/ data may be subject to inspection for audit purposes if required in future.
8. I understand that personal data about me as a researcher in this application will be held by the relevant RECs and that this will be managed according to the principles established in the Data Protection Act.
9. I understand that the REC may choose to audit this project at any point after approval.

Sharing information for training purposes: *Optional – please tick as appropriate:*

☑ I would be content for members of other Research Ethics Committees to have access to the information in the application in confidence for training purposes. All personal identifiers and references to researchers, funders and research units would be removed.

Principal Investigator:

Signature of Principal Investigator: .....
(This needs to be an actual signature rather than just typed. Electronic signatures are acceptable)

Print name: .....Emmanuel Ayodele..... Date: (dd/mm/yyyy): ....19/08/2019.....

Supervisor of student research:

I have read, edited and agree with the form above.

Supervisor's signature: .....
(This needs to be an actual signature rather than just typed. Electronic signatures are acceptable)

Print name: ..Dr Syed Ali Raza Zaidi.. Date: (dd/mm/yyyy): 19/08/2019.....

Please submit your form by email to the FREC or School REC's mailbox.

Remember to include any supporting material such as your participant information sheet, consent form, interview questions and recruitment material with your application.

To help speed up the review of your application:

- ❑ Answer the questions in plain English, avoid using overly technical terms and acronyms not in common use.
- ❑ Answer all the questions on the form, including those with several parts (refer to the guidance if you're not sure how to answer a question or how much detail is required).
- ❑ Include any relevant supplementary materials such as
    - ❑ Recruitment material (posters, emails etc)
    - ❑ Sample participant information sheet
    - ❑ Sample consent form. Include different versions for different groups of participants eg for children and adults, clearly indicating which is which.
    - ❑ Signed risk assessment (If you are unsure whether a risk assessment is required visit http://ris.leeds.ac.uk/HealthAndSafetyAdvice or contact your Faculty Health and Safety Manager for advice).

  Remember to include use version control and meaningful file names for the documents.
- ❑ If you are not going to be using participant information sheets or consent forms explain why not and how informed consent will be otherwise obtained.
- ❑ If you are a student it is essential that you discuss your application with your supervisor.
- ❑ Submit a signed copy of the application, preferably electronically. Students' applications need to be signed by their supervisors as well.

A.4 Participant Information sheet

School of Electronic and Electrical Engineering, Faculty of Engineering

UNIVERSITY OF LEEDS

PARTICIPANT INFORMATION SHEET

RESEARCH PROJECT: **Activity Classification via Weft Knit Data Glove**

You are invited to participate in the research project titled: *Activity classification via weft knit data glove*. If you have had any injuries to your fingers or hand, please decline to participate in this project without giving any reason. If you have had no injuries to your fingers and are between the ages of 20-35 and you wish to continue, please read the information below.

Purpose of the project

Data gloves can provide a cheap method of monitoring patients remotely. This can enable healthcare professionals to monitor several patients in the time it takes to visit one. However, the output data of the glove will not make sense to the healthcare professional unless it is converted to something meaningful. The aim of this project is to train and validate a classifier (an algorithm) with the data from healthy participants to enable it accurately predict the activities performed when a new user wears the glove. This algorithm will help to convert the data from the glove to meaningful information that healthcare professionals can easily understand. This study is undertaken as part of the lead researcher's PhD.

Selection of Participants

This research focuses on training the algorithm with healthy participants to ensure consistency in the data and processed results. Therefore, participants with injuries on their fingers are excluded.

What do I have to do?

The participant is required to wear the data glove and grasp light objects of different shapes. Objects include a coffee mug, ID card, pen, small box etc. The entire experiment will take only 20 minutes and will take place within one visit.

What are the possible disadvantages and risks of taking part

Participants will be required to sit for a short period during the experiment. There may be a risk of slight fatigue so it is advised that participants perform some grasping exercises for a few seconds to warm up the necessary joints. However, there are no health and safety risks that might require emergency prevention.

What are the possible benefits of taking part?

There are no financial benefits in taking part in this project. However, you are participating in research that has a potential for making the world a better place for people with disabilities.

Can I say NO?

Yes, YOU CAN! Please feel free to say no for whatsoever reason you may have. But if you do decide to participate, you will be given this information sheet to keep and you will be required to sign a consent form. Furthermore, you can withdraw your consent data unconditionally with no required reason.

How confidential is my data?

Your data will be fully pseudonymised. This means that your data will only be stored with the code number assigned to it. The consent form containing your code number and your name is only stored to allow identification of your data if you plan on withdrawing consent, so that it can be destroyed. Furthermore, the consent form will only be disclosed to the researcher and no one else. Any access to your data in publications (in form of results of the study) such as journals will only be in its pseudonymised form.

In addition, your data will be stored on a secure University of Leeds server in folders protected with strong passwords.

Can I WITHDRAW my data?

Yes! You can withdraw your data up to 3 weeks after the study and you don't have to give a reason. The limit of 3 weeks post-experiment is given because the data will be analysed and submitted for publications at which point withdrawal is impossible.

How is the research being funded/organised?

This research is part of the lead researcher's PhD project and there is no current available funding.

Contact information for complaints

Clare Skinner, Head of Research Integrity and Governance, Secretariat. c.e.skinner@leeds.ac.uk

Privacy Notice for Research

Please take some time to read this document. It is important to read this before participating in this study. ***Privacy Notice for Research.*** Hard copy versions will be printed if requested.

Contact for further information

The contact details of researcher:

Name (title, first name, last name)	Emmanuel Ayodele
Department/ School/ Institute	Faculty of Engineering School of Electronic and Electrical Engineering

	Institute of Robotics, Autonomous Systems and Sensing
Telephone number	+44(0)7931776779
University of Leeds email address	el15eoa@leeds.ac.uk

The contact details of main supervisor:

Name (title, first name, last name)	Dr Syed Ali Raza Zaidi
Department/ School/ Institute	Faculty of Engineering School of Electronic and Electrical Engineering Institute of Robotics, Autonomous Systems and Sensing
Telephone number	+44(0)113 343 5241
University of Leeds email address	S.A.Zaidi@leeds.ac.uk

References

[1] Z. Wang, J. Wang, H. Zhao, S. Qiu, J. Li, F. Gao, and X. Shi, "Using wearable sensors to capture posture of the human lumbar spine in competitive swimming," *IEEE Transactions on Human-Machine Systems*, vol. 49, no. 2, pp. 194–205, 2019. 1

[2] S. S. Rautaray and A. Agrawal, "Vision based hand gesture recognition for human computer interaction: a survey," *Artificial intelligence review*, vol. 43, no. 1, pp. 1–54, 2015. 1

[3] T. B. Moeslund, A. Hilton, and V. Krüger, "A survey of advances in vision-based human motion capture and analysis," *Computer vision and image understanding*, vol. 104, no. 2-3, pp. 90–126, 2006. 1

[4] K. E. Caine, A. D. Fisk, and W. A. Rogers, "Benefits and privacy concerns of a home equipped with a visual sensing system: A perspective from older adults," in *Proceedings of the human factors and ergonomics society annual meeting*, vol. 50, no. 2. SAGE Publications Sage CA: Los Angeles, CA, 2006, pp. 180–184. 1

[5] S. Liao, "The apple watch outsold the entire swiss watch industry in 2019," Feb 2020. [Online]. Available: https://edition.cnn.com/2020/02/14/tech/apple-swiss-watches/index.html 2

[6] J. Maier, "Made smarter review.(2017)," *Department for Business EIS. The Stationery Office. London*, 2017. 2

[7] J. S. Heo, J. Eom, Y.-H. Kim, and S. K. Park, "Recent progress of textile-based wearable electronics: a comprehensive review of materials, devices, and applications," *Small*, vol. 14, no. 3, p. 1703034, 2018. 2

[8] G. N. Islam, A. Ali, and S. Collie, "Textile sensors for wearable applications: A comprehensive review," *Cellulose*, vol. 27, no. 11, pp. 6103–6131, 2020. 2

[9] B. Almohammed, A. Ismail, and A. Sali, "Electro-textile wearable antennas in wireless body area networks: materials, antenna design, manufacturing techniques, and human body consideration—a review," *Textile Research Journal*, p. 0040517520932230, 2020. 2

[10] D. Patron, W. Mongan, T. P. Kurzweg, A. Fontecchio, G. Dion, E. K. Anday, and K. R. Dandekar, "On the use of knitted antennas and inductively coupled rfid tags for wearable applications," *IEEE transactions on biomedical circuits and systems*, vol. 10, no. 6, pp. 1047–1057, 2016. 2, 103

[11] J. Wang, S. Soltanian, P. Servati, F. Ko, and M. Weng, "A knitted wearable flexible sensor for monitoring breathing condition," *Journal of Engineered Fibers and Fabrics*, vol. 15, p. 1558925020930354, 2020. 2

[12] C. Isaia, S. A. McMaster, and D. McNally, "Study of performance of knitted conductive sleeves as wearable textile strain sensors for joint motion tracking," in *2020 42nd Annual International Conference of the IEEE Engineering in Medicine & Biology Society (EMBC)*. IEEE, 2020, pp. 4555–4558. 2

[13] O. Atalay, W. R. Kennon, and E. Demirok, "Weft-knitted strain sensor for monitoring respiratory rate and its electro-mechanical modeling," *IEEE Sensors Journal*, vol. 15, no. 1, pp. 110–122, 2015. 3, 13, 14, 25, 29, 35, 36, 40, 41, 45, 51, 62, 63, 69, 84, 103, 117

[14] H. Zhang, X. Tao, S. Wang, and T. Yu, "Electro-mechanical properties of knitted fabric made from conductive multi-filament yarn under unidirectional extension," *Textile research journal*, vol. 75, no. 8, pp. 598–606, 2005. 3, 13, 14, 29, 30, 31, 32, 45, 51, 63, 69, 84, 104, 117

[15] O. Atalay, A. Tuncay, M. D. Husain, and W. R. Kennon, "Comparative study of the weft-knitted strain sensors," *Journal of Industrial Textiles*, vol. 46, no. 5, pp. 1212–1240, 2017. 3, 29, 30, 104

[16] R. Postle and D. Munden, "Analysis of the dry-relaxed knitted-loop configuration: Part i: Two-dimensional analysis," *Journal of the Textile Institute*, vol. 58, no. 8, pp. 329–351, 1967. 5, 26, 49, 53, 62, 67, 110

[17] Y. Li, Y. A. Samad, T. Taha, G. Cai, S.-Y. Fu, and K. Liao, "Highly flexible strain sensor from tissue paper for wearable electronics," *ACS Sustainable Chemistry & Engineering*, vol. 4, no. 8, pp. 4288–4295, 2016. 9

[18] B. Glišić, Y. Yao, S.-T. E. Tung, S. Wagner, J. C. Sturm, and N. Verma, "Strain sensing sheets for structural health monitoring based on large-area electronics and integrated circuits," *Proceedings of the IEEE*, vol. 104, no. 8, pp. 1513–1528, 2016. 9

[19] S. Seyedin, P. Zhang, M. Naebe, S. Qin, J. Chen, X. Wang, and J. M. Razal, "Textile strain sensors: a review of the fabrication technologies, performance evaluation and applications," *Materials Horizons*, vol. 6, no. 2, pp. 219–249, 2019. 10

[20] J. Wu, D. Zhou, C. O. Too, and G. G. Wallace, "Conducting polymer coated lycra," *Synthetic Metals*, vol. 155, no. 3, pp. 698–701, 2005. 10

[21] T. Lee, W. Lee, S.-W. Kim, J. J. Kim, and B.-S. Kim, "Flexible textile strain wireless sensor functionalized with hybrid carbon nanomaterials supported zno nanowires with controlled aspect ratio," *Advanced Functional Materials*, vol. 26, no. 34, pp. 6206–6214, 2016. 10, 11

[22] M. Zhang, C. Wang, Q. Wang, M. Jian, and Y. Zhang, "Sheath–core graphite/silk fiber made by dry-meyer-rod-coating for wearable strain sensors," *ACS applied materials & interfaces*, vol. 8, no. 32, pp. 20 894–20 899, 2016. 10

[23] X. Wu, Y. Han, X. Zhang, and C. Lu, "Highly sensitive, stretchable, and wash-durable strain sensor based on ultrathin conductive layer@ polyurethane yarn for tiny motion monitoring," *ACS applied materials & interfaces*, vol. 8, no. 15, pp. 9936–9945, 2016. 10

[24] X. Wang, X. Fu, and D. Chung, "Strain sensing using carbon fiber," *Journal of Materials Research*, vol. 14, no. 3, pp. 790–802, 1999. 11

[25] A. Lekawa-Raus, K. K. Koziol, and A. H. Windle, "Piezoresistive effect in carbon nanotube fibers," *ACS nano*, vol. 8, no. 11, pp. 11 214–11 224, 2014. 11

[26] S. Ryu, P. Lee, J. B. Chou, R. Xu, R. Zhao, A. J. Hart, and S.-G. Kim, "Extremely elastic wearable carbon nanotube fiber strain sensor for monitoring of human motion," *ACS nano*, vol. 9, no. 6, pp. 5929–5936, 2015. 11

[27] Y.-L. Li, I. A. Kinloch, and A. H. Windle, "Direct spinning of carbon nanotube fibers from chemical vapor deposition synthesis," *Science*, vol. 304, no. 5668, pp. 276–278, 2004. 11

[28] X. Li, P. Sun, L. Fan, M. Zhu, K. Wang, M. Zhong, J. Wei, D. Wu, Y. Cheng, and H. Zhu, "Multifunctional graphene woven fabrics," *Scientific reports*, vol. 2, p. 395, 2012. 12

[29] Z. Tang, S. Jia, F. Wang, C. Bian, Y. Chen, Y. Wang, and B. Li, "Highly stretchable core–sheath fibers via wet-spinning for wearable strain sensors," *ACS applied materials & interfaces*, vol. 10, no. 7, pp. 6624–6635, 2018. 12, 13

[30] C. Wang, X. Li, E. Gao, M. Jian, K. Xia, Q. Wang, Z. Xu, T. Ren, and Y. Zhang, "Carbonized silk fabric for ultrastretchable, highly sensitive, and wearable strain sensors," *Advanced materials*, vol. 28, no. 31, pp. 6640–6648, 2016. 12

[31] Y.-h. Wu, R.-m. Zhen, H.-z. Liu, S.-q. Liu, Z.-f. Deng, P.-p. Wang, S. Chen, and L. Liu, "Liquid metal fiber composed of a tubular channel as a high-performance strain sensor," *Journal of Materials Chemistry C*, vol. 5, no. 47, pp. 12 483–12 491, 2017. 13, 14

[32] S. Chen, H. Liu, S. Liu, P. Wang, S. Zeng, L. Sun, and L. Liu, "Transparent and waterproof ionic liquid-based fibers for highly durable multifunctional sensors and strain-insensitive stretchable conductors," *ACS applied materials & interfaces*, vol. 10, no. 4, pp. 4305–4314, 2018. 13

[33] C. Isaia, D. S. McNally, S. A. McMaster, and D. T. Branson, "Effect of mechanical preconditioning on the electrical properties of knitted conductive textiles during cyclic loading," *Textile Research Journal*, vol. 89, no. 3, pp. 445–460, 2019. 13, 29, 37, 38, 46, 63, 77

[34] H. Zhang, X. Tao, T. Yu, and S. Wang, "Conductive knitted fabric as large-strain gauge under high temperature," *Sensors and Actuators A: Physical*, vol. 126, no. 1, pp. 129–140, 2006. 13

[35] J. Foroughi, G. M. Spinks, S. Aziz, A. Mirabedini, A. Jeiranikhameneh, G. G. Wallace, M. E. Kozlov, and R. H. Baughman, "Knitted carbon-nanotube-sheath/spandex-core elastomeric yarns for artificial muscles and strain sensing," *ACS nano*, vol. 10, no. 10, pp. 9129–9135, 2016. 13

[36] S. Seyedin, J. M. Razal, P. C. Innis, A. Jeiranikhameneh, S. Beirne, and G. G. Wallace, "Knitted strain sensor textiles of highly conductive all-polymeric fibers," *ACS applied materials & interfaces*, vol. 7, no. 38, pp. 21 150–21 158, 2015. 13, 40, 41, 62

[37] O. Atalay, W. R. Kennon, and M. D. Husain, "Textile-based weft knitted strain sensors: Effect of fabric parameters on sensor properties," *Sensors*, vol. 13, no. 8, pp. 11 114–11 127, 2013. 13, 18, 37, 45, 63, 74, 104, 125

[38] O. Atalay and W. Kennon, "Knitted strain sensors: Impact of design parameters on sensing properties," *Sensors*, vol. 14, no. 3, pp. 4712–4730, 2014. 13, 39, 46, 63, 104

[39] M. Amjadi, A. Pichitpajongkit, S. Lee, S. Ryu, and I. Park, "Highly stretchable and sensitive strain sensor based on silver nanowire–elastomer nanocomposite," *ACS nano*, vol. 8, no. 5, pp. 5154–5163, 2014. 15, 17

[40] X. Xiao, L. Yuan, J. Zhong, T. Ding, Y. Liu, Z. Cai, Y. Rong, H. Han, J. Zhou, and Z. L. Wang, "High-strain sensors based on zno nanowire/polystyrene hybridized flexible films," *Advanced materials*, vol. 23, no. 45, pp. 5440–5444, 2011. 15

[41] M. Hempel, D. Nezich, J. Kong, and M. Hofmann, "A novel class of strain gauges based on layered percolative films of 2d materials," *Nano letters*, vol. 12, no. 11, pp. 5714–5718, 2012. 15

[42] J. J. Park, W. J. Hyun, S. C. Mun, Y. T. Park, and O. O. Park, "Highly stretchable and wearable graphene strain sensors with controllable sensitivity for human motion monitoring," *ACS applied materials & interfaces*, vol. 7, no. 11, pp. 6317–6324, 2015. 15

[43] W. Obitayo and T. Liu, "A review: Carbon nanotube-based piezoresistive strain sensors," *Journal of Sensors*, vol. 2012, 2012. 15, 17

[44] N. Hu, H. Fukunaga, S. Atobe, Y. Liu, J. Li *et al.*, "Piezoresistive strain sensors made from carbon nanotubes based polymer nanocomposites," *Sensors*, vol. 11, no. 11, pp. 10 691–10 723, 2011. 15

[45] C. Li, E. T. Thostenson, and T.-W. Chou, "Dominant role of tunneling resistance in the electrical conductivity of carbon nanotube–based composites," *Applied Physics Letters*, vol. 91, no. 22, p. 223114, 2007. 15

[46] A. Oskouyi, U. Sundararaj, and P. Mertiny, "Tunneling conductivity and piezoresistivity of composites containing randomly dispersed conductive nano-platelets," *Materials*, vol. 7, no. 4, pp. 2501–2521, 2014. 15

[47] T. Yamada, Y. Hayamizu, Y. Yamamoto, Y. Yomogida, A. Izadi-Najafabadi, D. N. Futaba, and K. Hata, "A stretchable carbon nanotube strain sensor for human-motion detection," *Nature nanotechnology*, vol. 6, no. 5, p. 296, 2011. 16

[48] Y. Wang, L. Wang, T. Yang, X. Li, X. Zang, M. Zhu, K. Wang, D. Wu, and H. Zhu, "Wearable and highly sensitive graphene strain sensors for human motion monitoring," *Advanced Functional Materials*, vol. 24, no. 29, pp. 4666–4670, 2014. 16

[49] X. Li, R. Zhang, W. Yu, K. Wang, J. Wei, D. Wu, A. Cao, Z. Li, Y. Cheng, Q. Zheng *et al.*, "Stretchable and highly sensitive graphene-on-polymer strain sensors," *Scientific reports*, vol. 2, p. 870, 2012. 16, 17

[50] S. Tadakaluru, W. Thongsuwan, and P. Singjai, "Stretchable and flexible high-strain sensors made using carbon nanotubes and graphite films on natural rubber," *Sensors*, vol. 14, no. 1, pp. 868–876, 2014. 17

[51] M. Amjadi, K.-U. Kyung, I. Park, and M. Sitti, "Stretchable, skin-mountable, and wearable strain sensors and their potential applications: a review," *Advanced Functional Materials*, vol. 26, no. 11, pp. 1678–1698, 2016. 17, 18

[52] C. Yan, J. Wang, W. Kang, M. Cui, X. Wang, C. Y. Foo, K. J. Chee, and P. S. Lee, "Highly stretchable piezoresistive graphene–nanocellulose nanopaper for strain sensors," *Advanced materials*, vol. 26, no. 13, pp. 2022–2027, 2014. 17

[53] C. S. Boland, U. Khan, C. Backes, A. O'Neill, J. McCauley, S. Duane, R. Shanker, Y. Liu, I. Jurewicz, A. B. Dalton *et al.*, "Sensitive, high-strain, high-rate bodily motion sensors based on graphene–rubber composites," *ACS nano*, vol. 8, no. 9, pp. 8819–8830, 2014. 17

[54] Y. R. Jeong, H. Park, S. W. Jin, S. Y. Hong, S.-S. Lee, and J. S. Ha, "Highly stretchable and sensitive strain sensors using fragmentized graphene foam," *Advanced Functional Materials*, vol. 25, no. 27, pp. 4228–4236, 2015. 18

[55] M. Amjadi, Y. J. Yoon, and I. Park, "Ultra-stretchable and skin-mountable strain sensors using carbon nanotubes–ecoflex nanocomposites," *Nanotechnology*, vol. 26, no. 37, p. 375501, 2015. 18

[56] L. Cai, L. Song, P. Luan, Q. Zhang, N. Zhang, Q. Gao, D. Zhao, X. Zhang, M. Tu, F. Yang *et al.*, "Super-stretchable, transparent carbon nanotube-based capacitive strain sensors for human motion detection," *Scientific reports*, vol. 3, no. 1, pp. 1–9, 2013. 18

[57] D. J. Spencer, *Knitting technology: a comprehensive handbook and practical guide*. CRC press, 2001, vol. 16. 19, 21, 22, 23, 62, 105, 110, 121

[58] V. Schrank, M. Beer, M. Beckers, and T. Gries, "Polymer-optical fibre (pof) integration into textile fabric structures," in *Polymer optical fibres*. Elsevier, 2017, pp. 337–348. 19

[59] B. Gupta and J. Edwards, "Textile materials and structures for topical management of wounds," in *Advanced Textiles for Wound Care*. Elsevier, 2019, pp. 55–104. 19

[60] M. J. Denton and P. N. Daniels, *Textile terms and definitions*. Textile Institute, 2002. 19

[61] K. Gandhi, *Woven textiles: Principles, technologies and applications*. Woodhead Publishing, 2019. 21

[62] H. Hu and Q. He, "Knitting of basalt filament yarn," *Textile research journal*, vol. 81, no. 7, pp. 690–697, 2011. 21

[63] F. T. Peirce, "Geometrical principles applicable to the design of functional fabrics," *Textile Research Journal*, vol. 17, no. 3, pp. 123–147, 1947. 24, 63

[64] A. Kurbak, "Plain knitted fabric dimensions (part ii)," *Textile Asia*, vol. 78, pp. 36–44, 1998. 25

[65] A. Kurbak and O. Ekmen, "Basic studies for modeling complex weft knitted fabric structures part i: A geometrical model for widthwise curlings of plain knitted fabrics," *Textile Research Journal*, vol. 78, no. 3, pp. 198–208, 2008. 25, 26

[66] S. Kawabata, "Nonlinear mechanics of woven and knitted materials," in *Textile structural composites*, W. B. Kleijn and K. K. Paliwal, Eds. Amsterdam: Elsevier, 1989, ch. 3. 27, 45

[67] J. Wang, H. Long, S. Soltanian, P. Servati, and F. Ko, "Electromechanical properties of knitted wearable sensors: Part 1–theory," *Textile Research Journal*, vol. 84, no. 1, pp. 3–15, 2014. 28, 33, 34, 45

[68] D. Munden, "26—the geometry and dimensional properties of plain-knit fabrics," *Journal of the Textile Institute Transactions*, vol. 50, no. 7, pp. T448–T471, 1959. 28, 111

[69] G. Leaf, "4—models of the plain-knitted loop," *Journal of the Textile Institute Transactions*, vol. 51, no. 2, pp. T49–T58, 1960. 28

[70] G. Leaf and A. Glaskin, "43—the geometry of a plain knitted loop," *Journal of the Textile Institute Transactions*, vol. 46, no. 9, pp. T587–T605, 1955. 28

[71] K. Yang, G.-l. Song, L. Zhang, and L.-w. Li, "Modelling the electrical property of 1× 1 rib knitted fabrics made from conductive yarns," in *Information and Computing Science, 2009. ICIC'09. Second International Conference on*, vol. 4. IEEE, 2009, pp. 382–385. 29, 30

[72] J. Wang, H. Long, S. Soltanian, P. Servati, and F. Ko, "Electro-mechanical properties of knitted wearable sensors: Part 2–parametric study and experimental verification," *Textile Research Journal*, vol. 84, no. 2, pp. 200–213, 2014. 34, 40, 45

[73] R. Holm, *Electric contacts: theory and application*. Springer Science & Business Media, 2013. 38, 104

[74] L. Li, W. M. Au, K. M. Wan, S. H. Wan, W. Y. Chung, and K. S. Wong, "A resistive network model for conductive knitting stitches," *Textile research journal*, vol. 80, no. 10, pp. 935–947, 2010. 40, 62

[75] R. K. Raji, X. Miao, A. Wan, L. Niu, Y. Li, and A. Boakye, "Knitted piezoresistive smart chest band and its application for respiration patterns assessment," *Journal of Engineered Fibers and Fabrics*, vol. 14, p. 1558925019868474, 2019. 41, 42

[76] Y. Li, X. Miao, and R. K. Raji, "Flexible knitted sensing device for identifying knee joint motion patterns," *Smart Materials and Structures*, vol. 28, no. 11, p. 115042, 2019. 41, 62, 84

[77] R. Reddy K, S. Gandla, and D. Gupta, "Highly sensitive, rugged, and wearable fabric strain sensor based on graphene clad polyester knitted elastic band for human motion monitoring," *Advanced Materials Interfaces*, vol. 6, no. 16, p. 1900409, 2019. 41

[78] H. Zhang and X. Tao, "From wearable to aware: Intrinsically conductive electrotextiles for human strain/stress sensing," in *Biomedical and Health Informatics (BHI), 2012 IEEE-EMBS International Conference on*. IEEE, 2012, pp. 468–471. 44, 63, 120

[79] W.-L. Wu, H. Hamada, and Z.-i. Maekawa, "Computer simulation of the deformation of weft-knitted fabrics for composite materials," *Journal of the Textile Institute*, vol. 85, no. 2, pp. 198–214, 1994. 45

[80] F. T. Peirce, "5—the geometry of cloth structure," *Journal of the Textile Institute Transactions*, vol. 28, no. 3, pp. T45–T96, 1937. 45

[81] P. Popper, "The theoretical behavior of a knitted fabric subjected to biaxial stresses," *Textile Research Journal*, vol. 36, no. 2, pp. 148–157, 1966. 45

[82] N. J. Seo, W. Z. Rymer, and D. G. Kamper, "Delays in grip initiation and termination in persons with stroke: effects of arm support and active muscle stretch exercise," *Journal of neurophysiology*, vol. 101, no. 6, pp. 3108–3115, 2009. 59

[83] M. H. Schieber, C. Lang, K. Reilly, P. McNulty, and A. Sirigu, "Selective activation of human finger muscles after stroke or amputation," in *Progress in Motor Control*. Springer, 2009, pp. 559–575. 59

[84] C.-y. Park, J.-h. Bae, and I. Moon, "Development of wireless data glove for unrestricted upper-extremity rehabilitation system," in *ICCAS-SICE, 2009*. IEEE, 2009, pp. 790–793. 59

[85] R. V. Aroca, R. S. Inoue, L. M. Pedro, G. A. Caurin, and D. V. Magalhaes, "Towards a battery-free wireless smart glove for rehabilitation applications based on rfid," in *RFID, 2015 IEEE Brasil*. IEEE, 2015, pp. 1–5. 59

[86] C. OQuigley, M. Sabourin, S. Coyle, J. Connolly, J. Condall, K. Curran, B. Corcoran, and D. Diamond, "Characteristics of a piezo-resistive fabric stretch sensor glove for home-monitoring of rheumatoid arthritis," in *Wearable and Implantable Body Sensor Networks Workshops (BSN Workshops), 2014 11th International Conference on*. IEEE, 2014, pp. 23–26. 60

[87] G. S. Rash, P. P. Belliappa, M. P. Wachowiak, N. N. Somia, and A. Gupta, "A demonstration of the validity of a 3-d video motion analysis method for measuring finger flexion and extension," *Journal of Biomechanics*, vol. 32, no. 12, pp. 1337–1341, 1999. 60

[88] R. Y. Wang and J. Popović, "Real-time hand-tracking with a color glove," *ACM transactions on graphics (TOG)*, vol. 28, no. 3, p. 63, 2009. 60

[89] P. Braido and X. Zhang, "Quantitative analysis of finger motion coordination in hand manipulative and gestic acts," *Human Movement Science*, vol. 22, no. 6, pp. 661–678, 2004. 60

[90] O. Luzanin and M. Plancak, "Hand gesture recognition using low-budget data glove and cluster-trained probabilistic neural network," *Assembly Automation*, vol. 34, no. 1, pp. 94–105, 2014. 60, 61

[91] I.-K. Park, J.-H. Kim, and K.-S. Hong, "An implementation of an fpga-based embedded gesture recognizer using a data glove," in *Proceedings of the 2nd international conference on Ubiquitous information management and communication*. ACM, 2008, pp. 496–500. 60, 61

[92] C. Oz and M. C. Leu, "Recognition of finger spelling of american sign language with artificial neural network using position/orientation sensors and data glove," in *International Symposium on Neural Networks*. Springer, 2005, pp. 157–164. 60, 61

[93] R. Ozawa and N. Ueda, "Supervisory control of a multi-fingered robotic hand system with data glove," in *2007 IEEE/RSJ International Conference on Intelligent Robots and Systems*. IEEE, 2007, pp. 1606–1611. 60, 61

[94] A. Tognetti, N. Carbonaro, G. Zupone, and D. De Rossi, "Characterization of a novel data glove based on textile integrated sensors," in *2006 International Conference of the IEEE Engineering in Medicine and Biology Society*. IEEE, 2006, pp. 2510–2513. 61

[95] S. Pabon, E. Sotgiu, R. Leonardi, C. Brancolini, O. Portillo-Rodriguez, A. Frisoli, and M. Bergamasco, "A data-glove with vibro-tactile stimulators for virtual social interaction and rehabilitation," in *10th Annual Intl Workshop on Presence*, 2007, pp. 345–348. 61

[96] C.-S. Fahn and H. Sun, "Development of a data glove with reducing sensors based on magnetic induction," *IEEE Transactions on Industrial Electronics*, vol. 52, no. 2, pp. 585–594, 2005. 61

[97] P. Kumar, J. Verma, and S. Prasad, "Hand data glove: a wearable real-time device for human-computer interaction," *International Journal of Advanced Science and Technology*, vol. 43, 2012. 61

[98] G. Saggio, S. Bocchetti, C. A. Pinto, and G. Orengo, "Wireless data glove system developed for hmi," in *2010 3rd International Symposium on Applied Sciences in Biomedical and Communication Technologies (ISABEL 2010)*. IEEE, 2010, pp. 1–5. 61

[99] G. Saggio, F. Giannini, M. Todisco, and G. Costantini, "A data glove based sensor interface to expressively control musical processes," in *2011 4th IEEE International Workshop on Advances in Sensors and Interfaces (IWASI)*. IEEE, 2011, pp. 192–195. 61

[100] N. H. Adnan, K. Wan, A. Shahriman, S. K. Za'ba, H. Desa, and M. A. A. Aziz, "The development of a low cost data glove by using flexible bend sensor for resistive interfaces," in *The 2nd International Malaysia-Ireland Joint Symposium on Engineering, Science and Business*, 2012, pp. 579–587. 61

[101] A. Z. Shukor, M. F. Miskon, M. H. Jamaluddin, F. bin Ali, M. F. Asyraf, M. B. bin Bahar *et al.*, "A new data glove approach for malaysian sign language detection," *Procedia Computer Science*, vol. 76, pp. 60–67, 2015. 61

[102] J.-H. Kim, N. D. Thang, and T.-S. Kim, "3-d hand motion tracking and gesture recognition using a data glove," in *2009 IEEE International Symposium on Industrial Electronics*. IEEE, 2009, pp. 1013–1018. 61

[103] K. N. Tarchanidis and J. N. Lygouras, "Data glove with a force sensor," *IEEE Transactions on Instrumentation and Measurement*, vol. 52, no. 3, pp. 984–989, 2003. 61

[104] L. Lei and Q. Dashun, "Design of data-glove and chinese sign language recognition system based on arm9," in *2015 12th IEEE International Conference on Electronic Measurement & Instruments (ICEMI)*, vol. 3. IEEE, 2015, pp. 1130–1134. 61

[105] N. Tongrod, T. Kerdcharoen, N. Watthanawisuth, and A. Tuantranont, "A low-cost data-glove for human computer interaction based on ink-jet printed sensors and zigbee networks," in *International Symposium on Wearable Computers (ISWC) 2010*. IEEE, 2010, pp. 1–2. 61

[106] P.-C. Hsiao, S.-Y. Yang, B.-S. Lin, I.-J. Lee, and W. Chou, "Data glove embedded with 9-axis imu and force sensing sensors for evaluation of hand function," in *2015 37th annual international conference of the IEEE Engineering in Medicine and Biology Society (EMBC)*. IEEE, 2015, pp. 4631–4634. 61

[107] B. S. Lin, I. J. Lee, P. C. Hsiao, S. Y. Yang, and W. Chou, "Data glove embedded with 6-dof inertial sensors for hand rehabilitation," in *2014 Tenth International Conference on Intelligent Information Hiding and Multimedia Signal Processing*. IEEE, 2014, pp. 25–28. 61

[108] D. Lu, Y. Yu, and H. Liu, "Gesture recognition using data glove: An extreme learning machine method," in *2016 IEEE International Conference on Robotics and Biomimetics (ROBIO)*. IEEE, 2016, pp. 1349–1354. 61, 93

[109] F. L. Hammond, Y. Mengüç, and R. J. Wood, "Toward a modular soft sensor-embedded glove for human hand motion and tactile pressure measurement," in *2014 IEEE/RSJ International Conference on Intelligent Robots and Systems*. IEEE, 2014, pp. 4000–4007. 61

[110] B. Fang, D. Guo, F. Sun, H. Liu, and Y. Wu, "A robotic hand-arm teleoperation system using human arm/hand with a novel data glove," in *2015 IEEE International Conference on Robotics and Biomimetics (ROBIO)*. IEEE, 2015, pp. 2483–2488. 61

[111] I. E. McDowall, M. T. Bolas, R. C. Mead Jr, and C. Greuel, "Virtual reality glove system with fabric conductors," Oct. 3 2000, uS Patent 6,128,004. 61

[112] L. K. Simone, N. Sundarrajan, X. Luo, Y. Jia, and D. G. Kamper, "A low cost instrumented glove for extended monitoring and functional hand assessment," *Journal of neuroscience methods*, vol. 160, no. 2, pp. 335–348, 2007. 61

[113] Z. Shen, J. Yi, X. Li, M. H. P. Lo, M. Z. Chen, Y. Hu, and Z. Wang, "A soft stretchable bending sensor and data glove applications," *Robotics and biomimetics*, vol. 3, no. 1, p. 22, 2016. 61

[114] L. Li, W. M. Au, T. Hua, and K. S. Wong, "Design of a conductive fabric network by the sheet resistance method," *Textile research journal*, vol. 81, no. 15, pp. 1568–1577, 2011. 62

[115] L. Li, S. Liu, F. Ding, T. Hua, W. M. Au, and K.-S. Wong, "Electromechanical analysis of length-related resistance and contact resistance of conductive knitted fabrics," *Textile research journal*, vol. 82, no. 20, pp. 2062–2070, 2012. 62

[116] C. M. Bishop, *Pattern recognition and machine learning*. springer, 2006. 77

[117] N. Lv, X. Yang, Y. Jiang, and T. Xu, "Sparse decomposition for data glove gesture recognition," in *2017 10th International Congress on Image and Signal Processing, BioMedical Engineering and Informatics (CISP-BMEI)*. IEEE, 2017, pp. 1–5. 80

[118] P. D. Rosero-Montalvo, P. Godoy-Trujillo, E. Flores-Bosmediano, J. Carrascal-García, S. Otero-Potosi, H. Benitez-Pereira, and D. H. Peluffo-Ordóñez, "Sign language recognition based on intelligent glove using machine learning techniques," in *2018 IEEE Third Ecuador Technical Chapters Meeting (ETCM)*. IEEE, 2018, pp. 1–5. 80

[119] N. Tubaiz, T. Shanableh, and K. Assaleh, "Glove-based continuous arabic sign language recognition in user-dependent mode," *IEEE Transactions on Human-Machine Systems*, vol. 45, no. 4, pp. 526–533, 2015. 85

[120] J.-S. Kim, W. Jang, and Z. Bien, "A dynamic gesture recognition system for the korean sign language (ksl)," *IEEE Transactions on Systems, Man, and Cybernetics, Part B (Cybernetics)*, vol. 26, no. 2, pp. 354–359, 1996. 85

[121] S. A. Mehdi and Y. N. Khan, "Sign language recognition using sensor gloves," in *Proceedings of the 9th International Conference on Neural Information Processing, 2002. ICONIP'02.*, vol. 5. IEEE, 2002, pp. 2204–2206. 85

[122] K. Bernardin, K. Ogawara, K. Ikeuchi, and R. Dillmann, "A sensor fusion approach for recognizing continuous human grasping sequences using hidden markov models," *IEEE Transactions on Robotics*, vol. 21, no. 1, pp. 47–57, 2005. 85

[123] G. Heumer, H. B. Amor, M. Weber, and B. Jung, "Grasp recognition with uncalibrated data gloves-a comparison of classification methods," in *2007 IEEE Virtual Reality Conference*. IEEE, 2007, pp. 19–26. 85

[124] P. Rajpurkar, A. Y. Hannun, M. Haghpanahi, C. Bourn, and A. Y. Ng, "Cardiologist-level arrhythmia detection with convolutional neural networks," *arXiv preprint arXiv:1707.01836*, 2017. 85

[125] I. Goodfellow, Y. Bengio, and A. Courville, *Deep learning*. MIT press, 2016. 85

[126] F. Seide, G. Li, and D. Yu, "Conversational speech transcription using context-dependent deep neural networks," in *Twelfth annual conference of the international speech communication association*, 2011. 85

[127] G. Dahl, A.-r. Mohamed, G. E. Hinton *et al.*, "Phone recognition with the mean-covariance restricted boltzmann machine," in *Advances in neural information processing systems*, 2010, pp. 469–477. 85

[128] L. Deng, M. L. Seltzer, D. Yu, A. Acero, A.-r. Mohamed, and G. Hinton, "Binary coding of speech spectrograms using a deep auto-encoder," in *Eleventh Annual Conference of the International Speech Communication Association*, 2010. 85

[129] M. Atzori, M. Cognolato, and H. Müller, "Deep learning with convolutional neural networks applied to electromyography data: A resource for the classification of movements for prosthetic hands," *Frontiers in neurorobotics*, vol. 10, p. 9, 2016. 85

[130] Y. LeCun, L. Bottou, Y. Bengio, and P. Haffner, "Gradient-based learning applied to document recognition," *Proceedings of the IEEE*, vol. 86, no. 11, pp. 2278–2324, 1998. 85

[131] Q. Yao, R. Wang, X. Fan, J. Liu, and Y. Li, "Multi-class arrhythmia detection from 12-lead varied-length ecg using attention-based time-incremental convolutional neural network," *Information Fusion*, vol. 53, pp. 174–182, 2020. 85

[132] X. Fan, Q. Yao, Y. Cai, F. Miao, F. Sun, and Y. Li, "Multiscaled fusion of deep convolutional neural networks for screening atrial fibrillation from single lead short ecg recordings," *IEEE journal of biomedical and health informatics*, vol. 22, no. 6, pp. 1744–1753, 2018. 85

[133] S. Kiranyaz, T. Ince, and M. Gabbouj, "Real-time patient-specific ecg classification by 1-d convolutional neural networks," *IEEE Transactions on Biomedical Engineering*, vol. 63, no. 3, pp. 664–675, 2015. 85

[134] Z. Qin, Z. Jiang, J. Chen, C. Hu, and Y. Ma, "semg-based tremor severity evaluation for parkinson's disease using a light-weight cnn," *IEEE Signal Processing Letters*, vol. 26, no. 4, pp. 637–641, 2019. 85

[135] G. Ghazaei, A. Alameer, P. Degenaar, G. Morgan, and K. Nazarpour, "Deep learning-based artificial vision for grasp classification in myoelectric hands," *Journal of neural engineering*, vol. 14, no. 3, p. 036025, 2017. 86

[136] B. Fang, Q. Lv, J. Shan, F. Sun, H. Liu, D. Guo, and Y. Zhao, "Dynamic gesture recognition using inertial sensors-based data gloves," in *2019 IEEE 4th International Conference on Advanced Robotics and Mechatronics (ICARM)*. IEEE, 2019, pp. 390–395. 86, 102

[137] N. Diliberti, C. Peng, C. Kaufman, Y. Dong, and J. T. Hansberger, "Real-time gesture recognition using 3d sensory data and a light convolutional neural network," in *Proceedings of the 27th ACM International Conference on Multimedia*, 2019, pp. 401–410. 86

[138] M. A. Simão, O. Gibaru, and P. Neto, "Online recognition of incomplete gesture data to interface collaborative robots," *IEEE Transactions on Industrial Electronics*, vol. 66, no. 12, pp. 9372–9382, 2019. 86, 102

[139] S. Sundaram, P. Kellnhofer, Y. Li, J.-Y. Zhu, A. Torralba, and W. Matusik, "Learning the signatures of the human grasp using a scalable tactile glove," *Nature*, vol. 569, no. 7758, pp. 698–702, 2019. 86

[140] R. J. Schwarz and C. Taylor, "The anatomy and mechanics of the human hand," *Artificial limbs*, vol. 2, no. 2, pp. 22–35, 1955. 87

[141] G. Schlesinger, "Ersatzglieder und arbeitshilfen fur kriegsbeschadigte und unfallverletzte," *Der Mechanische Aufbau der Künstlichen Glieder*, pp. 312–661, 1919. 87

[142] J. Liu, F. Feng, Y. C. Nakamura, and N. S. Pollard, "A taxonomy of everyday grasps in action," in *2014 IEEE-RAS International Conference on Humanoid Robots*, 2014, pp. 573–580. 88

[143] W. Rawat and Z. Wang, "Deep convolutional neural networks for image classification: A comprehensive review," *Neural computation*, vol. 29, no. 9, pp. 2352–2449, 2017. 89, 90

[144] Y. Zhao and S. Zhou, "Wearable device-based gait recognition using angle embedded gait dynamic images and a convolutional neural network," *Sensors*, vol. 17, no. 3, p. 478, 2017. 89

[145] B.-Y. Su, J. Wang, S.-Q. Liu, M. Sheng, J. Jiang, and K. Xiang, "A cnn-based method for intent recognition using inertial measurement units and intelligent lower limb prosthesis," *IEEE Transactions on Neural Systems and Rehabilitation Engineering*, vol. 27, no. 5, pp. 1032–1042, 2019. 90

[146] A. Ibarguren, I. Maurtua, and B. Sierra, "Layered architecture for real time sign recognition: Hand gesture and movement," *Engineering Applications of Artificial Intelligence*, vol. 23, no. 7, pp. 1216–1228, 2010. 93

[147] N. S. Altman, "An introduction to kernel and nearest-neighbor nonparametric regression," *The American Statistician*, vol. 46, no. 3, pp. 175–185, 1992. 93

[148] C. Cortes and V. Vapnik, "Support-vector networks," *Machine learning*, vol. 20, no. 3, pp. 273–297, 1995. 93

[149] X. Yang, X. Chen, X. Cao, S. Wei, and X. Zhang, "Chinese sign language recognition based on an optimized tree-structure framework," *IEEE journal of biomedical and health informatics*, vol. 21, no. 4, pp. 994–1004, 2016. 93

[150] J. H. Friedman, J. L. Bentley, and R. A. Finkel, "An algorithm for finding best matches in logarithmic expected time," *ACM Transactions on Mathematical Software (TOMS)*, vol. 3, no. 3, pp. 209–226, 1977. 93

[151] N. Cristianini, J. Shawe-Taylor *et al.*, *An introduction to support vector machines and other kernel-based learning methods*. Cambridge university press, 2000. 94

[152] L. Breiman, J. Friedman, C. J. Stone, and R. A. Olshen, *Classification and regression trees*. CRC press, 1984. 95

[153] J. Hughes, A. Spielberg, M. Chounlakone, G. Chang, W. Matusik, and D. Rus, "A simple, inexpensive, wearable glove with hybrid resistive-pressure sensors for computational sensing, proprioception, and task identification," *Advanced Intelligent Systems*, 2020. 102

[154] S. A. McMaster, "Method for making electrically conductive textiles and textile sensor," Nov. 6 2018, uS Patent 10,119,208. 106

[155] S. Liu, Y. Liu, and L. Li, "The impact of different proportions of knitting elements on the resistive properties of conductive fabrics," *Textile Research Journal*, vol. 89, no. 5, pp. 881–890, 2019. 108

[156] S. Liu, C. Yang, Y. Zhao, X. M. Tao, J. Tong, and L. Li, "The impact of float stitches on the resistance of conductive knitted structures," *Textile research journal*, vol. 86, no. 14, pp. 1455–1473, 2016. 109

[157] A. Kurbak and O. Kayacan, "Basic studies for modeling complex weft knitted fabric structures part v: Geometrical modeling of tuck stitches," *Textile Research Journal*, vol. 78, no. 7, pp. 577–582, 2008. 111